False Vacuum Decay in Two-Higgs-Doublet Models Plus a Scalar or Pseudoscalar

Rickson Wielian

A thesis submitted for the degree of
Bachelor of Philosophy (Honours) - Science at
The Australian National University

October 2024

Declaration

This thesis is an account of research undertaken between February 2024 and October 2024 at the Research School of Physics, The Australian National University, Canberra, Australia. Except where acknowledged in the customary manner, the material presented in this thesis is, to the best of my knowledge, original and has not been submitted in whole or part for a degree in any university.

Rickson Wielian

24 October 2024

Acknowledgments

First, I would like to thank my supervisors Dr. Giorgio Busoni, Navneet Krishnan, and Prof. Cedric Simenel. Thank you to Giorgio for suggesting this research topic—it has been a wonderful experience for me learning and researching quantum field theory and particle physics. Thank you also for supporting me throughout this year, especially for your thorough feedback in editing this thesis. To Nav, thank you for your patience in answering all the quantum field theory and particle physics questions I've had throughout this year. Even though I am not strictly your responsibility, you have helped me greatly with this research project. Thank you too, for all the fun conversations we've had in the Physics building, they have helped make this year lighter. To Cedric, thank you for taking me under your wing and organising our weekly meetings—especially since I am sure you weren't expecting to have to supervise another honours student this year. Thank you for helping me stay on track to finish this honours project in time, and for your writing advice which has surely helped shape this thesis. Thank you to Patrick for your proofreading efforts and your detailed feedback. They were really helpful in editing this thesis.

I would also like to thank for everyone who has supported me growing up. Thank you to mother and father, who have raised me and supported me to try my own path. Thank you to ama, for your love, your kindness and your support too. I literally could not have survived without any of you. Thank you also to my middle school maths teacher Mr. Melchor, for helping me regain interest in maths after 7^{th} grade. I would not be here studying Physics without you. And finally, thank you to my brother, Darren. You have helped cheer me up in moments of stress.

Finally, thank you to all my past and present friends, including those who are no longer in contact with me. All of you have helped me understand myself better, and all of you have been there for me through significant periods of my life. I could not be my present self, here, without any of you.

Abstract

The Two-Higgs Doublet Model (2HDM) is one of the simplest extensions to the Standard Model of particle physics. Despite its simplicity, the 2HDM has the potential to resolve several outstanding problems in high-energy physics, such as baryogenesis, and the generation of neutrino masses. Additionally, its scalar and pseudoscalar extensions 2HDM+s/a are among the most promising simplified models for dark matter. These extensions are theoretically consistent, sufficiently generic to encompass a broad range of theoretical scenarios, and are rich with new physics. However, as with any quantum field theory, the 2HDM(+s/a) models have vast parameter spaces which can only be constrained through observations.

In this thesis, I constrain the 2HDM(+s/a) parameter spaces with the observation that our universe's vacuum has not decayed in the past 10^{10} years. The analysis is split into two parts. First, I analyse the behaviour of leading order vacua appearing at field values of $|\phi| < 10^4$ GeV. I find that in the 2HDM, when the new 2HDM masses $m_H, m_{H^\pm}, m_A$ are set to be large ($\gtrsim 800\,\text{GeV}$), no second vacuum is generated at either tree-level or one-loop order. Second, I examine radiatively-induced vacua appearing at $|\phi| \gtrsim 10^5\,\text{GeV}$. To do this, I extend Fubini's instanton solution to multiple fields, and calculate the leading order contribution to the tunneling rate. I find that when the 2HDM masses are degenerate, a large fraction of the low $\tan\beta \lesssim 3$ region is excluded by false vacuum decay. In addition, as opposed to flavour and electroweak constraints, mass degeneracies generically serve to destabilise the vacuum. Consequently, I expect false vacuum decay constraints to work together with flavour and electroweak constraints to efficiently rule out the 2HDM parameter space. As for the 2HDM+s/a models, I found that in addition to the constraints on the 2HDM, large dark matter Yukawa couplings $y_\chi \gtrsim 0.8$ are excluded by false vacuum decay.

Thus, this thesis provides a comprehensive study of constraints on the 2HDM($+s/a$) through false vacuum decay, and lays a foundation for future research on radiatively-induced false vacuum decay in theories with extended scalar sectors.

Contents

List of Figures

List of Tables

Chapter 1

Introduction

1.1 The Standard Model and Beyond

The Standard Model (SM) of particle physics is currently the most successful theory of fundamental particles in high-energy physics. For example, measurements of magnetic dipole moments of the electron and muon have agreed with SM predictions to over 6 significant figures. Measurements of meson decay rates have also agreed with Standard Model predictions to 4 significant figures [1, 2]. In addition, the SM has even predicted the existence of whole new particles such as the charm [3] and top [4, 5] quarks, as well as the W [6, 7], Z [8, 9], and Higgs [10, 11] bosons. However, even with all these successes, the SM is not without fault. The most significant limitations of the SM are:

1. *The SM has no candidate for dark matter (DM).* All the particles within the SM are either too strongly interacting, or too light to be dark matter candidates [12].

2. *The SM does not predict the observed baryon matter-antimatter asymmetry in the universe.* This is because the SM does not sufficiently violate a symmetry called 'CP symmetry' [13, 14], and the SM cannot support a strong first-order phase transition with the measured Higgs boson mass [14, 15].

3. *The SM has no mechanism to generate neutrino masses.* Though we are sure from neutrino oscillation observations that neutrinos must have nonzero masses [16].

These discrepancies between the SM and observations strongly suggest that the Standard Model must be modified somehow. Given the previous successes of quantum field theory (QFT), as well as field theory's general effectiveness at describing low energy phenomena (as will be discussed in 2), it is of course reasonable to modify the SM within the framework of QFT. This led to the proposals of various 'complete' QFTs which generalise the SM by adding new particles, such as the 'Minimal Supersymmetric Standard Model [17]' and the 'Little Higgs Model [18]'. However, these models suffer from introducing too many new particles and free parameters[1]. This means their parameter spaces are too large to probe with current experimental capabilities [19]. As such, focus has recently shifted to so-called 'simplified' models, introducing only a few new particles which we may directly probe through experiment. In addition, various complete models may reduce to the same simplified model[2], so simplified models have the additional advantage of being able to describe a broader range of theoretical scenarios [19]. The drawback is that simplified models will miss some features of the more complete models; however, these features are expected to only appear at higher energies. As such, they are less relevant to present and near-future experiments.

My project focuses on a simplified model known as the 'Two-Higgs-Doublet Model (2HDM) Plus a Scalar or Pseudoscalar ($+s/a$)'. The 2HDM is well-motivated as it may provide the foundation for more complete models which solve all three of the problems with the SM listed above:

1. In the 1980s, Silveira and Zee showed that DM-SM interactions mediated by the Higgs boson are naturally suppressed, as compared to interactions mediated by the other bosons [20]. Models which exploit this fact are now known as Higgs dark matter portal models. However, the parameter space for a single-Higgs portal has mostly been excluded from collider measurements of Higgs boson production and decay [21, 22], as well as from astrophysical signals [22]. This motivated the investigation of the next-to-minimal scenario of a two-Higgs dark matter portal. However, to consistently realise a dark matter portal with two Higgs doublets requires the introduction of an extra scalar [23] or pseudoscalar [24] particle. This is the motivation behind the 2HDM+s/a model under consideration in this Honours project.

2. As we will see in chapter 2, the 2HDM supports extra sources of CP-symmetry breaking. This means, depending on which region of 2HDM parameter space experiments favour, it is possible the 2HDM will have enough CP-breaking to explain the observed baryon matter-antimatter asymmetry.

3. The 2HDM also forms the basis of several models for neutrino mass generation.

[1]For example, the Minimal Supersymmetric Standard Model contains over 100 free parameters.
[2]As an example, the MSSM requires two Higgs doublets. So the MSSM reduces to the 2HDM.

This includes the well-known scotogenic model [25] which may describe both neutrino masses and dark matter, as well as models where small 'Dirac'[3] masses are generated due to a symmetry [26].

It is important to note, however, that the 2HDM is not the unique model which can solve these issues with the SM. Another example of a simplified dark matter model is the 'dark photon' model, which posits that DM particles may interact with other DM particles through a dark version of the electromagnetic force. The dark version of the photon would then generically mix with the SM photon, providing a possibility for DM-SM interactions through this dark photon [27]. In addition, CP-violation is a rather generic feature of SM extensions. This is because CP-violation can roughly be understood as a nonzero complex phase appearing in the model, which cannot be removed by symmetry transformations. However, for spontaneous CP-violation or a strong first-order phase transition to occur, extensions to the scalar sector of the SM are required. Since the 2HDM is one of the simplest extensions to the Higgs sector of the SM, it remains a well motivated candidate model for baryogenesis. Finally, the currently most popular theory for neutrino mass generation is the 'seesaw' mechanism, which proposes the existence of heavy right-handed neutrinos [28]. The heaviness of these right-handed neutrinos simultaneously explains why we haven't observed them, as well as why observed neutrino masses are so small.

All in all, it remains that the 2HDM is one of the minimal modifications to the Standard Model which can potentially solve the problems with the SM enumerated above. As such, it is important that we take it seriously and check it against experiments. In particle physics phenomenology, we do this by excluding the regions in parameter space which are ruled out by experiment. This is usually a daunting task since even minimal modifications to the SM can introduce around ~ 3 to 10 new free parameters into the model. As we will see in section 3.1, the 2HDM is no exception, and introduces 6 new free parameters. This means that phenomenologists must essentially rule out all of this 6 dimensional space, to effectively rule out the two-Higgs scenario. The focus of this thesis is to rule out regions in parameter space, based on the fact that we have not observed a process called 'false vacuum decay'. As we will see more explicitly in section 2.2, this strategy is very effective in the SM, as it produces the

[3] Dirac mass is a mass term which mix left and right handed fermions.

most stringent theoretical lower bound on the Higgs boson mass [29], before the LHC confirmed its existence in 2012 [10, 11]. So we expect that this strategy should be similarly effective in the 2HDM. However, to the best of our knowledge there has not been a comprehensive analysis of false vacuum decay in the 2HDM. Previous studies have only focused on either false vacuum decay for the creation of baryons [30, 31], or only focus on a specific case that is most analogous to the Standard Model [32]. In particular, all these studies only focus on a subset of possible decay channels.

The main objective of this Honours project is thus to obtain a comprehensive set of constraints on the 2HDM+s/a models due to false vacuum decay. As one would expect, the constraints produced in this project will rule out a large portion of parameter space, so that future efforts can be directed to only the regions allowed by false vacuum decay. On the other hand, on the off-chance that experiments confirm a 2HDM that is marked unstable in this study, the results in this thesis imply that new physics must appear at much lower energies ($\lesssim 10^8$ GeV) than previous theoretical upper bounds ($\lesssim 10^{16}$ GeV.) Thus, I expect that these constraints will inform future phenomenological and experimental work on the 2HDM.

1.2 Thesis Outline

The structure of this thesis is as follows:

Chapter 2: *Background Theory and Related Works*. Here, I begin by introducing quantum field theory, the notion of a vacuum, and the Callan-Coleman method for calculating tunneling rates between vacua. I then review how this Callan-Coleman method is applied to the Standard Model, and outline how the 2HDM differs from the Standard Model.

Chapter 3: *Nearby Vacua in the Two-Higgs-Doublet-Model*. This chapter marks the start of my own work. Here, I begin by reviewing how to translate the free parameters in the 2HDM to more physically meaningful quantities. I then briefly review the present state of theoretical and experimental bounds on the 2HDM. With these bounds in mind, I show that the presence of nearby vacua are increasingly disfavoured by experiments in the 2HDM.

Chapter 4: *Renormalisation-Induced Vacua and Metastability Constraints*. I finally apply the Callan-Coleman method to calculate tunneling rates in the 2HDM. The generalisation from the single-field to the multi-field case comes with a few difficulties. However, I show here that the difficulties miraculously do not matter, as the leading-order solutions can be obtained exactly in much the same way as the single-field case. Armed with these solutions, I performed the, to the best of our knowledge, first comprehensive study of metastability in the 2HDM.

Chapter 5: *Generalisation to Scalar and Pseudoscalar Extensions*. I adapt the procedure developed in the previous chapters to the 2HDM+s/a models. This chapter provides an example of how easily the results of Chapter 4 generalises to other models.

I then conclude with a discussion of how the results in this thesis inform our expectation of future experiments, and what the physical implications of various potential experimental results would be. Then, I will summarise some of the many possible future directions one can take with this research.

1.3 Notations and Conventions

- *Units.* Unless otherwise stated, I use $c = \hbar = 1$. This way, all quantities have units of [energy]^q for some rational number q. For reference, position and time have units of [energy]$^{-1}$. The standard unit of energy in this thesis will be GeV. Where c and $\hbar$ are made explicit, they are generally for pedagogical purposes, or to keep track of terms in semiclassical expansions.

- *n-loop and (next-to)^n-leading order and N^{n}LO.* Throughout this thesis I will use all of these terms interchangeably. In perturbative quantum field theory, leading-order contributions are generally referred as 'tree-level' contributions, and (next-to)^n-leading order (N^{n}LO) contributions are referred as 'n-loop' contributions[4].

- *Approximate order symbols.* I use the symbols $\lesssim$ and $\gtrsim$ throughout this thesis. The statement $a \lesssim b$ should be understood as the statement $a \ll b$ or $a \sim b$.

- *Coordinate planes.* To resolve any potential ambiguities, coordinate planes are named with the following template: '$\square \times \square$'. As an example, the xy-plane is now denoted the $x \times y$ plane.

[4] I have assumed that the tree-level contribution is nonzero, and thus 'leading-order'. This is true for this thesis but may not apply in other contexts.

Chapter 2

Background Theory and Related Works

2.1 Statistical and Quantum Field Theory

In this section I will begin by discussing the basics of field theory in sections 2.1.1 and 2.1.2. Most of this will initially be done within the perspective of statistical field theory but the results can be bridged over to quantum field theory with ease. I will then transition to purely discussing quantum field theory from the middle of section 2.1.3 onwards, where the statistical approach becomes less intuitively useful.

Note that this section involves a lot of equations. As such, the key equations which will be relevant to future chapters are boxed. The unboxed equations contain mostly steps in derivations, or definitions of symbols used in key equations.

2.1.1 Basic Principles and Correlation Functions

Fields are generically obtained as moving averages of physical quantities of underlying systems. Intuitive examples of fields include the local magnetisation of a ferromagnet or the local density of a fluid. Physical observables can then be obtained from these fields through correlation functions. This intuition holds true for both quantum and statistical field theories.

While it is certainly possible to introduce field theory from purely the quantum perspective, I believe it is more intuitive and pedagogical to begin with a statistical approach, where the underlying physical systems are easier to picture. This does not come at much cost, since statistical field theory (SFT) and QFT are intrinsically related. Indeed, as we will see, there is a mathematical equivalence between the classical SFT in d dimensions and the QFT in $d-1$ spatial dimensions.

Let us begin with an example. We would like to describe first a ferromagnet. To do that, we will model the ferromagnet as a 2D square lattice of spins $\boldsymbol{S}_{ij}$. In statistical mechanics, we describe such a lattice with a Hamiltonian like the following:

$$H = \underbrace{\sum_{ij} \boldsymbol{B} \cdot \boldsymbol{S}_{ij}}_{\text{onsite energy}} + \underbrace{\sum_{i,j,k,l} f(i-k, j-l) \boldsymbol{S}_{ij} \cdot \boldsymbol{S}_{kl} + \cdots}_{\text{2-body interactions}} . \tag{2.1}$$

Here, $\boldsymbol{B}$ is the external magnetic field, f is the distance-dependent coupling between the spins, and the dots signify that there might be higher order contributions to the Hamiltonian. However, Hamiltonians like this are impossible to solve analytically outside of toy model situations, like where only nearest-neighbour interactions are allowed [33, 34]. It remains however that we know of phenomena like phase transitions which persist even when these simplifying assumptions are broken. This is one of the original motivations behind studying SFT: To obtain a framework that captures phenomena which are independent of the minute details in the system.

To obtain a field theory, we define our field by taking an average of spins within some radius R much larger than the lattice spacing a:

$$\phi(x, y) = \frac{1}{N} \sum_{(x-ai)^2+(y-aj)^2 \leq R^2} \boldsymbol{S}_{ij}. \tag{2.2}$$

Here, N is the number of spins within the radius R.

The most general Hamiltonian to describe our system then becomes

$$H = \int d^2x \underbrace{\left[J\phi + K\phi^2 + L\phi^3 + \cdots \right]}_{\text{onsite energy}} + \underbrace{\left[A\partial_\mu\phi\partial^\mu\phi + B(\partial_\mu\partial^\mu\phi)^2 + \cdots \right]}_{\text{local interactions}} \equiv \int d^2x \mathcal{H}. \tag{2.3}$$

where the capital letters are constants to be chosen. Here, we have also defined the Landau energy density functional $\mathcal{H}$. To interpret the Hamiltonian above, the first square bracket includes terms that are only dependent on the field at a certain location. This should be understood to be the energy cost of the field to take on a certain independent value. Derivative terms on the other hand compare field values at adjacent points, due to the finite difference

$$\partial\phi = \frac{\phi(x+\epsilon)-\phi(x-\epsilon)}{2\epsilon} + O(\epsilon^2)$$
$$\partial^n\phi = \frac{1}{\epsilon^n}\sum_{k=-\lfloor n/2\rfloor}^{n-\lfloor n/2\rfloor}\binom{n}{k+\lfloor n/2\rfloor}\phi(x+k\epsilon)+O(\epsilon) \tag{2.4}$$

Indeed if we take the finite difference parameter ϵ on the order of the lattice spacing a, we see that in general then $2N^{\text{th}}$ derivative term approximately corresponds to N-nearest neighbour interactions.

Equipped with a Hamiltonian, we follow the usual procedure in statistical mechanics of writing down the partition function

$$Z = \sum_{\text{all microstates } i} e^{-\beta H_i} = \mathcal{N}\int \mathcal{D}\phi \exp\left(-\beta\int d^2x\mathcal{H}\right). \tag{2.5}$$

Here we have defined $\int \mathcal{D}\phi$ to be the sum over all possible field configurations ϕ and $\mathcal{N}$ is a normalisation constant. We may now see the connection between SFT and QFT. In quantum field theory, the energy density $\mathcal{H}$ is instead replaced by the Lagrangian density $\mathcal{L}$ and the $-\beta$ factor is instead replaced by $\frac{1}{\hbar}$. In addition, a spatial dimension must be substituted for a timelike dimension so we must perform a 'Wick rotation' $(x_1, x_2, \cdots, x_d) \mapsto (it, x_1, \cdots, x_{d-1})$. This Wick rotation will give us the factor of i appearing in (2.6). Performing these substitutions yields the Feynman path integral formalism for a quantum field theory:

$$Z = \mathcal{N}\int \mathcal{D}\phi \exp\left(\frac{i}{\hbar}\int d^2x\mathcal{L}\right). \tag{2.6}$$

As a result, the mathematical operations are the same in both QFT and SFT. It should be noted that the equivalence between QFT and SFT makes the success of QFTs intuitively clear: No matter what the underlying theory of everything could be, if we zoom out from the details and average over a large enough region, we will obtain a quantum field theory[1]. As we will see our intuition from classical statistical mechanics can often be imported into quantum field theory this way.

Continuing with SFT, all physical observables are then obtained from the partition

[1] Up to topological considerations which aren't important in this thesis.

function as usual by means of log derivatives. For example, the total magnetisation can be obtained via

$$\langle\phi\rangle = \frac{1}{Z}\sum \phi e^{-\beta H} = -\frac{1}{\beta}\frac{\partial \ln Z}{\partial J}. \tag{2.7}$$

In general, all observables in SFT (and similarly in QFT) are obtainable through n-point correlation functions (or Green's functions) which take the form

$$\langle\phi(x_1)\cdots\phi(x_n)\rangle = \frac{(-1)^n}{\beta^n Z}\frac{\delta^n Z[\boldsymbol{J}]}{\delta \boldsymbol{J}(x_1)\delta\cdots \boldsymbol{J}(x_n)}, \quad Z[\boldsymbol{J}] = \int \mathcal{D}\phi e^{-\beta\int d^dx(\mathcal{H}-\boldsymbol{J}(x)\cdot\phi(x))}. \tag{2.8}$$

In SFT the interpretation of this is rather straightforward: The correlation functions includes all the statistical correlations between spins of different distances, and encodes the response of the spin density ϕ under local changes in the external field J. In QFT the importance of these Green's functions is a little more obfuscated. But, it can be summarised by the Lehmann–Symanzik–Zimmermann (LSZ) reduction formula (2.9), which connects scattering amplitudes to Green's functions [35].

$$\begin{aligned}\langle \boldsymbol{p}_1\cdots \boldsymbol{p}_n|\, S\, |\boldsymbol{k}_1\cdots \boldsymbol{k}_m\rangle &\left[\prod_{i=1}^{n}\frac{\sqrt{Z}i}{p_i^2-m^2+i\epsilon}\right]\left[\prod_{i=1}^{m}\frac{\sqrt{Z}i}{k_i^2-m^2+i\epsilon}\right] \\ = \prod_{i=1}^{m}\int d^dx e^{ip_ix_i}\prod_{i=1}^{n}\int d^dy e^{-ik_iy_i}&\langle\phi(x_1)\cdots\phi(x_n)\phi(y_1)\cdots\phi(y_m)\rangle.\end{aligned} \tag{2.9}$$

Here, d is the spacetime dimension[2], p_i are the outgoing particle momenta, k_i are ingoing particle momenta, S is the scattering matrix, and Z is an unimportant renormalisation factor. The important factors for the present discussion are highlighted in blue. The LSZ reduction formula tells us that all observables from $m \to n$ scattering experiments are thus obtainable from the $m+n$-point correlation functions.

2.1.2 Renormalisation

The process of obtaining a field theory from an underlying system is many-to-one. Renormalisation is a process of connecting these different quantum field theories which describe the same underlying system.

Let us now go back to our averaging technique to define the field ϕ. In principle,

[2]In the above examples, $d=2$. Usually in particle physics, we set $d=4$.

we could have chosen a different averaging radius $\tilde{R}$ and that would give us a different field $\tilde{\phi}$. However, we must now also change the parameters of the theory $(J, K, L, A, B) \mapsto (\tilde{J}, \tilde{K}, \tilde{L}, \tilde{A}, \tilde{B})$ so that the SFT Hamiltonian (2.3) best approximates the lattice Hamiltonian (2.1) with our new averaging region. A straightforward way of recovering a theory with larger averaging radius $\tilde{R} > R$ is to integrate out the fluctuations operating on length scales in the intermediate region $[R, \tilde{R}]$, and reabsorb the integrated results into the free parameters $J, K, L, \cdots$. This line of reasoning will recover the Kadanoff-Wilson renormalisation group approach, which systematically connects theories with different averaging radii [34]. However, this Kadanoff-Wilson method is computationally intractable for QFTs as it breaks Lorentz and gauge symmetries [36]. Care must then be taken to ensure that the final results are Lorentz and gauge invariant. So, we will instead discuss a shortcut which will make QFT calculations easier. Since these SFTs obtained from different averaging radii describe the same underlying system, they should produce identical predictions[3]. This means that the n-point correlation functions $G^{(n)}$ should not change between the two theories:

$$G^{(n)}(\{J, K, L, \cdots\}, \phi, R) = G^{(n)}(\{\tilde{J}, \tilde{K}, \tilde{L}, \cdots\}, \tilde{\phi}, \tilde{R}) \tag{2.10}$$

If this relation were to hold for all R, then the derivative of $G^{(n)}$ with respect to R must be zero. This, along with the multivariable chain rule, gives us the Callan-Symanzik equation:

$$\frac{dG^{(n)}}{d\ln\mu} = \left(\frac{\partial}{\partial \ln\mu} + \sum_i \frac{d\lambda_i}{d\ln\mu}\frac{\partial}{\partial\lambda_i} + \frac{d\ln\phi}{d\ln\mu}\frac{\partial}{\partial\ln\phi} \right) G^{(n)} = 0 \tag{2.11}$$

where in this case $\mu = a/R$, λ_i are the parameters of the model (e.g. $J, K, L \cdots$ from the spin example) and $G^{(n)}$ are the n-point correlation functions. The definition of μ and the choice of logarithms is just convention. The connection between the Kadanoff-Wilson approach and the Callan-Symanzik equation approach is subtle but they both agree at length scales much greater than $R \gg a$ [37], so that there are no theoretical

[3]At this stage, this is a small leap in logic, since in principle we may expect that the act of averaging out the spins may produce a small nonzero R-dependent error. This subtlety will not be relevant for our purposes.

uncertainties.

For a quantum field theory the scale μ is instead the energy scale at which parameters are determined by experiment[4]. But the statement of the Callan-Symanzik equation is fundamentally the same: There is a continuum of equivalent QFTs, with different couplings $\lambda(\mu)$ and fields $\phi(\mu)$, which produce the same predictions $G^{(n)}$. And just like in SFT, in QFT, this Callan-Symanzik equation approach is accurate as long as the experimental energy scales are much smaller than the cutoff scale Λ, defined as the scale at which new physics emerge[5] [37, 38].

Another point of note, is that in the standard model, and the 2HDM(+s/a), we often take the cutoff scale Λ to be very large $\Lambda \gg \mu$. Using the Kadanoff-Wilson approach we can show that the parameters evolve approximately as[6] [34, 36]

$$\lambda(\mu) \approx \lambda(\Lambda) \left(\frac{\mu}{\Lambda}\right)^{-[\lambda]} \tag{2.12}$$

where $[\lambda]$ is the energy dimension of the parameter. So for parameters λ with $[\lambda] < 0$, the value of the parameter at lower energy $\lambda(\mu)$ is insensitive to what we set $\lambda(\Lambda)$ to be at higher energies. This means we may obtain an approximate low energy theory by neglecting all parameters λ with $[\lambda] < 0$. Such theories, where parameters of negative energy dimension are set to zero, are called perturbatively *renormalisable* theories. In spacetime dimension 4, the only renormalisable derivative terms are of the form $\partial_\mu\phi\partial^\mu\phi$. This way, the QFT Lagrangian can often be split into the form $\mathcal{L} = \partial_\mu\phi\partial^\mu\phi - V(\phi)$. Here, the derivative term can be interpreted as a kinetic energy term, and the V term can be interpreted as a potential energy term. We will only consider such renormalisable theories in this thesis.

Usually in the literature, the partial derivative of the parameters are called beta functions β and the partial derivative of the fields are called the anomalous dimensions γ. Explicitly,

$$\boxed{\beta_{\lambda_i} := \frac{d\lambda_i}{d\ln\mu}, \quad \gamma_\phi := \frac{d\ln\phi}{d\ln\mu}.} \tag{2.13}$$

[4]As an example. A measurement of a 2→2 scattering amplitude with centre-of-mass energy 100 GeV would fix one of the $\lambda_i(\mu)$ at a scale $\mu \approx 100\,\text{GeV}$.

[5]This can be in the form of another QFT, a fundamental theory of quantum gravity, or etc.

[6]For simplicity, I assume that $\lambda(\Lambda)$ is close to the 'Gaussian fixed point', which is often assumed for perturbative QFTs. For a more complete treatment of the connection between Kadanoff-Wilson renormalisation and perturbative renormalisability of QFTs, see [39].

In practice, these β and γ functions are calculated by computing the $G^{(n)}$ through perturbation theory, computing its explicit dependence on μ, and imposing (2.11) order by order in perturbation theory. This then tells us how λ_i and ϕ depend on the energy scale μ.

2.1.3 Effective Potentials

In the absence of outside sources, quantum and statistical systems naturally tend to minimise their free energy. In this subsection, I outline the derivation for computing the NLO expression (2.20) *and* (2.24) *for the free energy. These formulas will be used all throughout this thesis.*

In this honours project I am interested in calculating the most energetically favoured field configurations in the 2HDM(+s/a). To build up the tools to do this, let us ask the analogous question in SFT: What field configurations are energetically favoured at finite temperature?

From statistical mechanics we know that the relevant quantity to answer such a question is the Gibbs free energy. To construct it in field theory, we first write the Helmholtz free energy $-\beta F = \ln Z$ and take the Legendre transform [34]

$$G = F - \int d^d x \, \langle \phi(x) \rangle J(x) = F - \int d^d x \, \phi_{\text{cl}}(x) J(x). \tag{2.14}$$

Here, in the last equality we have made the definition $\phi_{\text{cl}}(x) = \langle \phi(x) \rangle$ as is commonly done in the literature [36, 40]. The subscript here is an abbreviation of 'classical'. Though, please don't take this 'classical' label too seriously. Now, taking the functional derivative,

$$\frac{\delta G}{\delta \phi_{\text{cl}}(x)} = \int d^d y \, \frac{\delta J(y)}{\delta \phi_{\text{cl}}(x)} \frac{\delta F}{\delta J(y)} - \frac{\delta J(y)}{\delta \phi_{\text{cl}}(x)} \phi_{\text{cl}}(y) - J(x) = -J(x). \tag{2.15}$$

where in the first equality we use the functional chain rule, and in the second equality we use the fact that $\frac{\delta F}{\delta J(x)} = \phi_{\text{cl}}(x)$ as we saw in (2.8) [36]. This equation (2.15) shows that in the absence of external fields $J = 0$, the favoured field configurations ϕ_{cl} are ones which make $G[\phi_{\text{cl}}]$ stationary.

Since G is an extensive[7] quantity, it is often more convenient to take out the

[7] As defined in statistical mechanics. G scales proportionally to the system volume.

extensive factor and define $V_{\text{eff}} = \frac{1}{L^d} G$ where L^d is the volume of the sample, or in the case of QFT, the extent of spacetime. This V_{eff} is known as the effective potential.

To compute the effective potential perturbatively, it is convenient to use the background field method [36]. We expand the field around ϕ_{cl} to get $\phi = \phi_{\text{cl}} + \eta$. Neglecting terms $O(\eta^3)$ that contribute at NNLO, the path integral then becomes

$$Z[J] = \int \mathcal{D}\eta \exp\left\{ -\beta \left([\mathcal{H}[\phi_{\text{cl}}] + J\phi_{\text{cl}}] + \left[\left.\frac{\delta \mathcal{H}}{\delta \phi(x)}\right|_{\phi_{\text{cl}}} + J \right] \eta(x) + \left.\frac{\delta^2 \mathcal{H}}{\delta\phi(x)\delta\phi(y)}\right|_{\phi_{\text{cl}}} \eta(x)\eta(y) \right) \right\} \tag{2.16}$$

For clarity, I have used a generalised Einstein summation convention where repeated function arguments x and y are integrated over. The first derivative term vanishes if we choose J so that ϕ_{cl} satisfies $\left.\frac{\delta \mathcal{H}}{\delta \phi}\right|_{\phi_{\text{cl}}} + J = 0$, the classical equation of motion[8]. Then, performing the gaussian path integral over η, we obtain

$$Z[J] = \left[\beta \det \left(\left.\frac{\delta^2 \mathcal{H}}{\delta\phi(x)\delta\phi(y)}\right|_{\phi_{\text{cl}}} \right) \right]^{-1/2} e^{-\beta(H(\phi_{\text{cl}}) + J\phi_{\text{cl}})} \tag{2.17}$$

Going through the Legendre transformations then gives us

$$G = \int d^d x \left(\mathcal{H} + \frac{1}{2\beta} \ln \det \left[\left.\frac{\delta^2 \mathcal{H}}{\delta\phi(x)\delta\phi(y)}\right|_{\phi_{\text{cl}}} \right] \right) + \text{constant} \tag{2.18}$$

Here, the constant is irrelevant to the physics, since only differences in the free energy have any physical meaning. To translate to QFT language, we need to only replace $\beta \to i/\hbar$ and $\mathcal{H} \to \mathcal{L}$. Now splitting the QFT Lagrangian in the form $\mathcal{L} = \partial_\mu \phi \partial^\mu \phi - V(\phi)$ we may obtain an expression for the QFT effective potential[9] [36]:

$$\begin{aligned} V_{\text{eff}} &= V(\phi) - \frac{i}{2L^d} \ln \det \left[\partial^2 + \frac{\partial^2 V}{\partial\phi\partial\phi} \right] \\ &= V(\phi) - \frac{i}{2} \int \frac{d^d k}{(2\pi)^d} \ln \left[-k^2 + \frac{\partial^2 V}{\partial\phi\partial\phi} \right]. \end{aligned} \tag{2.19}$$

To go from the first line to the second line, we have used the fact that $\ln \det = \text{Tr} \ln$

[8] This choice will not matter since G is independent of J.

[9] Since we are ultimately interested in the lowest energy field configurations, I will do what is commonly done in the literature and assume ϕ_{cl} is constant in space. This is because any variations in the field will come at a nonzero energy cost from the $\partial_\mu \phi \partial^\mu \phi$ term.

is the sum of log of eigenvalues of the operator $\partial^2 + \partial_\phi^2 V$. This operator is then diagonalised by going to momentum space. This method can be repeated for any types of fields and the integral in (2.19) can be analytically computed to yield the Coleman-Weinberg formula for the one-loop (NLO) contribution to the effective potential (2.20) [41].

$$\boxed{V_{\text{eff}}^{(1)}(\phi, \lambda, \mu) = \frac{1}{64\pi^2} \sum_{\text{particles } i} (-1)^{2s_i} n_i m_i^4(\phi) \left[\ln \left(\frac{m_i^2(\phi)}{\mu^2} \right) + c_i \right] + \Omega(\mu).} \tag{2.20}$$

Here, s_i is the particle spin, n_i denotes the multiplicity of the particle[10] and c_i is a constant which depends on the particle and the renormalisation scheme. For dimensional regularisation in the $\overline{MS}$ scheme, which is what we will use in this thesis, the values are $c_i = 3/2$ for scalars and fermions and $c_i = 5/6$ for vector bosons [42]. The $\Omega(\mu)$ term is due to the fact that the physics should be independent under constant shifts of the Gibbs free energy, so in principle we are free to set this to whatever we desire. However, for calculations it is convenient[11] take $\Omega(\mu) = -V_{\text{eff}}^{(1)}(\phi = 0, \mu)$. Also in this equation, m_i are the eigenvalues of the Hessian

$$m_i^2(\phi) = \text{Eigval}_i \left(\frac{\partial^2 \mathcal{L}}{\partial\phi\partial\phi} \right) \tag{2.21}$$

Note that this way of solving for the effective potential generates logarithm factors like $\ln(m_i^2/\mu^2)$. The n-loop contribution reads as

$$V_{\text{eff}}^{(n)} \propto \sum_{\{n_i\}} V_{n_1,\cdots,n_k} L_1^{n_1} L_2^{n_2} \cdots L_k^{n_k}, \quad L_i = \ln(m_i^2/\mu^2) \tag{2.22}$$

where here $\sum_i n_i \leq n$ and $V_{n_1,\cdots,n_k}$ are the coefficients of the expansion. If at any field point ϕ there is only one relevant energy scale $m_i^2 \sim M(\phi)^2$ then we can always choose $\mu = M(\phi)$ to keep the logarithms small. This choice generates the renormalisation-

[10] In more precise terms it is the real dimension of the representation in which the particle lives, excluding Poincare symmetry. (Spin multiplicity is given by the dimension of the spin $\mathfrak{su}(2)$ representation as usual.)

[11] This is because we want the potential to satisfy the Callan-Symanzik equation $\frac{dV}{d\ln\mu} = 0$. The choice $\Omega(\mu) = -V_{\text{eff}}^{(1)}(0, \mu)$ is a particularly simple way to ensure this.

group (RG) improved effective potential

$$V_{\text{eff,imp}}(\phi) = V(\lambda(M), \phi(M)) + V_{\text{eff}}^{(1)}(\phi(M), \lambda(M), M) \tag{2.23}$$

where the $\lambda(M)$ and $\phi(M)$ now depend on M through the β and γ functions (2.13).

For theories with a single field ϕ, the above approach works fine since by dimensional analysis, we always expect all m_i to be of order ϕ. So, we can always take $M = \phi$. However, in general theories with multiple fields, each field introduces an independent energy scale. This could cause the masses m_i to take on completely different energy scales, so that a single choice M to make all the logarithms small would not *a priori* exist.

Several methods have been proposed to obtain a consistent improvement of the effective potential in these cases. One method is to introduce multiple renormalisation scales μ_i, one for each parameter λ_i. However this results in a far more complicated version of the Callan-Symanzik equation (2.11) which becomes intractable to solve for realistic models [43]. Another method is to exploit the decoupling theorem, which states that higher energy scales $m_i \gg \mu$ can be systematically integrated out to generate an effective field theory at the scale μ. With the higher energy scales out of the way we can then perform renormalisation group improvement as in equation (2.23) [44]. This technique, however, requires us to choose the energy scales at which decoupling takes place in an ad-hoc manner using step functions. This would be complicated to implement in the 2HDM(+s/a). Finally, it has recently been shown that if one pushes the technique (2.23) to its limits, one can always find a choice of scale μ which would automatically take into account the contributions from the largest logarithms in (2.22) [42]. At the one-loop level (NLO), this choice is given by $\mu : V_{\text{eff}}^{(1)}(\phi(\mu), \lambda(\mu), \mu) = 0$. This gives the improved effective potential

$$\boxed{V_{\text{eff,imp}}(\phi) = V(\lambda(\mu_*), \phi(\mu_*)) + O(\lambda^3), \quad V_{\text{eff}}^{(1)}(\phi(\mu_*), \lambda(\mu_*), \mu_*) = 0} \tag{2.24}$$

where $O(\lambda^3)$ denotes two-loop and higher contributions. As a single-scale method, this form of the improved effective potential then automatically keeps logarithms small as long as there exists a scale $\mathcal{M}$ such that all the logarithms are rendered small [42]

$$\boxed{\max_i \left| \ln\left(\frac{m_i}{\mathcal{M}}\right) \right| \ll 4\pi} \tag{2.25}$$

Of course, when such a scale $\mathcal{M}$ does not exist, the approximation is invalidated. Thus, when using this method, it is important to double check whether such a scale $\mathcal{M}$ exists, before jumping to conclusions.

2.1.4 Tunneling Rate Calculations

It is possible that the universe has not had enough time in its life to settle down in the most energetically favoured state. In this subsection, I describe how we can deal with this issue quantitatively by outlining the derivation of the NLO tunneling rate formula (2.30) *and* (2.32) *in QFT.*

The previous subsection dealt with the theory required to identify the field configurations which would be energetically favoured. In quantum field theory these configurations are called vacua[12]. However, even if we find that a lower energy vacuum exists, compared to the vacuum required to reproduce experimental observations, it does not mean our theory is invalid yet. It could be that the two vacua are far enough separated, or that the energy cost to get from one vacuum to another is too large for our universe to transition down to the lower vacuum. This subsection deals with these problems quantitatively. We aim to calculate, or at least in some form approximate, the transition rate from the higher energy vacuum to a lower energy vacuum.

One approach to calculate this rate is by the Callan-Coleman 'bounce' instanton method, which was developed in [45, 46]. This method makes use of the fact that the leading Wentzel-Kramers-Brillouin (WKB) tunneling rate Γ in d dimensional quantum mechanics is identical to twice the abbreviated action[13] of a classical particle [48].

$$\Gamma \propto e^{-B}, \quad B = 2\int_\gamma \sqrt{2V(q)}\, ds. \tag{2.26}$$

Here the path γ must be taken as to minimise B, with the total energy of the particle

[12]In SFT, these would instead be called phases of matter.

[13]Loosely speaking, this is the action of a classical particle when the Hamiltonian is held constant and shifted to zero. See Chapter 9, Section 45D of [47] for a more rigorous and insightful discussion.

fixed at 0. The q_i are spatial coordinates and the line element ds is given by the standard metric $ds^2 = \sum_i dq_i^2$. By Maupertuis' principle in classical mechanics [47], this path can be obtained by solving the classical equations of motion

$$\frac{d^2 q}{dt^2} = \nabla V, \quad \frac{1}{2}\dot{q}^2 - V(q) = 0.$$

Note that the classical particle moves in a potential $-V$ which is the negative of the quantum mechanical barrier. Callan and Coleman proceed analogously in the field theory case, and obtain an equation of motion for the classical field ϕ_i [45, 46]

$$\left(-\frac{\partial^2}{\partial t^2} + \nabla^2\right)\phi_i = \frac{\partial V}{\partial \phi_i} \tag{2.27}$$

Coleman proved that the bounce action B can only be minimised if ϕ is Lorentz-invariant. In such case, the bounce PDE above can be reduce to an ODE in the radial variable $\rho^2 = x^\mu x_\mu = -t^2 + x^2 + y^2 + z^2$:

$$\boxed{\frac{\partial^2 \phi_i}{\partial \rho^2} + \frac{d-1}{\rho}\frac{\partial \phi_i}{\partial \rho} = \frac{\partial V}{\partial \phi_i}.} \tag{2.28}$$

To find the bounce solution, this ODE needs to be solved with the boundary condition $\phi'(0) = 0$ and $\phi(\infty) = \phi_{\text{FV}}$ the field value at the higher vacuum [45]. The solution to this equation ϕ_b can then be immediately plugged into the definition of the bounce action for field theory to calculate the exponential contribution to the tunneling rate [40]:

$$\Gamma \propto \exp\left(-2\int \sqrt{2U(\phi_b)}\, ds\right), \quad U(\phi) := \frac{1}{2}(\nabla\phi)^2 + V(\phi). \tag{2.29}$$

To obtain the next-order contribution in this approximation, Callan and Coleman considered fluctuations $\phi = \phi_b + \eta$ and integrated over Gaussian fluctuations much like we did in deriving the effective potential (2.19)[14]. The final result is given by

[14]This calculation involves a lot of subtleties regarding zero and negative eigenvalues as well as resumming 'multibounce' solutions to (2.28), and thus will be omitted from this thesis. Interested readers are encouraged to check [46] and [49].

[46, 50]

$$\boxed{\frac{\Gamma}{V} = \frac{B^2}{4\pi}\left|\frac{\mathrm{Sdet}'[-\partial^2 + V''(\phi_b)]}{\mathrm{Sdet}[-\partial^2 + V''(\phi_{\mathrm{FV}})]}\right|^{-\frac{1}{2}} e^{-B}.} \tag{2.30}$$

Here, $V = L^{d-1}$ is the spatial volume, Sdet $=$ det for bosons and Sdet $= 1/\det^2$ for fermions, and the prime in Sdet$'$ indicates that the zero eigenvalues are omitted.

In case there is only one energy scale M relevant to the problem, we can approximate the one-loop contribution to the decay rate via dimensional analysis. Both sides of the equation has energy dimension 4. The only dimensionful parameter that can appear in the RHS of (2.30) is M. As such, up to an $O(1)$ dimensionless prefactor,

$$\frac{\Gamma}{V} \approx M^4 e^{-B}. \tag{2.31}$$

The probability of decay is then given by integrating this rate over the observable universe. This gives

$$\boxed{P_{\mathrm{decay}} \approx M^4 T_X^4 e^{-B}} \tag{2.32}$$

where $T_X = 10^{10}\,\mathrm{yr}$ is the age of the universe.

Other approaches to calculate the tunneling rate exist. One example is the 'effective action' approach, which computes the tunneling rate directly from the Gibbs free energy 2.14. This is, however, impractical for perturbative calculations as successive terms in the perturbation series are not suppressed, resulting in poor convergence [40]. Another method, recently proposed, is the Andreassen-Farhi-Frost-Schwartz (AFFS) direct path-integral approach in [51]. However, this approach seems to only be advantageous in the development of tunneling theory and numerical lattice calculations where the relevant correlation functions can be directly approximated. In any case, this AFFS direct approach reproduces the first-order WKB approximation result when expanded to next-to-leading order in quantum mechanics, so it should reproduce (2.30) in QFT [51]. The Callan-Coleman formula (2.30) is thus the most suitable technique to calculate decay rates through perturbation theory.

Finally, now equipped with knowledge of tunneling rates, I would like to define some terminology which I will use throughout this thesis.

1. *Absolutely stable.* Our desired vacuum is absolutely stable if it is the true (global)

minimum of the effective potential.

2. *Metastable.* Our desired vacuum is metastable if it is not absolutely stable and if the tunneling rate Γ is not too large compared to the age of the universe T_X. That is, $\Gamma T_X \lesssim 1$.

3. *Unstable.* Our desired vacuum is unstable if it is both not absolutely stable and not metastable.

2.1.5 Higgs Mechanism

The Higgs mechanism provides a gauge-invariant way to give fundamental particles mass. Very roughly speaking, the way this works is as follows: The Higgs field is a field which takes on a nonzero value everywhere. Then, as fundamental particles propagate, they interact with this nonzero field. The energy from this interaction gives particles mass. This subsection expands upon the above picture in detail.

Since my project involves a model that extends the Higgs sector of the standard model, I will briefly introduce the Higgs mechanism here. There are two ingredients needed for the Higgs mechanism to take place: First, we need a gauge (local) symmetry. In the standard model, the Higgs mechanism acts on the electroweak gauge symmetry group $\mathrm{U}(2) \cong \mathrm{SU}(2)_L \times \mathrm{U}(1)_Y$[15]. This is done by letting the Higgs field Φ transform nontrivially under the gauge transformation:

$$\Phi \mapsto \underbrace{e^{i\frac{\theta_0}{2}}}_{\mathrm{U}(1)_Y} \underbrace{e^{i\frac{\theta_i \sigma_i}{2}}}_{\mathrm{SU}(2)_L} \Phi. \tag{2.33}$$

Here, $\theta_0, \cdots, \theta_3$ parametrise the elements of the gauge groups, and σ_i are the pauli matrices. This is what we mean by the Higgs Φ being a doublet[16]. The Higgs sector of the Standard Model lagrangian then reads as [36]

$$\mathcal{L}_{\text{Higgs}} = (D_\mu \Phi)^\dagger D^\mu \Phi - (-\mu_h^2 \Phi^\dagger \Phi + \lambda \Phi^\dagger \Phi \Phi^\dagger \Phi). \tag{2.34}$$

Here, we have the standard gauge covariant kinetic term $(D_\mu \Phi)^\dagger D^\mu \Phi$ that any phys-

[15]The group $\mathrm{U}(n)$ can be thought of as the set of unitary $n \times n$ matrices, equipped with matrix multiplication. $\mathrm{SU}(n)$ have the extra condition of matrices having determinant 1.

[16]More precisely, Φ is a doublet of the gauge group $\mathrm{SU}(2)_L$.

ical field must have, and a potential term $V(\Phi) = -\mu_h^2\Phi^\dagger\Phi + \lambda\Phi^\dagger\Phi\Phi^\dagger\Phi$ chosen specifically to make the Higgs mechanism work. We may use the U(2) symmetry of the lagrangian and perform transformations (2.33) so that at every point in space

$$\Phi(x) = \frac{1}{\sqrt{2}}\begin{pmatrix} 0 \\ \phi(x) \end{pmatrix} \tag{2.35}$$

where ϕ here is now a real scalar field. Remembering that the zeroth order approximation to the effective potential is simply the potential appearing in the Lagrangian, we can minimise this with respect to ϕ and find that $V(\phi)$ is minimised when

$$\phi = v := \frac{\mu_h}{\sqrt{\lambda}}.$$

This v is known as the vacuum expectation value (vev) of the Higgs field and is the second ingredient for the Higgs mechanism. To see how the Higgs vev gives the bosons mass, we simply expand the kinetic term for the Φ field to get [36]

$$(D_\mu\Phi)^\dagger(D^\mu\Phi) = -\frac{v^2}{8}\left[g^2(A_\mu^1)^2 + g^2(A_\mu^2)^2 + (-gA_\mu^3 + g'B_\mu)^2\right] + \ldots \tag{2.36}$$

where I have ignored all the irrelevant terms for brevity. Here, A^i are the gauge fields[17] associated to SU(2)$_L$ and B is the gauge field associated with U(1)$_Y$. Also, g and g' are parameters in the standard model representing the strengths of the electroweak force. This kinetic term thus expands to quadratic terms in the Lagrangian like $-\frac{g^2v^2}{8}(A^1)^2$.

To roughly understand why this gives rise to mass, we can look at the toy lagrangian $\mathcal{L}_{KG} = \frac{1}{2}\partial_\mu\phi\partial^\mu\phi - \frac{1}{2}m^2\phi^2$. By the Euler-Lagrange equations this gives the classical equation of motion $(\partial^\mu\partial_\mu + m^2)\phi = 0$ which is the Klein-Gordon equation for a particle with mass m. More generally, the squared masses of particles in QFT can be obtained from the eigenvalues of the Hessian of the effective potential at the vacuum (i.e. $m_i^2(\phi)$ from (2.21) evaluated at the vev $\phi = v$.) [36][18].

It should be noted that the discussion so far is a pedagogical simplification: In reality, the field Φ cannot formally attain a nonzero vev due to Elitzur's theorem

[17]Gauge fields are analogous to the electromagnetic potential $A_\mu = (\phi/c, \boldsymbol{A})_\mu$ of classical electromagnetism.

[18]Since we assumed ϕ_{cl} is constant, this only gives us an approximation of the particle masses. Nevertheless, this approximation to the mass of particle i will be accurate as long as $m_i^2(v) \lesssim v^2$ [40, 52].

[53]. This means the common saying that the Higgs mechanism is the spontaneous symmetry breaking of a gauge symmetry is strictly false. However, the procedure introduced in this subsection is not irredeemably broken. It has been shown that the Higgs mechanism actually arises in a gauge-invariant way, without any need of a nonzero vev. Only when we restrict to a specific gauge[19] does the Higgs mechanism mimic spontaneous symmetry breaking, as seen in this subsection [54].

2.2 Stability Bounds in the Standard Model

In the standard model, the only potential term comes form the Higgs sector. In this section, I outline how phenomenologists apply the background theory discussed in 2.1 to the SM Higgs potential. We find that our universe's vacuum in the standard model is metastable. So, when testing beyond-standard-model theories, it is important to be careful so that we do not worsen the situation and make the vacuum unstable. This is because such theories with an unstable vacuum would be inconsistent with the fact that we have not observed a false vacuum decay.

In the standard model, the question of whether our vacuum is stable or metastable has been investigated extensively [50, 55, 56]. There are two main reasons for this. First, before the confirmation of the Higgs boson's existence in 2012, vacuum stability bounds provided the most stringent lower bounds on the Higgs mass. This means that tunneling rate calculations helped guide collider experiments in identifying what energies were required to likely produce the Higgs boson [57]. Second, even after the measurement of the Higgs boson, the question of vacuum stability in the SM still incites a lot of curiosity. This is because the measured values of the Higgs and top quark masses seem to coincidentally place our universe near the critical point where the two vacua are degenerate. That is, the standard model suggests that we live very close to a phase transition. This has driven a lot of theorists to speculate on whether this could give us insight into unknown physics [58]. Though, much of this is speculation built on top of the assumption that the SM is valid at very high energies, so it is best to take them with a grain of salt[20].

The relevant potential in the standard model is the Higgs potential, which is shown

[19] As one would choose a gauge in electromagnetism.

[20] That is not to say that these investigations aren't valuable. After all, there is a chance that this coincidence is a hint of some deeper physics, and it does not hurt to be thorough.

in (2.34). Once we exploit the residual gauge symmetry (2.35) this becomes a potential in one scalar field

$$V(\phi) = -\frac{1}{2}\mu_h^2\phi^2 + \frac{1}{4}\lambda\phi^4. \tag{2.37}$$

Since there is only one field, we may obtain the one-loop RG-improved effective potential using the naïve choice $\mu = \phi$ so that

$$V_{\text{eff,imp}}(\phi) = -\frac{1}{2}\mu_h^2(\phi)\phi^2 + \frac{1}{4}\lambda(\phi)\phi^4 \approx \frac{1}{4}\lambda(\phi)\phi^4. \tag{2.38}$$

Here, as usual, μ and ϕ depend on its input parameter through the β functions, and the approximation on the RHS is due to the fact that λ and μ_h can only vary considerably at energy scales much larger than v. We will see this more explicitly in a moment.

Since our universe must lie in the vacuum at $\phi = v$, for $\phi \gg v$ the condition that a new, lower vacuum is generated in the effective potential is equivalent to the condition that $\lambda(\phi) < 0$ for some ϕ. The dependence of λ on μ for various choices of top mass is shown in figure 2.1a. The standard model Higgs potential is also shown 2.1b for a top mass of $m_t = 170\,\text{GeV}$. Crucially, we see that even when λ is only very slightly negative $|\lambda| \ll 1$, the potential quickly develops a minimum that is deeper than the desired minimum at $\phi = 246\,\text{GeV}$, for the theory to match experimental observations.

However, as we have seen from the previous subsection, the potential developing a deeper minimum does not immediately render our set of parameters broken. To rigorously rule out a set of parameters we must calculate the tunneling rate from our current desired vacuum to the deeper vacuum via equation (2.30). Then, we can only rule the set of parameters out if $\Gamma T_X \gtrsim 1$.

To calculate the tunneling rate in the standard model, we first find the leading order bounce solution which satisfies (2.28) with $d = 4$ and $V(\phi) = \lambda\phi^4$. Remarkably, this ODE admits a family of exact solutions given by [50, 59, 60]

$$\boxed{\phi_b(\rho) = \sqrt{\frac{2}{|\lambda|}}\frac{2\rho_0}{\rho^2 + \rho_0^2} \implies B = \frac{8\pi^2}{3|\lambda|}} \tag{2.39}$$

Here, ρ_0 can be any real number. This degeneracy in ρ_0 will be broken at one-loop

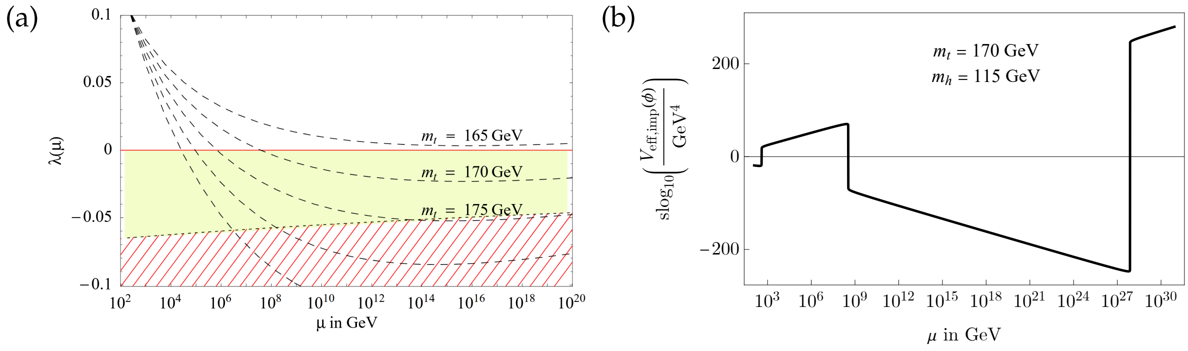

Figure 2.1: (a) Running of the λ parameter in the standard model for a Higgs mass of m_h =115 GeV and various top quark masses. When $\lambda(\mu)$ hits the green region, the potential develops a lower minimum. When $\lambda(\mu)$ goes below the red region the tunneling rate becomes significant compared to the age of the universe $\Gamma T_X \gtrsim 1$. This subfigure is reproduced from [50] with permission from the publisher Elsevier. (b) The Higgs improved effective potential (2.38), including the $-\frac{1}{2}\mu_h^2\phi^2$ term, with all parameters set to be the same as figure (a), and top quark mass $m_t = 170\,\mathrm{GeV}$. The slog_{10} function is defined to be $\mathrm{slog}_{10}(x) := \mathrm{sgn}(x)\log_{10}(1+|x|)$. We see that when $\lambda(\phi) < 0$ the potential becomes strongly negative, so the vacuum of our universe at $\phi = 246\,\mathrm{GeV}$ is no longer the global minimum.

order where we will be required to take $\rho_0 \sim 1/\mu$ to keep logarithms small. At this point, one might worry that this bounce is calculated using the zeroth order potential, while the new deeper minimum is only generated after RG-improvement. However this is not an issue as we can always flow our theory to a renormalisation scale μ such that $\lambda(\mu) < 0$. Since λ does not vary much while ϕ varies an order of magnitude (see 2.1a), the bounce calculated at this energy is a good approximation to the true bounce. In addition, the difference between using a leading-order bounce solution and NLO bounce solution in the calculation of (2.30) is formally an NNLO correction [50]. Another point of worry is that since we have chosen a renormalisation scale μ so that $\lambda(\mu) < 0$, the potential $V(\phi) = \lambda\phi^4$ no longer has a barrier. However, this isn't an issue in QFT since the derivative term $\nabla^2\phi$ in (2.29) supplies a barrier even if V doesn't have a barrier [60].

With this bounce solution, the authors computed the tunneling rate using the one-loop formula (2.30). The functional determinants in this formula is most easily calculated using the Gelfand-Yaglom method:

$$\frac{\det(-\partial^2 + W(\rho))}{\det(-\partial^2)} = \lim_{t\to\infty} \frac{\det u_W(\rho)}{\det u_0(\rho)} \tag{2.40}$$

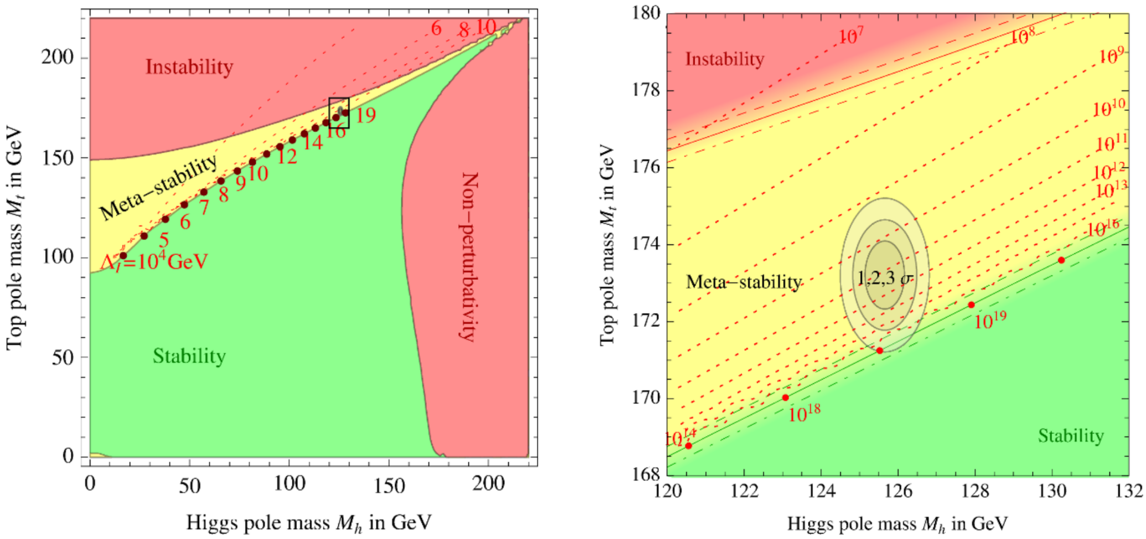

Figure 2.2: Vacuum stability bounds in the standard model. The right figure is a zoom-in view into the black rectangular inset in the left figure. The red contours represent the instability scales: The renormalisation scale μ at which $\lambda(\mu) < 0$. The grey regions in the right figure are the experimentally favoured regions from 2013 collider data at 1, 2, and 3 standard errors respectively. This figure is reproduced from [58] under the Creative Commons license from the publisher Springer.

Here, $u_W(\rho)$ is the eigenfunction of the operator $-\partial^2 + W$ with the lowest eigenvalue, and the det appearing on the RHS is over residual (spin, etc) degrees of freedom. With this method, and standard renormalisation techniques in quantum field theory, the authors derived the one-loop correction to the bounce action as [50]

$$\begin{aligned}\Delta B &= -\ln\left(\frac{B^2}{4\pi}\left|\frac{\mathrm{Sdet}'[-\partial^2 + V''(\phi_b)]}{\mathrm{Sdet}[-\partial^2 + V''(\phi_{\mathrm{FV}})]}\right|^{-\frac{1}{2}}\right) \\ &= -\frac{2}{3}(5+6L) + \frac{y_t^2}{6|\lambda|}(13+12L) + \frac{y_t^4}{6\lambda^2}(5+6L) - \frac{2g^2+g_Z^2}{12|\lambda|}(7+6L) \\ &\quad - \frac{2g^4+g_Z^4}{32\lambda^2}(1+2L) + f_h(\lambda) - f_t\left(\frac{y_t^2}{|\lambda|}\right) + f_g\left(\frac{g_Z^2}{|\lambda|}\right) + 2f_g\left(\frac{g^2}{|\lambda|}\right) \qquad (2.41)\end{aligned}$$

Here, $L = \ln(\rho_0\mu e^\gamma/2)$ with γ being the Euler-Mascheroni constant, $g_Z := g^2 + g'^2$, $f_h = \frac{7}{2}\ln|\lambda| - 8 \pm 1$, and $f_{t,g}$ are numerically determined functions given in [50]. We will not make use of this unruly expression in this thesis, but we will make note that the one-loop correction to the bounce is of order $O(y_t^4/|\lambda|^2)$. We also expect that the one-loop correction to the bounce will only be relevant when the leading-order tunneling time (2.32) is close to the age of the universe. With our solution (2.39), this gives approximately $|\lambda| \sim 0.05$. In addition, typical values of the yukawa top coupling are $y_t(\mu) \in [0.5, 0.75]$. Using these estimates, we can compute the relative magnitude of the one-loop correction as

$$\boxed{\frac{\Delta B}{B} \sim \frac{\left(\frac{y_t^4}{\lambda^2}\right)}{\left(\frac{8\pi^2}{3|\lambda|}\right)} = \frac{3y_t^4}{8\pi^2|\lambda|} \approx 10^{-1}.} \tag{2.42}$$

We will use this to estimate the impact of one-loop calculations in obtaining metastability bounds for the 2HDM+s/a.

Using (2.41), the authors of [50] showed that metastability is experimentally favoured in the standard model. This is shown in 2.2, which was taken from a study after the confirmation of the Higgs boson [58]. As we can see, the measured values of the Higgs and top masses live very closely to the metastability-instability bound. This is a reflection of the fact that vacuum stability bounds are some of the most stringent bounds we have on the standard model parameter space. This motivates us to look at the vacuum stability bounds of beyond-SM theories, as we need to constrain their parameter spaces to guide future experimental searches.

2.3 The Two-Higgs-Doublet Model

The Two-Higgs-Doublet Model postulates the existence of a second Higgs doublet. As a result, the 2-Higgs potential is much more complicated than the 1-Higgs potential and can support many new phenomena such as massive photons, and the creation of baryons in the early universe. This section details these new possibilities, and explicitly states the scenarios we will focus on in this thesis.

On top of the SM, the Two-Higgs-Doublet Model (2HDM) proposes the existence of the second Higgs doublet field. The reasons for this have been explained in Chapter 1 so I will not repeat them here. The 2HDM potential we consider is given by

$$\begin{aligned} V(\Phi_1, \Phi_2) =& m_{11}^2|\Phi_1|^2 + m_{22}^2|\Phi_2|^2 - (m_{12}^2\langle\Phi_1|\Phi_2\rangle + \text{h.c.}) + \frac{1}{2}\lambda_1|\Phi_1|^4 + \frac{1}{2}\lambda_2|\Phi_2|^4 \\ &+ \lambda_3|\Phi_1|^2|\Phi_2|^2 + \lambda_4\langle\Phi_1|\Phi_2\rangle\langle\Phi_2|\Phi_1\rangle + \frac{1}{2}(\lambda_5\langle\Phi_1|\Phi_2\rangle^2 + \text{h.c.}) \end{aligned} \tag{2.43}$$

Here, $|\Phi|^2 := \langle\Phi|\Phi\rangle$ and the bra-ket notation represents the standard inner product $\langle\Phi_1|\Phi_2\rangle = \Phi_1^\dagger\Phi_2$. The parameters m_{ij}^2 can be negative and the square only indicates that it has units of squared mass. Since we require the Lagrangian to be real, the parameters $m_{11}^2, m_{22}^2, \lambda_1, \cdots, \lambda_4$ are forced to be real. In the most general model m_{12}^2 and λ_5 are allowed to be complex. But while there is a lot of interesting phenomenology that can be done in the complex parameters case [61], the 2HDM with real m_{12} and λ_5 is still well-motivated. This is commonly done in the literature (see [62, 63]) for two main reasons. First, it is much easier to visualise the parameter space when these parameters are real. Second, this is an assumption of explicit CP-symmetry in the Lagrangian, which is well-motivated since experimentally, signatures of CP symmetry breaking are small, with a relative scale of $\sim 10^{-3}$ [64]. I have thus chosen to focus on the real parameters case as a first step in understanding the 2HDM parameter space.

In addition to the explicit CP-symmetry described above, we have imposed a $\mathbb{Z}_2$ symmetry given by $\mathcal{L}(\Phi_1, \Phi_2) = \mathcal{L}(\Phi_1, -\Phi_2)$. This symmetry is then 'softly' broken by reintroducing the m_{12}^2 term[21]. This, along with a choice of one of the Yukawa[22] assignments in table 2.1, prevents leading order contributions to flavour-changing-neutral-current processes [65, 66]. These are processes which change the total flavour while preserving electric charge (e.g. $\tau^- \to e^- + \gamma$), and they are highly suppressed in experiment [67].

Type	Top Family	Bottom Family	Tau Family
I	Φ_2	Φ_2	Φ_2
II	Φ_2	Φ_1	Φ_1
X	Φ_2	Φ_2	Φ_1
Y	Φ_2	Φ_1	Φ_2

Table 2.1: Summary of the different types of Yukawa (Higgs-fermion) interaction assignments in the 2HDM, which prevents flavour-changing neutral currents (FCNCs) at leading order. The doublet Φ_i in each column denotes the doublet which interacts with each fermion family.

[21]Soft-breaking just means that we reintroduce symmetry-breaking terms which have positive energy dimension. This is because, from (2.12), positive energy-dimension terms at μ are very sensitive to the high energy physics at Λ. This way, we are still taking into account the possibility that the high-energy theory at Λ is only very slightly $\mathbb{Z}_2$ asymmetric.

[22]These are interactions between the Higgs and fermions. These interactions give fermions mass in much the same way the Higgs gives Gauge bosons mass.

The 2HDM Higgs mechanism differs from the SM mechanism in one main way: The U(2) symmetry no longer leaves only one field component nonzero as in (2.35) — we are instead left with four:

$$\Phi_1 = \frac{1}{\sqrt{2}} \begin{pmatrix} \alpha \\ v_1 e^{i\theta} \end{pmatrix}, \quad \Phi_2 = \frac{1}{\sqrt{2}} \begin{pmatrix} 0 \\ v_2 \end{pmatrix}. \tag{2.44}$$

Here, v_1, v_2, α and θ are real. As such, to find the vacua of this model, we would naïvely need to investigate the effective potential in 4 fields. However, this is not always the case. For the photon to be massless, we require (Φ_1, Φ_2) to transform trivially under the electromagnetic charge $\mathrm{U}(1)_Q$ gauge group given by $(\Phi_1, \Phi_2) \mapsto e^{i\frac{t}{2} + i\frac{\sigma_3 t}{2}}(\Phi_1, \Phi_2)$. This is only possible if $\alpha = 0$. In addition, the complex phase θ would be a new source of CP-violation [68]. While these CP-violating vacua have interesting consequences for matter-antimatter asymmetry, I will instead focus on the case $\theta = 0$ in this thesis. The general case of CP-violating vacua will be relegated to future work. This is because my project was motivated by my supervisor's work on dark matter models. So, while relevant, matter-antimatter asymmetry is not our main interest. The SM-like vacuum is given by $\Phi_1 = (0, v_1/\sqrt{2}), \Phi_2 = (0, v_2/\sqrt{2})$ [66].

The discussion in the previous paragraph tells us how we can classify vacua by the implications they have on the theory. The results are summarised in Table 2.2. Remarkably, Ivanov showed that no minima of different types can coexist at leading order [69], so that if one vacuum is neutral, all vacua are forced to be neutral. Numerical studies have further showed that, at next-to-leading order, coexistence of charge-breaking and neutral minima occur only at a rate of $\sim 5\%$. So their existence can be immediately excluded at 95% confidence level [63]. This means that as a first step, it is reasonable to only consider the effective potential in two fields $V_{\text{eff}}(v_1, v_2)$.

Conventional Name	α	θ	Number of Massless Bosons
Neutral	0	0	1
Charge-breaking		0	0
CP-breaking	0		1

Table 2.2: Summary of the different types of vacua which can occur in the 2HDM. Empty cells indicates no constraint on the field. For the α and θ columns, zeroes indicate that the corresponding parameter is fixed to zero.

Chapter 3

Nearby Vacua in the Two-Higgs-Doublet Model

In this chapter, I investigate the vacuum structure of the 2HDM within $< 10^4$ *GeV of the origin. This will include all leading-order vacua, but will not include vacua induced by RG-running, which typically appear at the* 10^{10} *GeV scale. All calculations and proofs presented (mainly from section 3.3 onward) are, unless otherwise stated through relevant citations, the result of my own work.*

I begin by reviewing how to translate the parameters appearing in the 2HDM to physical observables in section 3.1. I will then review present constraints on the 2HDM in section 3.2. With these constraints in mind, I show in section 3.3 that the presence of a lower vacuum at leading order is gradually disfavoured by experiments in the 2HDM. In sections 3.4 and 3.5, I then show that the leading-order results still hold at one-loop level.

3.1 Input Variables for the 2HDM

Most of the free parameters m_{ij}, λ_k appearing in the potential (2.43) do not have direct interpretations in terms of measurable quantities. As a result, it would be inefficient to scan over the whole 8-dimensional parameter space, when most of the points would correspond to scenarios which would conflict with previous experiments. To make our parameter scan more efficient, it is common practice within the field to calculate tree-level approximations to observables, like particle masses, in terms of the potential parameters m_{ij}, λ_k. Then we invert the analytical relations to write the potential in terms of tree-level observables as input parameters. These calculations are routine and appear frequently in papers on the 2HDM [70]. However, I will outline the procedure here for completeness.

To calculate observables, like the masses of various particles, we first need to identify a minimum of the potential. To do this, we find the gradient of the potential and impose that it must be zero at a specified location (v_1, v_2). This condition gives the equations (3.1) below, which can be used to solve for m_{11}^2 and m_{22}^2 in terms of the other variables.

$$\begin{aligned} m_{11}^2 v_1 - m_{12}^2 v_2 + \frac{\lambda_1 v_1^3}{2} + \frac{1}{2}(\lambda_3 + \lambda_4 + \lambda_5) v_2^2 v_1 = 0 \\ m_{22}^2 v_2 - m_{12}^2 v_1 + \frac{\lambda_2 v_2^3}{2} + \frac{1}{2}(\lambda_3 + \lambda_4 + \lambda_5) v_1^2 v_2 = 0 \end{aligned} \tag{3.1}$$

It is customary to write $(v_1, v_2) = (v\cos(\beta), v\sin(\beta))$ since measurements of the W/Z boson and top quark masses fix $v = 246.21964(6)$ GeV when measured at low energies[1] $\mu \ll v$ [71]. In addition, the angle β is physically significant as it controls the mixing strength between the two Higgs doublets. The effects of this mixing manifests in measurements of decays of the charged B meson to an antilepton and a neutrino $B^+ \to l^+ \nu_l$ [66]. This way, we can directly calculate β from measured decay rates.

Once we have ensured that (v_1, v_2) is a stationary point of the potential, the leading order particle masses are given by the Hessian of the potential at (v_1, v_2). Since our minimum is neutral (see table 2.2), the Hessian matrix is block-diagonal with 2×2 blocks. Parametrising each block in terms of Pauli matrices then gives us the eigenvalues:

$$\frac{\partial^2 V}{\partial \phi_i \partial \phi_j} = a_i \sigma_i \implies m_\pm^2 = a_0 \pm \sqrt{a_1^2 + a_2^2 + a_3^2}.$$

Here, $m_\pm$ are the two masses calculated in each 2×2 block, and I use the convention that σ_0 is the identity. Ignoring the masses fixed to zero by symmetry, this gives 4 particle masses. These include the standard model Higgs m_h, the new neutral heavy Higgs m_H, the charged Higgs $m_{H^\pm}$, and the Higgs pseudoscalar m_A. In addition to these masses, it is common to take the angle α diagonalising the neutral Higgs 2×2 matrix as another input parameter. This is because the angle $\alpha - \beta$ directly modifies the coupling between the Higgs particles and the gauge bosons and fermions. For example, the 2HDM rate for the Higgs production process $ZZ \to h$ is $\sin^2(\alpha - \beta)$ times the SM rate. To agree with the Standard Model (and experiments), we thus require $\cos(\alpha - \beta) \to 0$, which is commonly dubbed the alignment limit [66, 72].

[1] Here, μ is the renormalisation scale.

So far, we have enough information to exchange 7 of the 8 initial parameters to physical input parameters. One physical choice for the final input parameter is to keep m_{12}^2, as it can in principle be determined by h or $H \to \gamma\gamma$ decay rates [70]. However, this will make our change of variables badly behaved near $\beta = \frac{\pi}{2}$, because in this limit $\lambda_1 \sim \sec(\beta)^3 \to \infty$ diverges rapidly. Since $\beta \to \frac{\pi}{2}$ is exactly the limit the 2HDM recovers the standard model [66], it is desirable for our work that we keep the change of variables well-behaved in this limit. I therefore keep λ_1 as an input parameter instead. The parameters appearing in the potential can then be calculated as

$$\begin{aligned}
m_{12}^2 &= \cot(\beta)\left(m_h^2 \sin^2((\alpha-\beta)+\beta) + m_H^2 \cos^2((\alpha-\beta)+\beta) - \lambda_1 v^2 \cos^2(\beta)\right) \\
\lambda_2 &= \frac{\csc^2(\beta)\left(-m_{12}^2 \cot(\beta) + m_h^2 \cos^2((\alpha-\beta)+\beta) + m_H^2 \sin^2((\alpha-\beta)+\beta)\right)}{v^2} \\
\lambda_3 &= -\frac{m_{12}^2 \csc(\beta)\sec(\beta)}{v^2} + \frac{\csc(2\beta)\left(m_H^2 - m_h^2\right)\sin(2(\alpha-\beta)+2\beta)}{v^2} + \frac{2m_{H^\pm}^2}{v^2} \\
\lambda_4 &= \frac{m_{12}^2 \csc(\beta)\sec(\beta)}{v^2} + \frac{m_A^2 - 2m_{H^\pm}^2}{v^2} \\
\lambda_5 &= \frac{m_{12}^2 \csc(\beta)\sec(\beta)}{v^2} - \frac{m_A^2}{v^2} \\
m_{11}^2 &= m_{12}^2 \tan(\beta) - \frac{1}{2}v^2\left(\lambda_1 \cos^2(\beta) + (\lambda_3+\lambda_4+\lambda_5)\sin^2(\beta)\right) \\
m_{22}^2 &= m_{12}^2 \cot(\beta) - \frac{1}{2}v^2\left(\lambda_2 \sin^2(\beta) + (\lambda_3+\lambda_4+\lambda_5)\cos^2(\beta)\right)
\end{aligned} \tag{3.2}$$

Since we are only keeping one unphysical parameter λ_1 as an input, it is straightforward to convert between λ_1 and m_{12}^2 given all the other physical inputs, using the first equation in (3.2). To summarise, the equations (3.2) perform the following change of variables:

$$\begin{pmatrix} m_{11}^2 & m_{22}^2 & m_{12}^2 & \lambda_1 \\ \lambda_2 & \lambda_3 & \lambda_4 & \lambda_5 \end{pmatrix} \leftarrow \begin{pmatrix} v & \beta & \alpha-\beta & \lambda_1 \\ m_h & m_H & m_{H^\pm} & m_A \end{pmatrix}.$$

3.2 Summary of Existing Constraints

With our physical input parameters in place, we would like to know what input parameters are physically reasonable. To do this, I will briefly review the current constraints placed on the 2HDM parameter space.

3.2.1 Theoretical Constraints

First, we require that our theory is theoretically consistent. To do this, three theoretical constraints are commonly used to rule out regions in parameter space [62, 63]: First, perturbative unitarity (PU) requires that the scattering process calculated through perturbation theory be unitary, so that the scattering amplitude calculations are self-consistent. The bounded-from-below (BFB) condition simply requires that the tree-level potential be bounded from below. This ensures that the theory has a well-defined vacuum at tree-level, so that we may begin our perturbation theory. Finally, perturbativity simply requires that all dimensionless quantities are sufficiently small so that perturbation theory remains accurate. For the 2HDM these conditions are given by [66][2]

Perturbative unitarity:

$$\begin{gathered}\left|\frac{3(\lambda_1+\lambda_2)}{2}+\sqrt{\frac{9}{4}(\lambda_1-\lambda_2)^2+(2\lambda_2+\lambda_4)^2}\right|\leq 8\pi,\\ \left|\frac{\lambda_1+\lambda_2}{2}+\frac{1}{2}\sqrt{(\lambda_1-\lambda_2)^2+4\lambda_4^2}\right|\leq 8\pi,\quad \left|\frac{\lambda_1+\lambda_2}{2}+\frac{1}{2}\sqrt{(\lambda_1-\lambda_2)^2+4\lambda_5^2}\right|\leq 8\pi,\\ |\lambda_3+2\lambda_4-3\lambda_5|\leq 8\pi,\quad |\lambda_3-\lambda_5|\leq 8\pi,\quad |\lambda_3+2\lambda_4+3\lambda_5|\leq 8\pi,\\ |\lambda_3+\lambda_5|\leq 8\pi,\quad |\lambda_3+\lambda_4|\leq 8\pi,\quad |\lambda_3-\lambda_4|\leq 8\pi.\end{gathered}\tag{3.3}$$

Bounded from below:

$$\lambda_1\geq 0,\quad \lambda_2\geq 0,\quad \lambda_3\geq -\sqrt{|\lambda_1\lambda_2|},\quad -|\lambda_5|+\lambda_3+\lambda_4\geq -\sqrt{|\lambda_1\lambda_2|}.\tag{3.4}$$

Perturbativity:

$$|\lambda_i|\leq 4\pi.\tag{3.5}$$

In the literature, these constraints are often used as a first point of comparison to other proposed constraints, or as a way to quickly rule out unreasonable sets of parameters [62, 63, 73, 74]. Furthermore, as these are the only theoretical constraints which often appear in the literature, they will provide a good point of comparison

[2]The derivation of these bounds are not my work.

against our vacuum metastability constraints[3].

3.2.2 Experimental Constraints

While experimental constraints are not as directly comparable to our vacuum metastability constraints as theoretical constraints, we must still take them into account if we are to do any real phenomenology. I will briefly summarise the main constraints which will guide our parameter scans.

1. *First, I will often take all the new scalar masses*[4] $m_{H^*,A}$ *to be degenerate. In the event I break this degeneracy, I will often take either* $m_H = m_{H^\pm}$ *or* $m_{H^\pm} = m_A$*.* The degenerate mass case $m_H = m_{H^\pm} = m_A$ is often the starting point in 2HDM analyses [62, 73] since mass differences between $m_H, m_{H^\pm}$ and m_A causes the quantity
$$\Delta\rho := \frac{M_W}{M_Z \cos\theta_W} - 1$$
to differ from the standard model value of approximately 10^{-3} [73], where it is strongly suppressed due to 'custodial' symmetry [75, 76]. Here, θ_W is a standard model parameter called the Weinberg angle[5]. However, it is possible to evade this constraint with nondegenerate masses as long as $m_H = m_{H^\pm}$ or $m_{H^+} = m_A$, and the mass difference is not too large. In any case, we will also see later in 3.3.1 that large mass differences will quickly cause the theory to be nonperturbative, so that the theoretical constraint (3.5) is anyway violated.

2. *Second, I will mostly focus on regions where either* $\tan\beta > 2$ *or* $m_{H^*/A} \gtrsim 800\,GeV$ *or both.* A recent and comprehensive analysis of the experimental bounds on the 2HDM, using all known experimental data, is provided in [77]. Notably, for the type-II 2HDM, the scalar masses are forced to be $m_{H^*,A} > 1000\,\text{GeV}$ due to constraints on flavour physics[6]. However, this constraint is loosened for the type-I 2HDM, where masses $m_{H^*/A} \lesssim 600\,\text{GeV}$ are allowed as long as

[3]While one could argue that we are using the experimental fact that our universe has not decayed in 10^{10} years, it is difficult to perform a direct experiment to test the vacuum stability of our universe. As a result, vacuum metastability constraints are often regarded as theoretical constraints in the literature (see for example [74]).

[4]Here and henceforth, H^* denotes H and $H^\pm$.

[5]It is the angle which diagonalises the quadratic form in (2.36).

[6]Flavour physics concerns processes which change the total flavour quantum number (electron number, strangeness, etc). Examples include decays from one type of quark to another $b \to s\gamma$.

$\tan\beta > 3$. In any case, for both type-I and type-II models, flavour constraints force $\tan\beta > 1$, with a preference for $\tan\beta > 2 \pm 0.3$ at a 95% confidence level.

3.3 Analytical Results at Tree-Level

Now that we have reviewed the present state of experimental bounds on the 2HDM, we are ready to analyse the question of vacuum stability in the 2HDM in earnest.

Barroso *et al.* have previously shown that at tree level our desired minimum (v_1, v_2) is the global minimum if and only if [70]

$$D := m_{12}^2(m_{11}^2 - k^2 m_{22}^2)(\tan\beta - k) > 0. \tag{3.6}$$

Here, $k := (\lambda_1/\lambda_2)^{1/4}$ and $\tan\beta$ is assumed to be positive. This assumption is due to the fact that the potential is symmetric under the reflection $m_{12}^2 \to -m_{12}^2, \quad \tan\beta \to -\tan\beta$. However, this work was done back in 2013 and the experimental situation has changed considerably since the paper's publication. In particular, Barroso *et al.* scanned the parameter space where the new scalar masses $m_{H^*/A}$ are within the range $125 - 900\,\text{GeV}$. However, in light of more recent experimental data, it has become important to understand the regions of parameter space supporting higher masses $m_H \gtrsim 1\,\text{TeV}$.

I will begin by discussing the case of degenerate scalar masses. Taking the limit where $m_H = m_{H^+} = m_A \gg v, m_h$, we have that

$$\lambda_{2,3,4,5} \propto \frac{m_H^2}{v^2}\cos(\alpha - \beta) + O(1)$$

However, to keep our theory perturbative, we require at least that all couplings are not too large $\lambda_i \lesssim 4\pi$. To do this, we power count[7] with $\alpha - \beta \sim \frac{\pi}{2} + av^2/m_H^2$ so that

[7] We can think of $\epsilon := v/m_H$ as a 'small' perturbation parameter, and perform perturbation theory as usual. Here, I simply assign $\cos(\alpha - \beta) \propto \epsilon^2$ so that $\lambda_{2,3,4,5} \sim O(1)$. Here and henceforth, these sets of rules for organising the series expansions will be called 'power counting rules', which is a term adapted from effective field theory.

$\lambda_{2,3,4,5}$ does not become too large. This way, to leading order,

$$
\begin{aligned}
m_{22}^2 &= m_H^2 \cos^2(\beta) + O(1) \\
m_{11}^2 &= m_H^2 \sin^2(\beta) + O(1) \\
m_{12}^2 &= m_H^2 \sin(\beta)\cos(\beta) + O(1) \\
\frac{\lambda_1}{\lambda_2} &= \frac{\lambda_1 v^2 \tan^2(\beta)}{-2av^2[\cot(\beta)+\tan(\beta)] + m_h^2[\tan^2(\beta) - \cot^2(\beta)] + \lambda_1 v^2 \cot^2(\beta)} + O(v^2/m_H^2)
\end{aligned}
\tag{3.7}
$$

Then, substituting these approximations into our expression for D in (3.6), we get that

$$
\begin{aligned}
D &= m_{12}^2 m_{22}^2 \left(\frac{m_{11}^2}{m_{22}^2} - k^2 \right) (\tan\beta - k) \\
&= m_H^4 \sin(\beta)\cos^3(\beta)(\tan^2\beta - k^2)(\tan\beta - k) + O(m_H^2).
\end{aligned}
\tag{3.8}
$$

Now, noticing that

$$
\begin{aligned}
(\tan^2\beta - \kappa^2)(\tan\beta - \kappa) = (\tan\beta + \kappa)(\tan\beta - \kappa)^2 \geq 0, \\
\mathrm{sgn}(\sin\beta\cos\beta) = \mathrm{sgn}(\tan\beta) \geq 0.
\end{aligned}
$$

we finally see that in this approximation we always have $D \geq 0$. That is, our desired minimum is the global minimum of the tree-level potential. Upon consideration this is not too surprising: The masses of the new scalars correspond to the second derivative of the potential at the minimum. If this second derivative is large then it would be much harder for the potential to curve back down and develop a second minimum. However, our analytical proof so far has two flaws: First, I have not discussed what happens when the masses are nondegenerate. Second, it is conceivable *a priori* that the $O(m_H^2)$ contribution to D has a large numerical prefactor. These large prefactors would only be possible if $\tan\beta$ is large. Then, a large negative term of the form $-\tan(\beta)m_H^2$ may render D negative. I will discuss both these cases next, and we will see that no second minimum can develop in these cases either.

3.3.1 Nondegenerate Masses

With the same power counting as above, when the masses are allowed to be nondegenerate, the $\lambda_{3,4,5}$ couplings become

$$\begin{aligned}
\lambda_3 &= \frac{4\Delta_{H^\pm} m_H}{v^2} + O(1) \\
\lambda_4 &= \frac{2m_H(\Delta_A - 2\Delta_{H^\pm})}{v^2} + O(1) \\
\lambda_5 &= -\frac{2\Delta_A m_H}{v^2} + O(1)
\end{aligned} \tag{3.9}$$

where here $\Delta_\Box := m_H - m_\Box$. Thus, we see that the theory can only be perturbative if the mass differences are of order $\Delta_* \lesssim v^2/m_H$. For an indicative $m_H = 1\,\mathrm{TeV}$ this means $\Delta_\Box$ should stay on the order of $\lesssim 100\,\mathrm{GeV}$.

This way, even with mass nondegeneracies, the relations (3.7) are unchanged. This means our conclusion that the desired minimum is always the global minimum in the limit $m_H \gg v$ is unchanged.

3.3.2 Large $\tan\beta$ Limit

Taking the limit of large $\tan\beta$, without any other assumptions, we find that

$$\begin{aligned}
m_{11}^2 =& \frac{1}{4}\left(-\frac{2\sin(2(\alpha-\beta))\left(m_h^2 - m_H^2\right)}{\pi - 2\beta} + 3\cos(2(\alpha-\beta))\left(m_h^2 - m_H^2\right) + m_h^2 + m_H^2\right) \\
&+ O\left(\beta - \frac{\pi}{2}\right).
\end{aligned} \tag{3.10}$$

This means that to remove the singularity in our description near $\beta = \frac{\pi}{2}$, we need $\alpha - \beta = O(\beta - \frac{\pi}{2})$ or $\alpha - \beta - \frac{\pi}{2} = O(\beta - \frac{\pi}{2})$. I consider only the second situation as the first one is too far from the alignment limit $\cos(\alpha - \beta) \to 0$, so it would not be relevant to experiments. To do this, I make the substitution $\beta = \frac{\pi}{2} + \delta$ and $\alpha - \beta = \frac{\pi}{2} + a\delta$ and organise the resulting perturbation series in δ. Note that for sufficiently large $\tan\beta$, we find $m_{12}^2 = -m_H^2\delta + O(\delta^3)$. Since $\tan(\beta) > 0 \implies \delta < 0$, this gives $m_{12}^2 > 0$ always. Also, $\tan\beta - k > 0$ since $\tan\beta \gg k$. Hence,

$$m_{12}^2(m_{11}^2 - k^2 m_{22}^2)(\tan\beta - k) < 0 \implies m_{11}^2 < k^2 m_{22}^2.$$

Now since $m_{22}^2 = -m_h^2/2 + O(\delta^2)$, we can safely assume that $\mathrm{sgn}(m_{22}^2) < 0$. This way, $m_{11}^2 < 0$ is a necessary condition for the desired vacuum to be unstable.

This result is not surprising: when $\tan\beta \to \infty$ we are in a situation largely analogous to $m_{12} \to 0$, in which case the potential takes the form

$$V = m_{11}^2\phi_1^2 + m_{22}^2\phi_2^2 + \lambda_1\phi_1^4 + \lambda_2\phi_2^4 + (\lambda_3 + \lambda_4 + \lambda_5)\phi_1^2\phi_2^2.$$

In this case, a second minimum can only be generated if $m_{11}^2 < 0$. To show that there is no second minimum, the strategy is to find the critical point where $m_{11}^2 = 0$ and show that for sufficiently large masses, λ_3 is forced to be large. This would mean we cannot simultaneously keep the theory perturbative while generating a second minimum. Expanding m_{11}^2 to second order in δ we have

$$\begin{aligned} m_{11}^2 =& \frac{1}{4}\left((2a+3)\left(m_H^2 - m_h^2\right) + m_h^2 + m_H^2\right) \\ &+ \frac{1}{4}\delta^2\left(\frac{1}{6}\left((2a+3)\left(m_H^2 - m_h^2\right) + 3\lambda_1 v^2\right) - \frac{1}{6}(2a+3)^3\left(m_H^2 - m_h^2\right) - \frac{9\lambda_1 v^2}{2}\right) + O(\delta^4) \end{aligned} \tag{3.11}$$

Setting this equal to zero, we may solve for a by perturbation theory $a = a^{(0)} + a^{(1)}\delta + a^{(2)}\delta^2$ and obtain

$$a^{(0)} = \frac{2m_H^2 - m_h^2}{m_h^2 - m_H^2}, \quad a^{(1)} = 0, \quad a^{(2)} = \frac{m_h^4\left(m_H^2 - 6\lambda_1 v^2\right) + m_h^2\left(m_H^4 + 12\lambda_1 m_H^2 v^2\right) - 6\lambda_1 m_H^4 v^2}{3\left(m_h^2 - m_H^2\right)^3}.$$

Using this solution, we find that with the same power counting

$$\lambda_3 = \frac{2m_{H^\pm}^2}{v^2} - \lambda_1\delta^2 + O(\delta^4). \tag{3.12}$$

This shows that in the large $\tan\beta$ limit, at the critical transition point where the second minimum is created, λ_3 grows as $m_{H^\pm}^2/v^2$. For sufficiently large $m_{H^\pm}/v$ we will thus always be driven out of the perturbative regime. Putting in the maximal values $\lambda_3 = \lambda_1 = 4\pi$ and a fairly large $\delta = \frac{\pi}{4}$, I conclude that there can only be a second minimum if $m_{H^\pm} < 800\,\mathrm{GeV}$.

Combining this result with the previous subsections, a second minimum cannot be created when the new scalar masses $m_{H^*/A}$ are too large $\gtrsim 800\,\mathrm{GeV}$, irrespective of the value of $\tan\beta$.

3.4 Choice of Renormalisation Scale in the $\overline{MS}$ Scheme

Before we compute the absolute stability bounds in the 2HDM at one-loop level, let us first discuss an issue that generically occurs when we work in the $\overline{MS}$ scheme and allow a mass hierarchy $m_h, v \ll m_H$: The one-loop corrections frequently become nonperturbative.

This issue can be easily seen using a minimal toy model. Consider a theory of two scalar fields ϕ_1, ϕ_2 with a potential given by $V(\phi_1, \phi_2) = \frac{1}{2}M^2\phi_1^2 + \lambda_{12}\phi_1^2\phi_2^2 + \frac{1}{4}\lambda(\phi_2^2 - v^2)^2$. For the sake of the argument, we will assume the mass M is much larger than the vev v and m_{12}. Then, a typical one-loop contribution to the effective potential reads like

$$V^{(1)} = \frac{1}{64\pi^2}m(\phi)^4\left(\ln\left(\frac{m(\phi)^2}{\mu^2}\right) + \frac{3}{2}\right) + \Omega(\mu) \tag{3.13}$$

where $\Omega(\mu) = -V(\phi = 0, \mu)$ as usual and the leading $m(\phi)^2$ contribution is given by

$$m(\phi)^2 = M^2 + 2\lambda_{12}\phi_2^2.$$

For the Higgs mechanism to work we require a minimum at some nonzero point v_1, v_2. For our toy potential this minimum occurs at $\phi_1 = 0, \phi_2 = v$. Keeping only leading terms in M^2/v^2 to simplify our analysis gives

$$V^{(1)}(0, v) = \frac{1}{64\pi^2}(M^2 + 2\lambda_{12}v^2)^2\left(\ln\left(\frac{M^2 + 2\lambda_{12}v^2}{\mu^2}\right) + \frac{3}{2}\right) + \Omega + O(v^4). \tag{3.14}$$

The important thing to note here is that the one loop contribution is large and is an increasing function of v. Usually, in the literature, the renormalisation scale μ is fixed at the vev v for convenience. For $M = 10^3\,\text{GeV}$ and $v = 246\,\text{GeV}$, we would find that the logarithm is of order ~ 3. This itself is not an issue but combined with the prefactor of $(M^2 + 2\lambda_{12}v^2)^2$, we find that the relative one-loop correction as compared

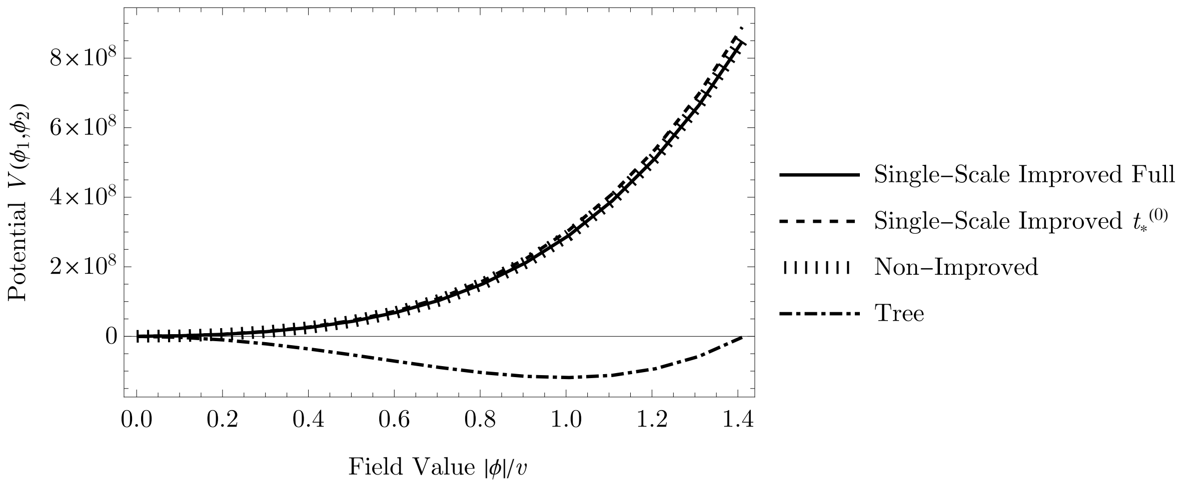

Figure 3.1: Comparison of typical 2HDM tree-level and one-loop nonimproved and improved potentials with $\mu = v$ and $m_H/v = 3$. Here, $|\phi| := \sqrt{\phi_1^2 + \phi_2^2}$ and $\phi_2/\phi_1 = \tan\beta$. The $t_*^{(0)}$ approximation is described in [42] and is provided here only for comparison. We see that the one-loop potentials all no longer have a minimum where the tree-level potential has a minimum.

to the tree-level potential $|V^{(0)}(0,v)| \approx \lambda v^4/4$ is

$$\frac{V^{(1)}(0,v)}{|V^{(0)}(0,v)|} \approx \frac{1}{4\pi^2}\frac{2\lambda_{12}M^2 + \lambda_{12}M^2\ln\left(\frac{M^2}{v^2}\right)}{\lambda v^2} \approx 2 > 1. \tag{3.15}$$

Here, I have assumed that $\lambda = \lambda_{12} = 1$ for convenience. This means that the one-loop contribution actually destroys the minimum at $\phi_2 = v$. This can be seen in the example in figure 3.1, where I have plotted the potentials for the 2HDM. Here, I also plot the improved effective potential as calculated numerically, as well as using the analytical $t_*^{(0)}$ approximation described in [42]. We see that no matter which method we use, due to large one-loop corrections, the one-loop potentials all no longer have a minimum at the desired point $\sqrt{\phi_1^2 + \phi_2^2} = v$. That is: the improved effective potential is insufficient to keep the one-loop corrections small, and our perturbation theory is completely spoiled.

This issue has been observed in previous one-loop studies of the 2HDM potential [30, 63]. A known way to address this issue is to move from the $\overline{MS}$ renormalisation scheme in favour of a more physical renormalisation scheme where we fix the one-loop vev v and one-loop scalar masses to the tree level values. To do this, we add to the potential a counterterm potential of the form

$$V_{\text{counter}} = \delta m_{11}^2 |\Phi_1|^2 + \delta m_{22}^2 |\Phi_2|^2 - (\delta m_{12}^2 \langle \Phi_1 | \Phi_2 \rangle + \text{h.c.}) + \frac{1}{2}\delta\lambda_1 |\Phi_1|^4 + \frac{1}{2}\delta\lambda_2 |\Phi_2|^4 \\ + \delta\lambda_3 |\Phi_1|^2 |\Phi_2|^2 + \delta\lambda_4 \langle \Phi_1 | \Phi_2 \rangle \langle \Phi_2 | \Phi_1 \rangle + \frac{1}{2}(\delta\lambda_5 \langle \Phi_1 | \Phi_2 \rangle^2 + \text{h.c.}) \tag{3.16}$$

and choose the $\delta m_{ij}, \delta\lambda_k$ so that

$$\nabla V_{\text{counter}} = -\nabla V^{(1)}, \quad \frac{\partial^2 V_{\text{counter}}}{\partial\phi_i \partial\phi_j} = -\frac{\partial^2 V^{(1)}}{\partial\phi_i \partial\phi_j}. \tag{3.17}$$

Basler *et al.* and Cline *et al.* showed that this is in general possible for the 2HDM with general neutral or CP-breaking vacua [30, 78]. However, this method will be inconvenient for our purposes. Indeed, barring some miracle, the counterterms would in general be dependent on the masses $m_h, m_{H^*/A}$. This would make our scheme mass-dependent, and mass-dependent schemes are inconvenient as the calculation of β and γ functions become much more difficult. This was not an issue in Basler *et al.*'s study [30] since they were focused on non-improved one-loop potentials. But since I will be looking at the RG-improved potential, it is desirable to keep our scheme mass-independent.

I thus aim to approximate (3.17) as well as possible within the $\overline{MS}$ scheme. To do this, I first approximate the one-loop potential with the RG-improved potential, which takes the form of the tree-level potential, but with parameters $\lambda(\mu(\phi))$ dependent on the field ϕ itself. At the vev, this reads

$$\begin{aligned} V(v) + V_{\text{counter}}(v) &= V^{(0)}(\lambda(\mu_0), v) + V^{(1)}(\lambda(\mu_0), v) + V_{\text{counter}}(v) \\ &= V^{(0)}(\lambda(\mu(v)), \phi(\mu(v))) + V_{\text{counter}}(v) \\ &\overset{!}{=} V^{(0)}(\lambda(\mu_0), v). \end{aligned} \tag{3.18}$$

Here, in the last line, I have made explicit the key assumption of this approach: To approximately fulfill equation (3.17), I will choose the counterterms exactly so that at the vev, we obtain the tree-level potential.

To see how this works in detail, let us look at our choice (3.18) more closely. Since both the improved effective potential and the counterterm potential take the form of the tree-level potential but with only modified parameters ($\lambda(\mu(\phi))$ and $\delta\lambda$ instead of just λ,) the parameters will factor out. So, if we choose the counterterms $\delta\lambda$ so that the total contribution to the potential reads as

$$\underbrace{\lambda(\mu_0)}_{V^{(0)}} + \underbrace{[\lambda(\mu(\phi)) - \lambda(\mu_0)]}_{V^{(1)}} + \underbrace{[\lambda(\mu_0) - \lambda(\mu(v))]}_{V_{\text{counter}}}, \tag{3.19}$$

then, at $\phi = v$, the $V^{(1)}$ and V_{counter} contributions cancel exactly. Notice however, that if we choose $\mu_0 = \mu(v)$, then the counterterm contribution becomes zero. This way we automatically absorb the counterterms into our tree-level and one-loop contributions. As a result, $V_{\text{counter}} = 0$ and we stay within the $\bar{M}S$ scheme.

Of course, this will not lead to the exact fulfillment of (3.17). For a point close to the vev $v + \eta$, we have

$$\begin{aligned} V(v+\eta) + V_{\text{counter}}(v+\eta) &= V^{(0)}(\lambda(\mu_0), v) + \eta \frac{dV^{(0)}}{d\phi} + O(\eta^2) \\ &= V^{(0)}(\lambda(\mu_0), v) + \eta \beta_\lambda \frac{d\ln\mu}{d\phi}\frac{dV^{(0)}}{d\lambda} + O(\eta^2) \end{aligned} \tag{3.20}$$

If $\frac{d\ln\mu}{d\phi}$ is sufficiently small ($\ll 4\pi$), as I will later prove, we find that the potential is modified from the tree-level value by something proportional to β_λ. Now, as long as the theory is perturbative, this β_λ function must be small (of one-loop order), so we expect that the one-loop minimum and one-loop masses are only shifted slightly.

There is still one theoretical ambiguity though. Since our initial choice μ_0 is arbitrary, $\mu(v)$ is also in some sense arbitrary. As such, we can repeat this procedure indefinitely by first setting the initial renormalisation scale at μ_{n-1} and defining $\mu_n = \mu(v)$. More precisely,

$$\mu_n : V^{(1)}(\lambda(\mu_n), v(\mu_n), \mu_n) = 0 \;\text{ where }\; \lambda(\mu_{n-1}) = \lambda, \quad v(\mu_{n-1}) = v, \tag{3.21}$$

Here, the λ, v appearing without arguments are the tree-level inputs, and the $\lambda(\mu), v(\mu)$ dependence on μ are given by the RGEs (2.13). The canonical choice of renormalisation scale which will best approximate (3.17) is thus given by $\bar{\mu} = \lim_{n\to\infty} \mu_n$. By the contraction mapping theorem, this $\bar{\mu}$ is given by $\bar{\mu} : V^{(1)}(\lambda, \phi, \bar{\mu}) = 0$. This equation has previously been investigated in a different context in [42]. The solution is given by a straightforward algebraic manipulation to be

$$\bar{\mu} = \mu_0 \exp\left(\frac{V^{(1)}(v, \mu_0)}{2\mathbb{B}(v)}\right), \quad \mathbb{B} = \frac{1}{64\pi^2}\sum_i m_i(\phi)^4. \tag{3.22}$$

Let us now examine when this solution will keep the one-loop corrections small. As usual, we will require the logarithms $\ln(m^2_{h,H^*,A}/\bar{\mu}^2)$ to be small. Since we customarily choose $\mu_0 = v$ and $\ln(m^2_{h,H^*,A}/v^2) \ll 4\pi$, this is equivalent to keeping $\ln(\bar{\mu}^2/\mu_0^2) = \frac{V^{(1)}}{\mathbb{B}}$ small.

To do this, we simply note that $V^{(1)}$ and $\mathbb{B}$ are both of order M^4. So, the only way $\frac{V^{(1)}}{2\mathbb{B}}$ can become large is if $V^{(1)}$ contains large logarithms, or if $\mathbb{B}$ is near a root.

The first case is not too big of a problem: Logarithms can only be large for all renormalisation scales μ at the vev if we have $\ln(m_H^2/m_h^2) \gtrsim 4\pi$. This is avoided as long as $m_H \ll 60\,\text{TeV}$ which we will always fulfill.

The second case is a hint of instability in our method: The condition $\mathbb{B} = 0$ defines a hypersurface in the space of parameters and fields (λ, ϕ). As such, as we scan the parameter space, we will be almost guaranteed to encounter at lease one point where $\mathbb{B} = 0$. In this case, our approximation (3.22) breaks down completely. It turns out though, by virtue of $\mathbb{B} = 0$ being a lower dimensional surface, this instability occurs in sufficient isolation that it will not impact our final conclusions. This will be discussed more precisely in section 3.5 and chapter 4.

Finally, it is time to go back and justify that the correction term in (3.20) is truly small. To do this, I will take a result from [42] which states that the expression in (3.22) is actually identical to the leading order choice of renormalisation scale which enters the RG-improved potential. That is, $\mu(\phi)$ in (3.18) is to leading order given by

$$\mu(\phi) = \bar{\mu} \exp\left(\frac{V^{(1)}(\phi, \bar{\mu})}{2\mathbb{B}(\phi)}\right).$$

Then, the $\frac{\partial \ln \mu}{\partial \phi}$ term appearing in (3.20) is given by

$$\frac{\partial \ln \mu}{\partial \phi} \sim \frac{V^{(1)'}\mathbb{B} - V^{(1)}\mathbb{B}'}{2\mathbb{B}^2}.$$

Here, primes denote differentiation with respect to ϕ. Similar to our analysis of (3.22),

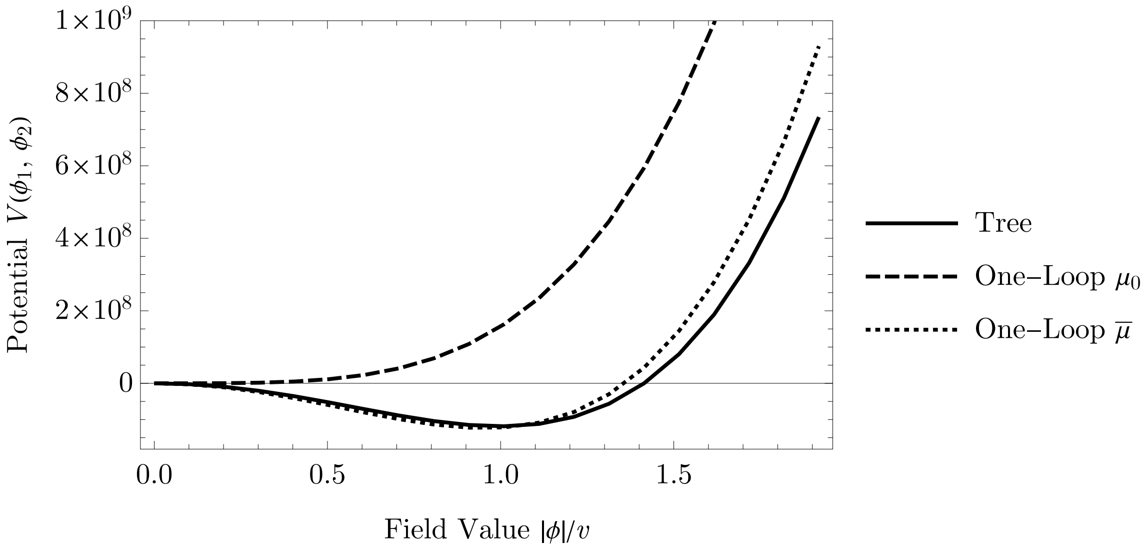

Figure 3.2: Comparison of 2HDM effective potentials at tree-level, one loop calculated at μ_0, and one-loop calculated at $\bar{\mu}$ in (3.22). Here, $|\phi| := \sqrt{\phi_1^2 + \phi_2^2}$ and $\phi_2/\phi_1 = \tan\beta$. The parameters are chosen such that $m_{H^*,A}/v = 3$ so that the vev is at $|\phi|/v = 1$ in the horizontal axis. We see that while the one-loop corrections at μ_0 destroys the minimum at $|\phi| = v$, the one-loop corrections at $\bar{\mu}$ does not shift observables like the vev and the mass (curvature of the potential at $|\phi| = v$) much. As such, our choice $\bar{\mu}$ improves the convergence of the perturbation theory.

this can only be large if $V^{(1)}$ contains large logarithms or if $\mathbb{B}$ is near a root. As such, there are no further conditions for the validity of our approximation (3.22).

Figure 3.2 shows an explicit comparison of the one-loop potential calculated conventionally with $\mu_0 = v$, and calculated with our improved approximation $\bar{\mu}$. This figure demonstrates how the one-loop corrections can be large at μ_0, but small at $\bar{\mu}$, so that the perturbation expansion $V = \sum_n V^{(n)}$ is expected to converge faster with $\bar{\mu}$.

3.5 One-Loop Results

3.5.1 Comparison of Improved and Unimproved potentials

Before we compute the one-loop absolute stability bounds, let us first discuss one more subtlety regarding the one-loop calculations. Both the nonimproved one-loop correction $V^{(1)}$ and the RG-improved one-loop correction $V^{(1)}_{\text{imp}}$ are viable candidates for the one-loop stability bounds calculations. Each of the two, *a priori*, come with their own theoretical advantages and disadvantages, and it is not clear whether we should use one over the other:

1. The RG-improved correction keeps logarithms which may appear in the one-loop corrections small. This means it is valid in a much larger domain than the non-improved potential. Indeed this is the original motivation for obtaining the RG-improved potential. At large field values $\sqrt{\phi_1^2+\phi_2^2} \gg v$ the unimproved potential is unreliable while the RG-improved potential is still reliable to one-loop order.

2. The RG-improvement effectively reorders the perturbation series to include all the dominant logarithms into the one loop correction. Therefore, we selectively mix higher-order corrections into our one-loop results. This means the RG-improved potential is not strictly consistent in the conventional perturbation theory. However, this is not an issue if the remaining terms in the RG-improved perturbation series are negligibly small.

As we will see, however, this will not matter in the end since the difference between the improved and unimproved potentials are almost always negligible in the region $\sqrt{\phi_1^2+\phi_2^2} \lesssim 10^4\,\text{GeV}$. Indeed one of the requirements for RG-improved potential is that, if $\mu(\phi) \sim \bar{\mu}$, then $V^{(1)}_{\text{imp}} = V^{(1)} + O(\text{2-loop})$. The renormalisation group technique we use has been proven to satisfy this requirement asymptotically [42].

However, these asymptotics do not guarantee that the non-improved and improved potentials agree for all field values $|\phi| < 10^4\,\text{GeV}$. I will thus verify that the difference between the RG-improved and unimproved potentials is small in the region of interest $|\phi| = \sqrt{\phi_1^2+\phi_2^2} \lesssim 10^4\,\text{GeV}$.

To do this, I sampled random input parameters and ensured that they satisfy 'perturbative unitarity' and 'bounded-from-below' constraints. This way, I obtained 13 input parameters which satisfy both PU and BFB constraints. Then, for each sampled input parameter, I sampled approximately 50 points logarithmically spaced in the radial coordinate $|\phi|$ and 6 points linearly spaced in the polar coordinate $\arctan(\phi_2/\phi_1)$. The relative corrections from one-loop calculations and RG-improvement are then calculated for each of these points. The results are summarised in figure 3.3.

In figure 3.3a, we see that the one-loop corrections are typically $\lesssim 10\%$ when $|\phi| \lesssim 10^4\,\text{GeV}$. Figure 3.3b then shows that the improvement procedure is typically

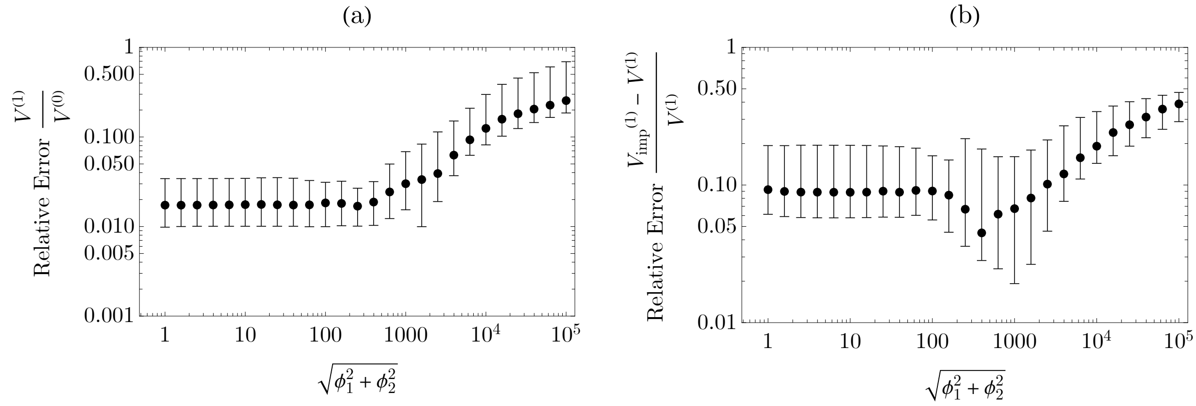

Figure 3.3: Average relative corrections from (a) the unimproved one-loop calculations and (b) the RG-improvement procedure. The error bars indicate not the standard deviations, but the interquartile ranges.

$\lesssim 20\%$ of the one-loop corrections when $|\phi| \lesssim 10^4$ GeV. Since we expect the two-loop corrections to be roughly on the size of $\lesssim 10\%$ of the one-loop corrections, we see that the difference between the one-loop improved and unimproved potentials is negligible to one-loop order, when $|\phi| \lesssim 10^4$ GeV. This means that we are free to choose either the improved or unimproved potentials in the calculation of our stability bounds.

In the next subsection, I will use the full RG-improved effective potential to calculate the absolute stability bounds. This is because I already have the RG-improved potential implemented and there is little reason to not use it at this stage. However, the results of this subsection show that this is not needed: Future work may use only the unimproved potential when calculating absolute stability bounds for nearby vacua $|\phi| \lesssim 10^4$.

3.5.2 Absolute Stability Bounds

Now that we have discussed how to unambiguously calculate the one-loop effective potential, it is time to finally obtain the stability bounds. I compute the bounds numerically as follows:

1. Start with a set of input parameters $v, m_{h,H^*,A}, \lambda_1, \tan\beta, \cos(\alpha - \beta)$, and calculate the parameters appearing in the 2HDM potential m_{ij}^2, λ_k.

2. Set the initial renormalisation scale to $\bar{\mu}$ according to (3.22).

3. Calculate the one-loop shift in the vev. To do this, I start from the tree-level vev

$\boldsymbol{v}_0 = (v\cos\beta, v\sin\beta)$ and perform Newton-Raphson iterations[8]

$$\boldsymbol{v}_{n+1} = \boldsymbol{v}_n - \left(\frac{\partial^2 V}{\partial\phi\partial\phi}\right)^{-1} \nabla V$$

until the estimated error $\|\boldsymbol{v}_{n+1} - \boldsymbol{v}_n\|$ is less than a relative tolerance of 10^{-4}. Call the result $\boldsymbol{v}$

4. Globally minimise the one-loop effective potential in the two neutral scalar fields ϕ_1 and ϕ_2. This is done using the NMinimize function in Mathematica 14.0. Call the result $\boldsymbol{w}$.

5. If the error $\|\boldsymbol{v} - \boldsymbol{w}\|$ is less than a relative tolerance of 10^{-3}, call the set of input parameters absolutely stable. Else, it is either metastable or unstable.

6. Repeat from step 1 with a new set of inputs.

As stated earlier in this chapter, the parameters v and m_h are fixed to 246 GeV and 125 GeV respectively by experiments. I then scanned through the $m_{H^*,A}, \tan\beta$ and the $\cos(\alpha-\beta), \tan\beta$ planes to gain an understanding of how absolute stability constrains the parameter space. These vacuum stability bounds are then compared against (perturbative) unitary and bounded-from-below constraints, to see what relative improvement my vacuum stability bounds give. The results are summarised in figure 3.4 and they are in line with our tree-level analysis: At masses higher than $m_{H^*,A} > 800$ GeV, I find no set of input parameters which supports a lower vacuum, while evading the PU, BFB, and perturbativity bounds[9].

The one-loop results in figure 3.4 are not too surprising. Indeed as I have loosely argued in section 3.3, when $m_{H^*,A} \gg m_h, v$, the second derivatives are large and positive. This way, the one-loop corrections are not big enough to generate a second minimum. To see the effect of modifying the λ_1 input parameter, I have also plotted the $m_{H^*,A}, \tan\beta$ parameter scans at $\lambda_1 = 0.5, 1.5$ in figure 3.5. From these plots we see that the behaviour of the absolute stability bounds is qualitatively in line with the analytical arguments around (3.12). As λ_1 increases, the critical value $m_{H^*,A}$ above which we have no second minimum also increases.

[8] The FindMinimum function in Mathematica 14.0 does not return the correct local minimum. So I wrote my own implementation.

[9] The 'PU and BFB' bound in figure 3.4 is usually stricter than just perturbativity.

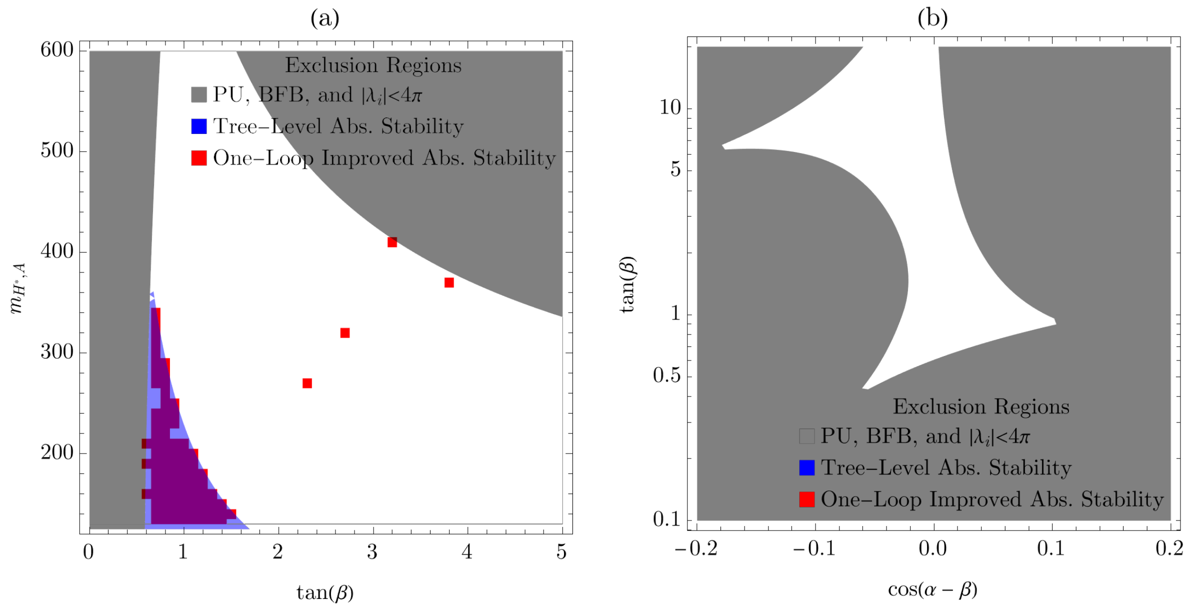

Figure 3.4: Parameter scans of 2HDM summarising the one-loop absolute stability results, as well as the tree-level stability results. Our absolute stability constraints (red, blue) are superimposed with other theoretical constraints (gray) commonly used in the literature. Namely, perturbative unitarity (PU), bounded-from-below (BFB) and perturbativity $|\lambda_i| < 4\pi$. Note that the white regions are absolutely stable and the purple region is not absolutely stable at both tree-level and one-loop. The scattered red points which do not agree with their surroundings are due to the numerical instabilities described in section 3.4. (a) Parameter scan in the $m_{H^*,A}, \tan\beta$ plane. The other parameters are fixed at $\lambda_1 = 1$, $\cos(\alpha - \beta) = 0.1$ to stay close to the alignment limit. We see that for new scalar masses of $m_{H^*,A} \gtrsim 400\,\text{GeV}$ there are no longer any unstable points. This agrees with the results of section 3.3. (b) Parameter scan in the $\cos(\alpha - \beta), \tan\beta$ plane. The other parameters are set to $\lambda_1 = 1, m_{H^*,A} = 800\,\text{GeV}$. We see that, in agreement with our analytical arguments 3.3, we find no parameters which supports a lower vacuum.

Finally, while my results do not exclude any potentially interesting regions of parameter space when $m_{H^*,A} > 1\,\text{TeV}$, they may have physical consequences on baryogenesis[10]. Namely, one of the main ingredients for baryogenesis in the early universe is a strongly first-order phase transition [14]. The 2HDM has thus been extensively studied in the context of baryogensis as the 2HDM can modify the SM electroweak phase transition to become strongly first order [30, 68].

However, to investigate cosmological phase transitions, we would need to study the 2HDM effective potential more thoroughly. This is because in the early universe, thermal corrections to the effective potential become important. These thermal corrections,

[10]The creation of baryons.

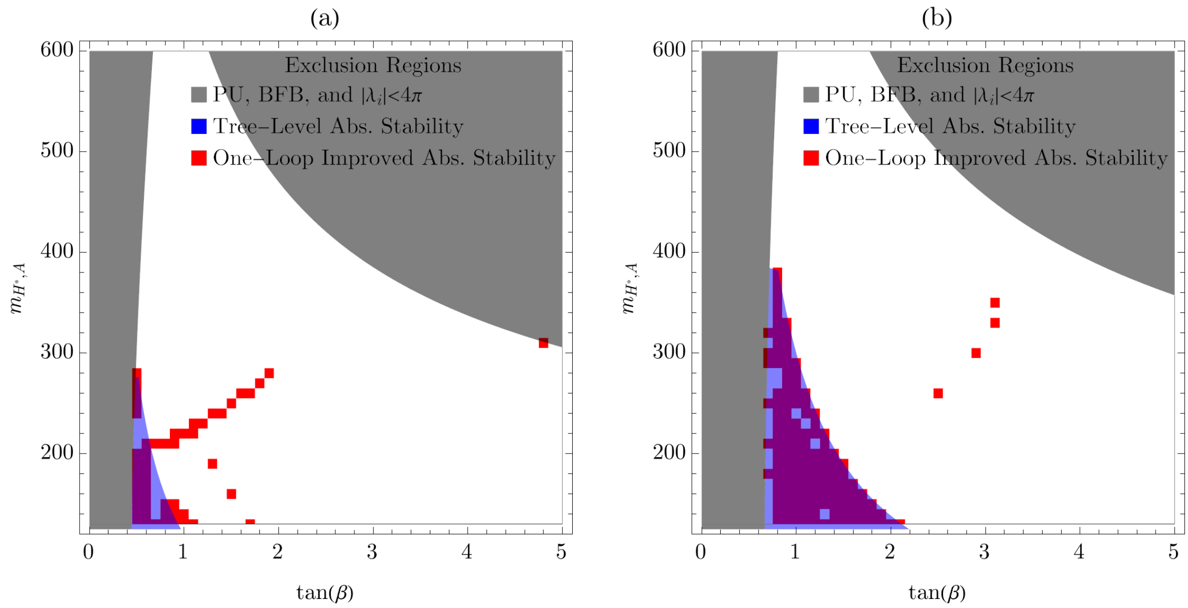

Figure 3.5: Same as figure 3.4 but with (a) $\lambda_1 = 0.5$ and (b) $\lambda_1 = 1.5$ respectively. The qualitative behaviour is in agreement with the analytical results from equation (3.12): As we increase λ_1, the critical mass $m_{H^*,A}$, above which there is no second minimum, increases. We see that the one-loop results do not differ from the tree-level results in any significant way. All disagreements seen in the above plots can be attributed to numerical instabilities.

at one-loop order, take the form [30, 79]

$$V^{(1)}_{\text{thermal}} = \frac{1}{2\pi^2}\sum_i (-1)^{2s_i} n_i T^4 \int_0^\infty dx\, x^2 \ln\left(1 + (-1)^{2s_i+1} e^{-\sqrt{x^2+\overline{m}_i^2/T^2}}\right). \tag{3.23}$$

Here, $\overline{m}_i$ are (2.21) but with thermal corrections included, n_i and s_i are identical with (2.20), and T is the temperature. So unless the one-loop thermal corrections are very large[11], $\left\|\frac{\partial^2 V^{(1)}_{\text{thermal}}}{\partial\phi\partial\phi}\right\|_2 \gtrsim m^2_{H^*,A}$, a second minimum cannot be generated outside the $\tan\beta = \phi_2/\phi_1$ direction. While this is not an issue for the standard one-step phase transitions considered in ref. [30, 80], these phase transitions are anyway excluded when $m_{H^\pm} \gtrsim 700\,\text{GeV}$ [80]. What my results in this thesis show is that multi-step phase transitions, such as those considered in [81, 82, 83], are likely disfavoured in the 2HDM with $m_{H^*,A} \gtrsim 800\,\text{GeV}$. As a result, the findings in this thesis, along with ref. [80], suggest that strongly first-order phase transitions in the 2HDM may be highly disfavoured when $m_{H^*,A} \gtrsim 800\,\text{GeV}$. However, due to time constraints, I will not investigate thermal corrections to the effective potential further in this thesis. I will thus leave it as an interesting potential direction for future work.

[11] In terms of the entry-wise (Frobenius) norm.

Chapter 4

Renormalisation-Induced Vacua and Metastability Constraints

In this chapter, I investigate the vacuum structure of the 2HDM due to the renormalisation scale dependence of the couplings $\lambda(\mu)$. These new vacua typically only appear at large field values $\gtrsim 10^5$ GeV, as opposed to the leading-order vacua found in chapter 3. All calculations and proofs presented are, unless otherwise stated through relevant citations, the result of my own work.

4.1 Bounces in the Two-Higgs-Doublet Model

As discussed in subsection 2.1.4, to compute the tunneling rate requires us to solve the bounce equation (2.28). In general, this would be a very complicated non-conservative equation with no general analytical solutions. However, in this chapter, I focus primarily on vacua induced by the RG-dependence of the couplings $\lambda(\mu)$. In ref. [42], Chataignier *et al.* showed that, just like in the single-field case, when we take the large-field limit $|\phi| = \sqrt{\phi_1^2 + \phi_2^2 + \cdots + \phi_n^2} \to \infty$, the RG-scale of the improved effective potential scales asymptotically like $\ln \mu \sim \ln |\phi| \to \infty$. I will make this claim more precise for the 2HDM in section 4.2, where I examine the validity of the RG-improvement technique for $|\phi| \gg v$. However, I will first make use of this fact to simplify the multi-field bounce equation.

Since the β functions are in general small $O\left(\frac{\lambda^2}{(4\pi)^2}\right)$, $\lambda(\mu)$ can only differ significantly from $\lambda(\mu_0)$ if $|\ln(\mu/\mu_0)| \gg 1$. Taking $\mu \sim |\phi|$ and $\mu_0 \sim v$ as usual, we see that unless we are in the large-field limit $|\phi| \gg v$, the RG-improved potential will not substantially differ from the leading-order potential. Indeed, we have also seen this numerically in figure 3.3, where the improved potential does not differ by more than $\sim 2\%$ from the one-loop or tree-level potentials unless $|\phi| \gtrsim 10^5$ GeV.

Taking advantage of these large fields, we may neglect any non-leading sub-quartic terms in the potential and write

$$V_{\text{eff}} \approx V_{\text{eff}}^{\{4\}} := \frac{1}{2}\lambda_1(\mu)|\Phi_1|^4 + \frac{1}{2}\lambda_2(\mu)|\Phi_2|^4 + \lambda_3(\mu)|\Phi_1|^2|\Phi_2|^2 + \lambda_4(\mu)\langle\Phi_1|\Phi_2\rangle\langle\Phi_2|\Phi_1\rangle \\ + \frac{1}{2}(\lambda_5(\mu)\langle\Phi_1|\Phi_2\rangle^2 + \text{h.c.}). \tag{4.1}$$

Here, the superscript {4} makes explicit that this is the quartic part of the 2HDM potential. Notably, $V_{\text{eff}}^{\{4\}}$ is homogeneous with degree 4: $V_{\text{eff}}^{\{4\}}(\lambda\Phi_1, \lambda\Phi_2) = \lambda^4 V_{\text{eff}}^{\{4\}}(\Phi_1, \Phi_2)$. Just as in (2.44) and (2.35), we may write the two doublets in terms of the real fields ϕ_*

$$\Phi_1(\boldsymbol{x}) = \begin{pmatrix} \phi_\alpha(\boldsymbol{x}) \\ \phi_1(\boldsymbol{x}) + i\phi_i(\boldsymbol{x}) \end{pmatrix}, \quad \Phi_2(\boldsymbol{x}) = \begin{pmatrix} 0 \\ \phi_2(\boldsymbol{x}) \end{pmatrix}. \tag{4.2}$$

Then, the Lorentz-symmetric bounce equation (2.28) reads as

$$\frac{\partial^2 \boldsymbol{\phi}}{\partial \rho^2} + \frac{3}{\rho}\frac{\partial \boldsymbol{\phi}}{\partial \rho} = \frac{\partial V_{\text{eff}}^{\{4\}}(\boldsymbol{\phi})}{\partial \boldsymbol{\phi}} \tag{4.3}$$

with $\boldsymbol{\phi} = (\phi_1, \phi_2, \phi_\alpha, \phi_i)$ and $\rho^2 = x^\mu x_\mu$. Inspired by Fubini's success in solving the single-field case [59, 60], I similarly make the change of variables $\boldsymbol{\psi} = \boldsymbol{\phi}/\rho$ and $t = \ln \rho$. This transforms our bounce equation into the auxiliary classical equation of motion[1]

$$\frac{\partial^2 \boldsymbol{\psi}}{\partial t^2} = \boldsymbol{\psi} + \frac{\partial V_{\text{eff}}^{\{4\}}(\boldsymbol{\psi})}{\partial \boldsymbol{\psi}}. \tag{4.4}$$

We may interpret this equation as the motion of a single particle with coordinates $\boldsymbol{\psi}$ subject to the following auxiliary Hamiltonian:

$$\mathcal{H} = \frac{1}{2}\boldsymbol{\pi}^2 - \frac{1}{2}\boldsymbol{\psi}^2 - V_{\text{eff}}^{\{4\}}(\boldsymbol{\psi}) \tag{4.5}$$

where $\boldsymbol{\pi}$ is interpreted as the canonical conjugate momentum of $\boldsymbol{\psi}$. Therefore, I have reduced the calculation of the leading-order contribution to the QFT tunneling rate with potential $V_{\text{eff}}^{\{4\}}(\boldsymbol{\phi})$, down to the trajectory of a classical particle subject to a modified, flipped potential $-\frac{1}{2}\boldsymbol{\psi}^2 - V_{\text{eff}}^{\{4\}}(\boldsymbol{\psi})$. In the single-field case, this is the end of the story: A Hamiltonian system in one spatial variable always admits an exact

[1] It should be noted that this procedure only works because $V_{\text{eff}}^{\{4\}}$ is homogeneous with degree 4.

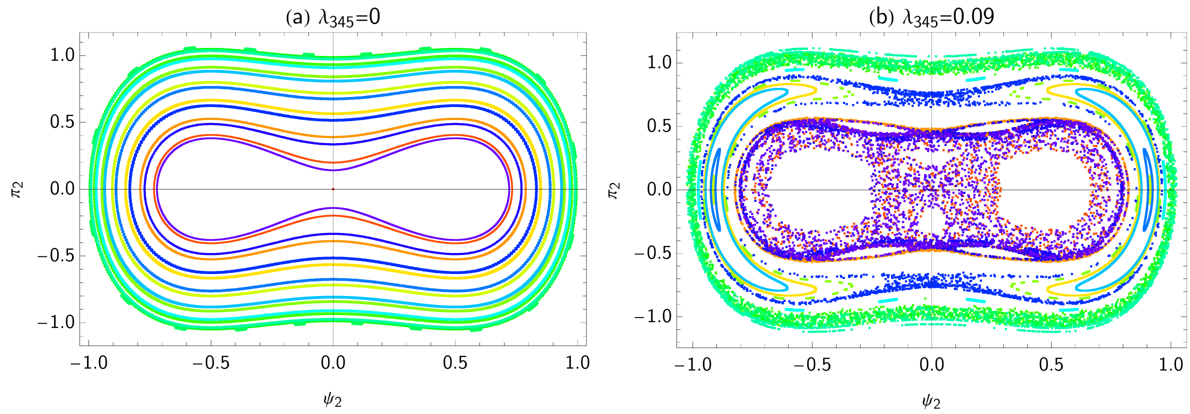

Figure 4.1: Poincare section of the auxiliary Hamiltonian system (4.5) at $\pi_1 = 0, \mathcal{H} = 1$ with $\lambda_1 = \lambda_2 = -1$. (a) The Poincare section at the integrable point $\lambda_{345} = 0$. The trajectories of the particle in phase space is constrained to a 2D torus, which intersects with the 2D poincare section in the 3D isoenergy surface to produce regular 1D curves. (b) The Poincare section at a near-integrable point $\lambda_{345} = 0.09$. Most of the trajectories are no longer constrained to regular curves in the Poincare section, indicating that there is no second conserved quantity. The mixing of the purple and orange trajectories suggests the onset of chaos.

analytical solution. In the case of $V_{\text{eff}}^{\{4\}} = \lambda\phi^4$, the solution satisfying the bounce boundary conditions below equation (2.28) is given in equation (2.39).

However, the multi-field case is not as easy. Indeed, our difficulty already appears in the 2-field case, with[2] $\psi_\alpha = \psi_i = 0$. In which case, the potential takes the form

$$V_{\text{eff}}^{\{4\}}(\boldsymbol{\psi}) = \lambda_1\psi_1^4 + \lambda_2\psi_2^4 + \lambda_{345}\psi_1^2\psi_2^2, \quad \lambda_{345} := \lambda_3 + \lambda_4 + \lambda_5. \tag{4.6}$$

When $\lambda_{345} = 0$ the potential separates into two independently solvable components, and the system is again exactly solvable. However, as we move away from this point, we see from figure 4.1b that the trajectories are no longer constrained to 2-dimensional surfaces. This means that there is no second conserved quantity, and so, we are forced to abandon a general analytical solution to the system (4.5).

But, we are lucky: the Hamiltonian system (4.5) is sufficiently nice so that exact radial solutions survive. To see why, note that the potential is a sum of a spherically symmetric component $-\frac{1}{2}\boldsymbol{\psi}^2$ and a homogeneous component $-V_{\text{eff}}^{\{4\}}$. Writing the

[2]Note that this choice automatically satisfies 2 of the 4 equations in (4.4).

fields in spherical coordinates $(\|\boldsymbol{\psi}\|, \boldsymbol{\theta})$, if for some set of angles $\boldsymbol{\theta}_*$ we have that

$$\left.\frac{dV_{\text{eff}}^{\{4\}}}{d\boldsymbol{\theta}}\right|_{\boldsymbol{\theta}_*} = 0 \tag{4.7}$$

then by homogeneity, this holds for all radii $\|\boldsymbol{\psi}\| \in \mathbb{R}$. By the classical equation of motion $\ddot{\boldsymbol{\theta}} \propto \frac{dV_{\text{eff}}^{\{4\}}}{d\boldsymbol{\theta}}$, this means the homogeneous component $-V_{\text{eff}}^{\{4\}}$ admits radial solutions: $\boldsymbol{\psi}(t) \propto \boldsymbol{\psi}(t')$ for all $t, t' \in \mathbb{R}$. This radial solution then survives in the modified potential $-\frac{1}{2}\boldsymbol{\psi}^2 - V_{\text{eff}}^{\{4\}}$ since the spherically symmetric component is constant in $\boldsymbol{\theta}$.

Indeed, if we denote the critical set of angular variables $\boldsymbol{\theta}_*$, then we can define an effective quartic parameter

$$\lambda_{\text{eff}} := V_{\text{eff}}^{\{4\}}(\|\boldsymbol{\psi}\| = 1, \boldsymbol{\theta}_*) \implies V_{\text{eff}}^{\{4\}}(\psi, \boldsymbol{\theta}_*) = \lambda_{\text{eff}}\psi^4. \tag{4.8}$$

Here, I have defined $\psi = \|\boldsymbol{\psi}\|$ for clarity. Since the trajectory is now constrained to a radial line, we can solve for the motion of $\boldsymbol{\psi}$ the same way we would in the single field case (2.39). This gives,

$$\phi(\rho) = \frac{\psi(\ln\rho)}{\rho} = \sqrt{\frac{2}{|\lambda_{\text{eff}}|}}\frac{2\rho_0}{\rho^2 + \rho_0^2} \implies B = \frac{8\pi^2}{3|\lambda_{\text{eff}}|}. \tag{4.9}$$

This allows us to directly calculate the leading-order tunneling rate using equation (2.32). However, before we continue, I would like to make a couple of remarks:

1. A bounce can only exist if there is a valid turning point for the particle $\boldsymbol{\psi}_{\text{turn}}$: $-\frac{1}{2}\boldsymbol{\psi}_{\text{turn}}^2 - V_{\text{eff}}^{\{4\}}(\boldsymbol{\psi}_{\text{turn}}) = 0$. Furthermore, the condition (4.7) ensures that the radial bounces traverse the steepest radial directions. So, it is sufficient to show that $-\frac{1}{2}\boldsymbol{\psi}^2 - V_{\text{eff}}^{\{4\}}(\boldsymbol{\psi}) = 0$ at some point in field configuration space. Indeed due to the homogeneity of $V_{\text{eff}}^{\{4\}}(\boldsymbol{\psi})$, this is exactly equivalent to the condition that $V_{\text{eff}}^{\{4\}}(\boldsymbol{\psi})$ is not bounded-from-below (BFB). Since this is exactly the same condition for the improved effective potential to develop a new lower minimum (see figure 2.1 or [42]), this suggests that the radial bounces I have derived are the physically significant solutions.

2. Of course, there are other solutions to the equations of motion given by (4.5).

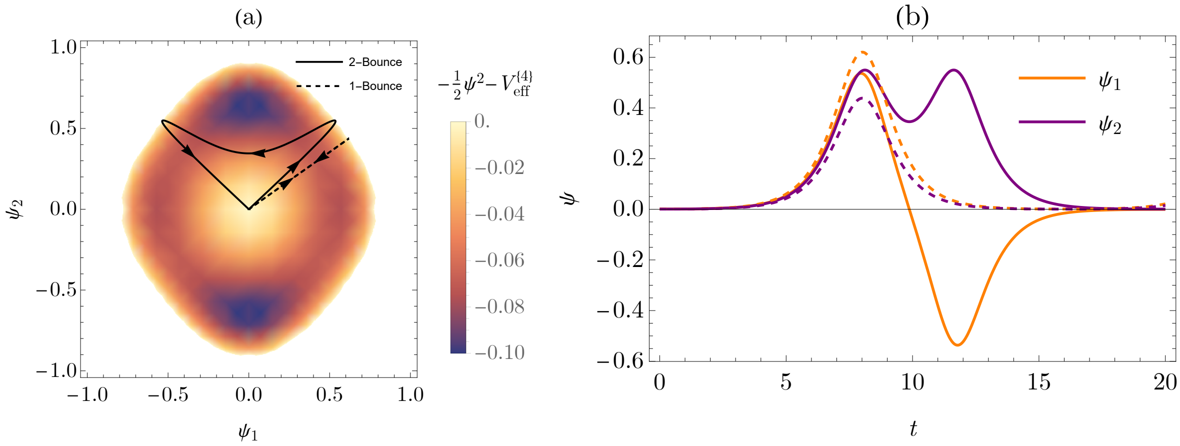

Figure 4.2: Comparison of minimal radial bounce derived in the main text (dashed) with a nonminimal 2-bounce solution (continuous). The parameters of the potential are chosen as $\lambda_1 = -0.8, \lambda_2 = -0.6, \lambda_{345} = -2$. (a) The bounce solutions visualised in field configuration space. The background density plot shows the potential of the auxiliary classical system (4.5). We see that the (continuous) 2-bounce solution visits two different vacua before returning to $\boldsymbol{\psi} = 0$ as required by the boundary condition. The radial 1-bounce solution is also shown in dashed lines for comparison. (b) The 2-bounce (continuous) and 1-bounce (dashed) solutions plotted against time. This shows that we need more time to complete the 2-bounce as compared to the 1-bounce.

> Indeed, as hinted in the previous remark, there are even other solutions which satisfy the bounce boundary conditions (below equation (2.28)). However, I argue that these bounces contribute negligibly to the tunneling rate. Indeed, we may visualise these extended bounce solutions in figure 4.2. Here, we see that the new 2-bounce requires the particle to move over a $\sim 50\%$ longer distance, and over a $\sim 50\%$ longer period of time. Hence, the 2-bounce will contribute with a much larger bounce action as compared to the radial bounce $B^{(\text{2-bounce})} \gg B^{(\text{1-bounce})}$. Since the tunneling rate contribution from each bounce is $\propto \exp(-B)$, the 2-bounce contribution to the tunneling rate will thus be exponentially suppressed as compared to the radial 1-bounce contribution.

Having argued that the only physically significant solutions are the radial bounces, we can specialise to the specific case of the 2HDM. The detailed derivation of the λ_{eff} is long, tedious, and not very insightful, so I will omit it here. In any case the general procedure has been outlined in equations (4.7) and (4.8). Defining the field space angles $\boldsymbol{\theta} = (\eta, \theta, \xi)$ as

$$\psi_2 = \psi \sin(\eta), \quad \psi_a = \psi \cos(\eta)\cos(\xi),$$
$$\psi_1 = \psi \cos(\eta)\cos(\theta)\sin(\xi), \text{ and } \psi_i = \psi \cos(\eta)\sin(\theta)\sin(\xi). \tag{4.10}$$

I summarise the radial bounces appearing in the 2HDM in table 4.1. Each solution appearing in the λ_{eff} column of table 4.1 can be used to derive a BFB condition. Specifically, the potential is BFB if and only if $\lambda_{\text{eff}} > 0$. However, it is generally more efficient to obtain the BFB conditions using linear algebra shortcuts. One way to do this is by writing $V_{\text{eff}}^{\{4\}}$ as a quadratic form, and requiring the quadratic form be co-positive, as is done in [84]. This is especially efficient in more complicated theories like the 2HDM+s/a [23]. However, these shortcuts usually obfuscate the calculation of λ_{eff}, so they aren't as useful for our purposes[3].

BFB Condition	Angles	λ_{eff}
$\lambda_1 > 0$	$\eta = 0$	$\frac{\lambda_1}{2}$
$\lambda_2 > 0$	$\eta = \frac{\pi}{2}$	$\frac{\lambda_2}{2}$
$\lambda_3 > -\sqrt{\lambda_1\lambda_2}$	$\xi = 0, \quad \eta = \arctan\left(\sqrt{\frac{\lambda_2-\lambda_3}{\lambda_1-\lambda_3}}\right)$	$\frac{\lambda_1\lambda_2-\lambda_3^2}{2(\lambda_1+\lambda_2-2\lambda_3)}$
$\lambda_3+\lambda_4+\lambda_5 > -\sqrt{\lambda_1\lambda_2}$	$\theta = 0, \xi = \frac{\pi}{2}$ $\eta = \arctan\left(\sqrt{\frac{\lambda_2-\lambda_3-\lambda_4-\lambda_5}{\lambda_1-\lambda_3-\lambda_4-\lambda_5}}\right)$	$\frac{\lambda_1\lambda_2-(\lambda_3+\lambda_4+\lambda_5)^2}{2(\lambda_1+\lambda_2-2(\lambda_3+\lambda_4+\lambda_5))}$
$\lambda_3+\lambda_4-\lambda_5 > -\sqrt{\lambda_1\lambda_2}$	$\theta = \frac{\pi}{2}, \xi = \frac{\pi}{2}$ $\eta = \arctan\left(\sqrt{\frac{\lambda_2-\lambda_3-\lambda_4+\lambda_5}{\lambda_1-\lambda_3-\lambda_4+\lambda_5}}\right)$	$\frac{\lambda_1\lambda_2-(\lambda_3+\lambda_4-\lambda_5)^2}{2(\lambda_1+\lambda_2-2(\lambda_3+\lambda_4-\lambda_5))}$

Table 4.1: Summary of the different radial bounce solutions present in the 2HDM. The angles in the second column satisfy equation (4.7). Each solution corresponds to the violation of one of the BFB conditions given in (3.4). This violated BFB condition is shown in the first column. The second column shows the direction in field configuration space at which the bounce solution traverses. The angles are defined in (4.1). The final column shows the analytical form of λ_{eff} which directly appears in our bounce solution (4.9).

[3]It is possible to derive λ_{eff} using linear algebra methods but it is more complicated than performing the procedure (4.8) for the 2HDM($+s/a$) models. However, for future reference, I expect that linear algebra methods are more efficient in models more complicated than the 2HDM$+s/a$, especially for numerical calculations.

4.2 Validity of the Single-Scale Improvement

Now that we have identified the relevant directions in field space for our tunneling rate calculations, it is time to go back and verify that all our approximations are valid. The single-scale improvement technique as introduced in 2.1.3 is valid as long as all the field-dependent masses $m_i^2(\boldsymbol{\phi})$ are of similar orders of magnitude. However, as we will see, while this is sufficient, it is not always necessary.

In the approximation $V \approx V^{\{4\}}$, comparing the field-dependent masses is rather simple. All the field dependent masses are eigenvalues of the Hessian, and since $V^{\{4\}}$ is homogeneous with degree 4, we find that the Hessian and hence the eigenvalues are also homogeneous with degree 2. As a result, the field dependent masses m_i^2 become only functions of the parameters λ_i and the angles $\boldsymbol{\theta}$. Importantly, since the potential $V^{\{4\}}$ does not contain any inverse powers of λ_i or $\sin\boldsymbol{\theta}$ or $\cos\boldsymbol{\theta}$, the Hessian and the eigenvalues must also not contain any inverse powers. This means, as long as the theory is perturbative $\lambda_i \lesssim O(1)$, the field dependent masses are always of order $m_i^2 \lesssim O(\|\boldsymbol{\phi}\|^2)$. For example, looking at the direction $\eta = \pi/2$, corresponding to the second row in table 4.1, the field dependent masses take the form

$$m^2(\boldsymbol{\phi}) = \left(\frac{\lambda_3}{2}, \frac{3\lambda_2}{2}, \frac{\lambda_3+\lambda_4+\lambda_5}{2}, \frac{\lambda_2}{2}, \frac{\lambda_3+\lambda_4-\lambda_5}{2}, \frac{\lambda_2}{2}, \frac{\lambda_3}{2}, \frac{\lambda_2}{2}\right) \times \|\boldsymbol{\phi}\|^2. \tag{4.11}$$

If we take $\mu^2 = \frac{\lambda_2}{2}\|\boldsymbol{\phi}\|^2$, then as long as $\lambda_2 \sim \lambda_3 \sim \lambda_4 \sim \lambda_5$, we have $\ln\left(m^2(\boldsymbol{\phi})/\mu^2\right) \lesssim 1$ and the single-scale improvement method works.

But what happens if for example $\lambda_3 \ll \lambda_2$? At first glance, one might think that then $|\ln\left(m_1^2(\boldsymbol{\phi})/\mu^2\right)| = |\ln(\lambda_3/\lambda_2)| \gg 1$ and the perturbation theory is spoiled[4]. But this is not actually the case. Let us denote the component parallel to the radial bounce $\phi_\parallel$ and the direction of the $\frac{\lambda_3}{2}\phi_\parallel^2$ eigenvector $\phi_\perp$. Then the potential in this direction reads as

$$V^{\{4\}} = \frac{1}{8}\lambda_2\phi_\parallel^4 + \frac{1}{4}\lambda_3\phi_\parallel^2\phi_\perp^2 + \dots.$$

When $\lambda_3 \ll \lambda_2 \lesssim 1$, we approach the limit where the $\phi_\perp$ field decouples from the $\phi_\parallel$ field, so we expect that the contributions from $\phi_\perp$ will be small. More concretely, perturbation theory yields an asymptotic series in the perturbation parameter λ_3. So

[4]Remember that the perturbation theory is spoiled when we have large logarithms.

the difference between the n^{th}-order effective potential and the effective potential at all orders of λ_3 scales as $o(\lambda_3^n)$. So the perturbation theory is not spoiled after all.

Similarly, for $\lambda_2 \ll \lambda_3 \lesssim 1$ we are not in much trouble. This is because for metastability constraints we are typically interested in $|\lambda_2| \gtrsim 0.01$. So, $|\ln(\lambda_3/\lambda_2)| \lesssim 5 < 4\pi$.

The above arguments generalise to all the rows appearing in table 4.1. As such, we conclude that the single-scale-improved potential is suitable at the large-field limit.

4.3 Landau Pole Constraints

Frequently, in quantum field theory, the RGEs (2.11)-(2.13) are not very well-behaved. As nonlinear systems of differential equations, almost all choices of initial conditions frequently lead to unphysical poles in the solutions. Usually, this is not an issue. For example, in quantum electrodynamics, the Landau pole occurs at an energy scale of $\gg 10^{200}$ GeV [36]. In the standard model, I calculated the Landau pole to occur at[5] $\sim 10^{40}$ GeV. In both of these cases the Landau pole occurs well beyond the Planck scale $\Lambda_{\text{pl}} \sim 10^{18}$ to 10^{19} GeV where we expect standard quantum field theory to break down, to make way for quantum gravity. As a result, we expect that the SM Landau pole would have no implication on theory or experiment whatsoever.

However, this is not the case when the Landau pole occurs at lower energies. The calculation of metastability constraints requires us to look at the 2HDM+s/a model at higher energies. So we must take into account the existence of Landau poles to ensure that our prediction is theoretically consistent. Indeed a Landau pole at a scale below the Planck scale Λ_{pl} would mean that our QFT must break down *before* the Landau pole[6].This could be due to the existence of new fields which become important at higher energies, or due to nonperturbative phenomena like colour confinement in QCD [86]. In both cases, we require that physics beyond the Landau pole be described by a new theory, beyond the model we are studying. In the former case, however, such fields must appear at energies much lower Λ_{new} than the Landau pole Λ_{L}. This is because new fields can only modify existing parameters at one-loop order through the

[5]using 2021 recommended values for measured observables [71] and 2-loop beta functions as calculated using the Mathematica package SARAH [85]

[6]This is because perturbative QFT can only make meaningful predictions for perturbative couplings $\lambda_i < 4\pi$.

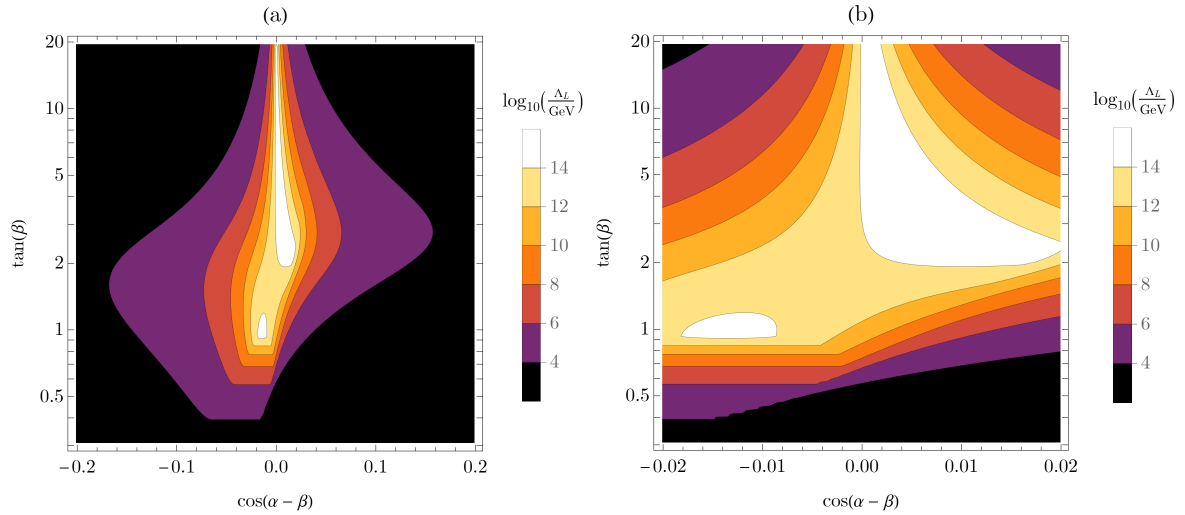

Figure 4.3: The renormalisation scale Λ_L at which the 2HDM encounters a Landau pole, with $\lambda_1 = 0.6, m_{H^*/A} = 1000\,\text{GeV}$. Figure (b) shows the same data as figure (a) but with $10\times$ magnification in the $\cos(\alpha-\beta)$ axis. We see that the requirement that the Landau poles are sufficiently high energy constrains the 2HDM to values of $|\cos(\alpha-\beta)| \lesssim 0.05$.

β function. Roughly speaking,

$$\lambda^{\text{new}}(\Lambda) - \lambda^{\text{2HDM}}(\Lambda) = \int_{\ln\Lambda_{\text{new}}}^{\ln\Lambda} \delta\beta(\ln\mu)\, d\ln\mu \tag{4.12}$$

where $\delta\beta$ is the difference in the beta function of the 2HDM and the new theory.

So, new fields must appear several orders of magnitude in energy before the Landau pole, to have a nonnegligible effect. After all, if $\lambda^{\text{2HDM}}(\Lambda)$ is large, we need the RHS of (4.12) to be large for $\lambda^{\text{new}}(\Lambda)$ to be perturbative.

With all this taken into account, I will by default exclude parameter points for which $\Lambda_L < 10^{10}\,\text{GeV}$. This way, if new particles are detected in future colliders at $\sim 10^4\,\text{GeV}$, they will have ample room to remove the Landau pole at[7] $\gtrsim 10^{10}\,\text{GeV}$.

I plot the 2HDM Landau poles in figure 4.3. Here, we see that the condition $\Lambda_L > 10^{10}\,\text{GeV}$ typically constrains $|\cos(\alpha-\beta)| \lesssim 0.02$ when $\lambda_1 \sim 0.6$ and $m_H \sim 1000\,\text{GeV}$. This is much stricter than the PU and BFB constraints (see for example fig 3.4), which typically allow values up to $|\cos(\alpha-\beta)| \sim 0.2$. As such, we conclude that the Landau pole constraint $\Lambda_\text{L} > 10^{10}\,\text{GeV}$ excludes a large region of unphysical parameters.

[7] In any case, a Landau pole at energies too small $\sim 10^6\,\text{GeV}$ would indicate that the β functions are large, so the theory would be close to being nonperturbative. In such a case our one-loop approximations would not be very precise anyway.

4.4 Stability Constraints Results

We are almost ready to calculate the constraints false vacuum decay impose on the 2HDM. However, there is one more subtlety to address.

With the choice $\bar{\mu}$ given in equation 3.22, the one-loop minimum, and the Hessian of the one-loop potential, do not coincide with their tree-level values. Of course, this is unavoidable when working within a mass-independent renormalisation scheme like $\overline{MS}$, so we must deal with the consequences.

The typical order of the one-loop corrections to the vev and masses are 10%. In addition, the vev typically gets negative one-loop corrections while the mass typically gets positive one-loop corrections. It turns out that both of these corrections work to destabilise the desired vacuum, and unfortunately this is sufficient to modify our (meta)stability conclusions for a significant region of parameter space. An example is shown in figure 4.4 where I plot the regions excluded by absolute stability and metastability for the tree-level m_h, v set to their experimental (all-orders) value, and for m_h, v shifted by 10%. We see that in figure 4.4a, only a small fraction of parameter space in the bottom left is excluded. To contrast, figure 4.4b shows that most of the parameter space is excluded by absolute and metastability constraints. This shows that it is imperative we take the one-loop Higgs mass m_h and vev v as inputs, rather than their tree-level values. For the 2HDM, I do this as follows

1. Calculate the one-loop potential with tree-level inputs $m_h^{(\text{tree})} = m_h^{(\text{exp})}, v^{(\text{tree})} = v^{(\text{exp})}$. Here, the superscript (exp) denotes the physical, experimentally-obtained value for m_h. The superscript (tree) denotes the tree-level approximation.

2. Calculate the one-loop mass and vev of the one-loop potential. This is done using the Newton-Raphson method as described in section 3.5.2, and using the default Eigenvalue function in Mathematica 14. Denote them $m_h^{(\text{one-loop})}$ and $v^{(\text{one-loop})}$.

3. Obtain new estimates for the tree-level quantities $m_h^{(\text{new,tree})}, v^{(\text{new,tree})}$ using an iteration of Newton's method:

$$\begin{pmatrix} m_h^{(\text{new,tree})} - m_h^{(\text{exp})} \\ v^{(\text{new,tree})} - v^{(\text{exp})} \end{pmatrix} = \frac{\partial(m_h^{(\text{tree})}, v^{(\text{tree})})}{\partial(m_h^{(\text{one-loop})}, v^{(\text{one-loop})})} \begin{pmatrix} m_h^{(\text{one-loop})} - m_h^{(\text{exp})} \\ v^{(\text{one-loop})} - v^{(\text{exp})} \end{pmatrix} \tag{4.13}$$

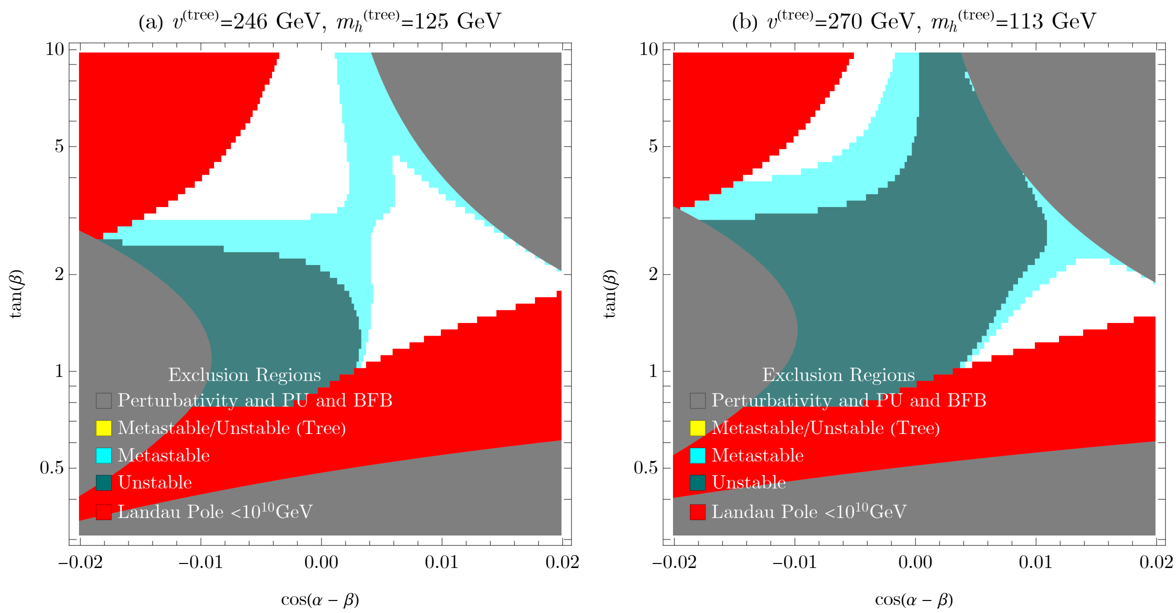

Figure 4.4: Comparison of stability bounds computed with (a) tree-level inputs set to experimental values, and (b) tree-level inputs set to be shifted by 10% of the experimental values. We see that the metastability bounds are very sensitive to these 10% changes of tree-level inputs so one-loop effects become important. Here, and in future plots, light cyan denotes non absolutely-stable but metastable vacua. Dark cyan on the other hand denotes unstable vacua.

Here, the Jacobian matrix $\frac{\partial(m_h^{(\text{tree})}, v^{(\text{tree})})}{\partial(m_h^{(\text{one-loop})}, v^{(\text{one-loop})})}$ can be obtained by computing the one-loop masses and vevs at different tree-level inputs, and finding the plane of best fit. Typically, I find that

$$\frac{\partial(m_h^{(\text{tree})}, v^{(\text{tree})})}{\partial(m_h^{(\text{one-loop})}, v^{(\text{one-loop})})} = \begin{pmatrix} 1.29 & -0.226 \\ -0.551 & 1.49 \end{pmatrix} \pm O(10\%). \tag{4.14}$$

Here, $O(10\%)$ is an abuse of notation to mean that each entry varies by approximately 10% when we vary the 2HDM parameters.

4. Compute the one-loop masses with the new inputs, and obtain the L^2 norm of relative error ϵ, as defined below.

$$\epsilon := \sqrt{\left(\frac{m_h^{(\text{new,one-loop})} - m_h^{(\text{exp})}}{m_h^{(\text{exp})}}\right)^2 + \left(\frac{v^{(\text{new,one-loop})} - v^{(\text{exp})}}{v^{(\text{exp})}}\right)^2}. \tag{4.15}$$

I use this to verify that the metastability bounds are correct to one-loop order.

With the one-loop SM-like Higgs mass and vev set to their experimentally observed

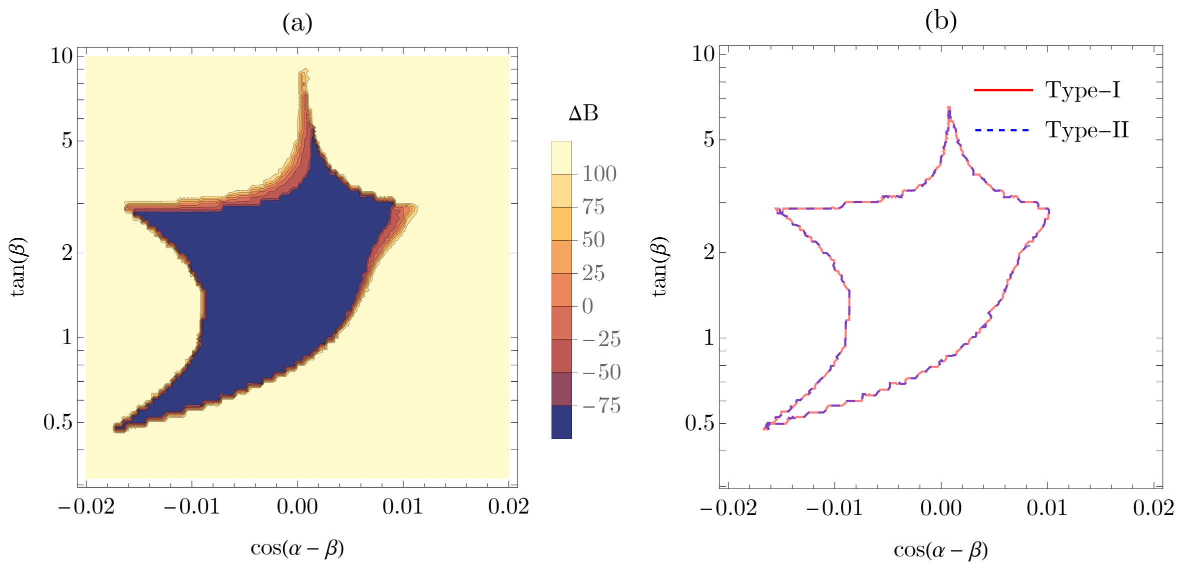

Figure 4.5: Uncertainty estimates for the region excluded by non-metastability $\Gamma T_X > 1$. (a) Contour plot of the smallest ΔB for which the parameter point is unstable. The light yellow region requires $\Delta B > 100$, and the dark blue region is unstable for $\Delta B < -100$. We see that for one-loop corrections of order ~ 40, the metastability results are largely unchanged. (b) Boundary of the region excluded by requiring metastability, as calculated in the Type-I and Type-II 2HDMs. We see that the excluded regions are identical in the two types. The analogous boundaries for Type-X and Type-Y are also identical to the above plot, but I omit them here for clarity of presentation.

value, we can now obtain the promised metastability bounds for the 2HDM. In this thesis, I chose to compute the tunneling times using the leading order expressions (2.32) and (4.9) for two main reasons. First, it has previously been observed in the Standard Model that the one-loop determinant factor is generally small enough to not be important [40, 50]. Second, the calculation of these functional determinants are lengthy and will require more time than I have in this Honours project. As a result, their calculation will be relegated to future work. In any case, in figure 4.5a, I estimate the impact of the one-loop functional determinants on my conclusions using equation (2.42). We see that the region excluded by metastability is insensitive to $\Delta B \sim \pm 10^{-1} B = \pm 40$, so we expect that one-loop corrections play a small role.

Similar to the SM [50], the leading order expressions (2.32) and (4.9) reduce the condition of metastability to checking that for all μ,

$$\lambda_{\text{eff}}(\mu) > \frac{-6.58}{101 - \ln(v/\mu) + 0.25\Delta B}. \tag{4.16}$$

Here, $v = 246\,\text{GeV}$ is the standard model vev as usual, and the μ dependence of $\lambda_{\text{eff}}(\mu)$

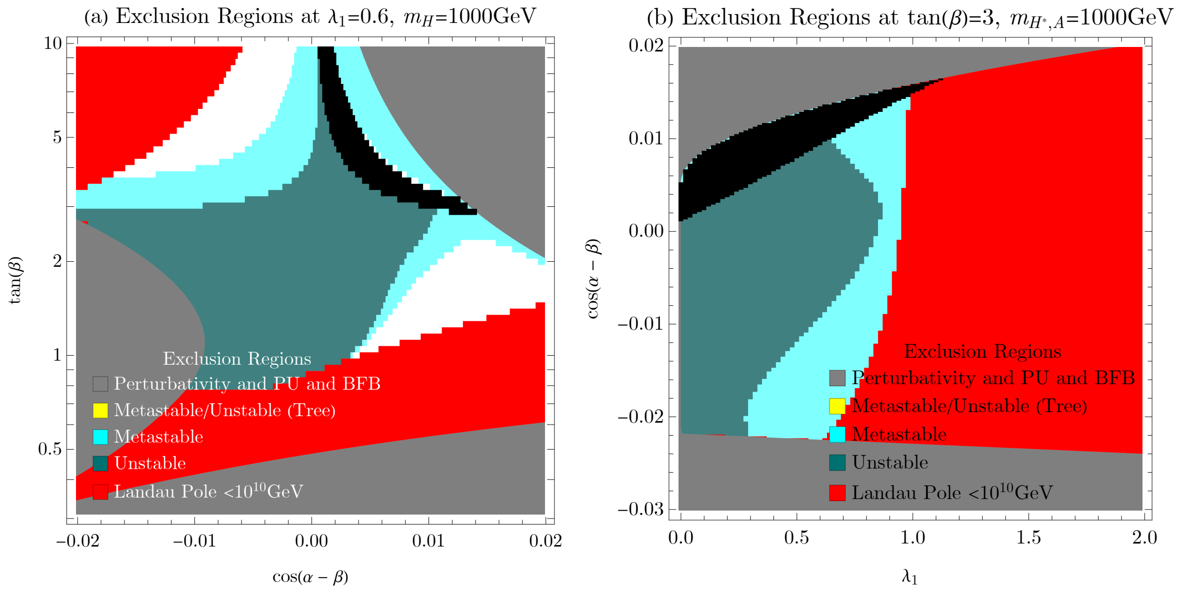

Figure 4.6: Stability bounds after one iteration of Newton's method (4.13). All the inconclusive regions with error $\epsilon > 0.03$ are coloured black. (a) Parameter scan in the $\tan\beta \times \cos(\alpha - \beta)$ plane. The other parameters are set to $\lambda_1 = 0.6$ and $m_{H^*,A} =$ 1000 GeV. We see here that metastability excludes most of the low $\tan\beta$ regions. (b) Parameter scan of the $\lambda_1 \times \cos(\alpha - \beta)$ plane. The other parameters are set to $\tan(\beta) = 3$ and $m_{H^*,A} = 1000$ GeV. We see that the Landau pole constraint $\Lambda_L > 10^{10}$ GeV excludes all the regions with $\lambda_1 > 1$.

is calculated using one-loop[8] beta functions as obtained from the Mathematica package SARAH. It should be noted that while I used the beta functions of the type-I 2HDM, the metastability constraints are actually insensitive to the Yukawa assignments. This is because the Yukawa couplings of the bottom and tau particles ~ 0.01 are much smaller than the Yukawa coupling of the top quark ~ 1. As such, the results here apply equally well to the type-II, X, and Y models. This argument is validated by the numerical scan in figure 4.5b, where we see the region excluded by tunneling rate calculations is identical between the type-I and type-II 2HDMs[9].

Computing the metastability bounds using equation (4.16) gives us the results in figure 4.6. One thing to notice is that these result differ significantly from figure 4.4. This validates the need to correct the tree-level inputs using our one-loop estimates. After these corrections are taken into account, the vast majority of parameter space satisfies $\epsilon < 0.03$ (non-black regions). I chose the cutoff to be 3% for two main reasons:

[8] I chose to use the one-loop beta functions in this thesis for consistency with chapter 3. However, one can use the two-loop beta functions directly in the calculations to obtain slightly more precise results. However, to be consistent this will also require us to calculate the one-loop determinants (2.30).

[9] I have since noticed that the metastability bounds do differ when $\tan\beta \gtrsim 30$. Since this does not affect the conclusions drawn in this thesis, I address this in future work.

First, we expect that two-loop corrections are of order 0.3 to 3% anyway, so there is no point in being more precise. Second, the calculated stability bounds are robust against 3% shifts in the input parameters, so there is not much to gain in being more precise.

In figure 4.6a, we see that most of the low $\tan\beta$ region is unstable, unless $\cos(\alpha-\beta)$ is sufficiently positive. For the type-II 2HDM this is a new and severe constraint: The 95% confidence interval on $\cos(\alpha-\beta)$ due to flavour and collider constraints is $[-0.02, 0.0016]$ [77]. This means that the type-II 2HDM, with degenerate $m_{H^*,A}$, now strongly favours the $\tan\beta > 3$ region. For the type-I 2HDM, at $m_{H^*,A} = 1000\,\text{GeV}$, flavour and collider constraints place $\cos(\alpha-\beta) \in [-0.1, 0.05]$ [77], so the situation is quite similar. However the type-I 2HDM supports $\cos(\alpha-\beta) > 0.05$ at smaller masses $m_{H^*,A} < 1000\,\text{GeV}$ so we cannot rule out $\tan\beta < 3$ immediately.

In figure 4.6b, we see mainly how the Landau pole constraint $\Lambda_L > 10^{10}\,\text{GeV}$ varies with λ_1. We see that for sufficiently low $\lambda_1 \lesssim 0.5$ the Landau pole constraint does not vary much. This means that low values of λ_1 are all equally viable. On the other hand, larger values $\lambda_1 \gtrsim 0.8$ are disfavoured by the existence of the low energy Landau pole. Notice however that the stability bounds become more stringent for smaller λ_1. This means that the bounds in figure 4.6a hold for all $\lambda_1 \lesssim 0.6$ and thus can directly be used to inform future experimental searches.

Finally, as we would like to understand the behaviour of the metastability constraints on the full parameter space, I also scanned the plane of mass splittings $m_A - m_H \times m_H^{\pm} - m_H$ and the plane $m_H \times \tan(\beta)$. The results are shown in figure 4.7.

In figure 4.7a, we see that mass splittings quickly cause the 2HDM to violate the other theoretical bounds (grey), or the Landau pole constraint (red). Since these mass-degeneracies quickly lead to conflict with experiment, this result is theoretically pleasing: Since we expect *a priori* that the successor to the standard model should not have a Landau pole at low energies, we can exclude parameter points with highly nondegenerate masses $m_{H^{\pm}/A} - m_H \gtrsim 100\,\text{GeV}$. As it turns out, recent experimental constraints for the type-II 2HDM require that mass splittings be smaller than approximately $m_{H^{\pm}/A} - m_H \lesssim 100\,\text{GeV}$ [77]. This way, the Landau pole constraint in 4.7a naturally excludes a large portion of parameter space in conflict with present experimental data.

It is also interesting to note that, in figure 4.7a, mass splittings consistently stabilise

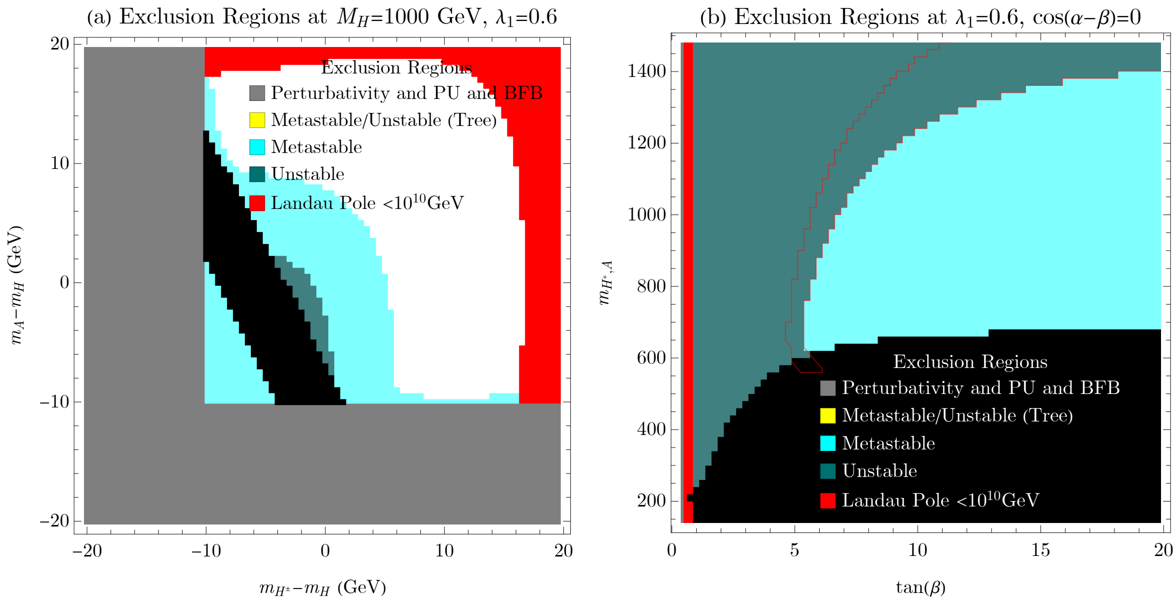

Figure 4.7: Stability bounds after one iteration of Newton's method (4.13). All the regions with error $\epsilon > 0.03$ are coloured black. (a) Parameter scan in the $m_A - m_H \times m_H^{\pm} - m_H$ plane. The other parameters are set to $\lambda_1 = 0.6$ and $m_H = 1000\,\text{GeV}$, $\cos(\alpha - \beta) = 0$ and $\tan\beta = 5$. We see that mass splittings generally stabilise the vacuum, but causes Landau poles to appear at low energy. (b) Parameter scan of the $\tan(\beta) \times m_{H^*,A}$ plane. The other parameters are set to $\lambda_1 = 0.6$, $\cos(\alpha - \beta) = 0$. The red line becomes light blue (metastable but not absolutely stable) when $\Delta B = -30$.

the vacuum. Indeed for $\tan\beta = 5$, $\cos(\alpha - \beta) = 0$, the degenerate mass point is barely unstable, but mass splittings of $m_{H^\pm/A} - m_H \gtrsim 10\,\text{GeV}$ is enough to turn it absolutely stable. Since these mass splittings modify flavour and electroweak observables [62, 77], more precise measurements of these flavour and electroweak observables may be able to rule out most of the $\tan\beta \lesssim 3$ region of 2HDM parameter space in the near future.

On the other hand, we see from figure 4.7b that higher scalar masses slightly destabilise the vacuum. This is however, a very slight effect. Indeed, setting $\Delta B = -30$ recovers the region outlined red in figure 4.7b. Thus, we see that the destabilising effect of increasing $m_{H^*,A}$ is on the order of the one-loop functional determinant correction.

Finally, we would like to verify how seriously we can take the metastability constraints presented in this chapter. Just like with the Landau pole, the instability or metastability of our vacuum is due to the renormalisation scale dependence of the parameters $\lambda_{1,\cdots,5}(\mu)$. So, in analogy with section 4.3, I will define the 'instability scale' Λ_I to be the critical renormalisation scale at which the vacuum becomes unstable. That is, Λ_I is the lowest renormalisation scale for which (4.16) is satisfied.

If new physics were to appear before Λ_I, then, it is entirely possible that a vacuum

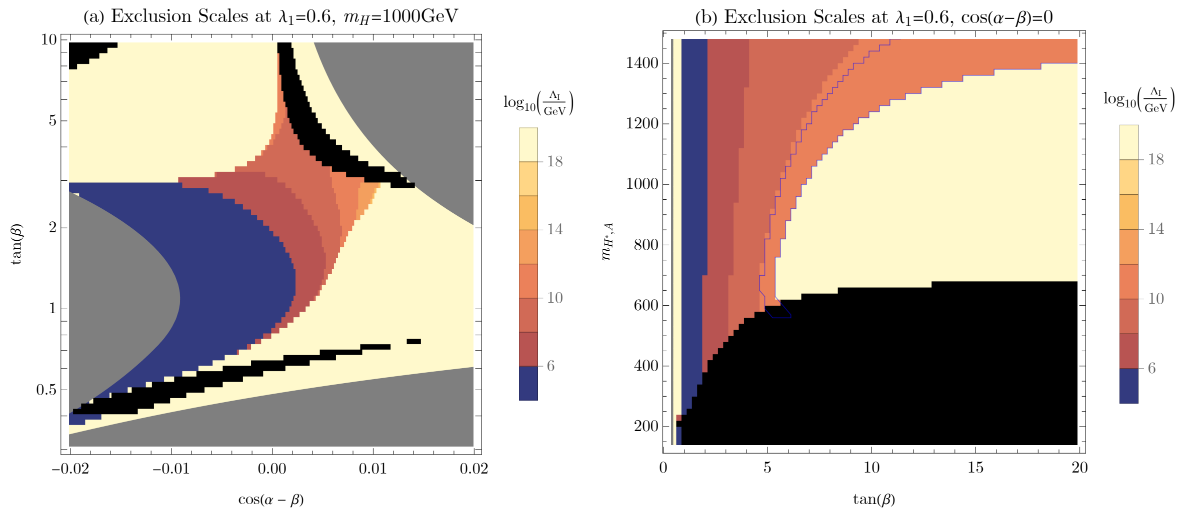

Figure 4.8: Parameter scan of the renormalisation scale Λ_I at which $\lambda_{\text{eff}}(\Lambda_M)$ critically satisfies (4.16). (a) Parameter scan in the $\tan\beta \times \cos(\alpha - \beta)$ plane, with other parameters identical to figure 4.6a. We see that most of the regions excluded by tunneling rate calculations is excluded with $\Lambda_I < 10^{10}$ GeV. We also see that a significant portion of parameter space is excluded at $\Lambda_I < 10^{6}$ GeV. (b) Parameter scan in the $\tan\beta \times m_{H^*,A}$ plane, with other parameters identical to figure 4.7b. The blue outline is identical to the red outline in figure 4.7b. All the excluded regions seem to have $\Lambda_I \lesssim 10^{12}$ GeV.

calculated to be metastable in the 2HDM is stabilised in the new theory. However, this new physics should appear order of magnitudes before Λ_I in energy. So, for a reasonable estimate, we can assume that if $\Lambda_I < 10^8$ GeV, then there is little hope for new physics to stabilise the vacuum. Interestingly, we see in figure 4.8 that when the vacuum becomes unstable it generally does so at scales $\Lambda_I \lesssim 10^{10}$ GeV, with a majority becoming unstable at $\Lambda_I \lesssim 10^8$ GeV. So, we expect that the results in this chapter are reasonably robust against new physics.

Note that even if experiments somehow confirm a 2HDM with parameters marked unstable in this study, then we can still learn something new: It would mean that there must be new particles appearing at a scale $\Lambda \lesssim 10^8$ GeV. In addition, the new particles must as a whole give a positive contribution to $\lambda_{\text{eff}}(\Lambda_I)$, so that the vacuum is stabilised. This would be a big improvement to the current theoretical upper bounds for new physics, which are the GUT scale $\Lambda_{\text{GUT}} \sim 10^{16}$ GeV and the Planck scale $\Lambda_{\text{pl}} \sim 10^{18}$ GeV.

This concludes my study of metastability constraints in the 2HDM. In the next chapter, I will generalise the techniques implemented in this chapter to the 2HDM+s/a models, and obtain their metastability constraints.

Generalisation to Scalar and Pseudoscalar Extensions

In this chapter, I generalise the technique developed in chapter 4 to the 2HDM+s/a models. I analyse the metastability constraints appearing in the 2HDM+s/a model and show that the results of chapter 4 can be directly used to constrain the 2HDM+s/a parameter space. All calculations and proofs presented are, unless otherwise stated through relevant citations, the result of my own work.

5.1 Input Variables in the 2HDM+s/a

The potentials for the 2HDM+s/a models are given by [23, 24, 62]

$$
\begin{aligned}
V_{2\mathrm{HDM}+s/a} &= V_{2\mathrm{HDM}} + V_{s/a}, \\
V_a &= \frac{1}{2}m_{a_0}^2 a_0^2 + \frac{1}{3}\mu_a a_0^3 + \frac{\lambda}{4}a_0^4 + \mu_{12a}(i\langle\Phi_1|\Phi_2\rangle a_0 + \text{h.c.}) + \lambda_{11a}\|\Phi_1\|^2 a_0^2 + \lambda_{22a}\|\Phi_2\|^2 a_0^2, \\
V_s &= \frac{1}{2}m_{s_0}^2 s_0^2 + \frac{1}{3}\mu_s s_0^3 + \frac{\lambda}{4}s_0^4 + \mu_{12s}(\langle\Phi_1|\Phi_2\rangle s_0 + \text{h.c.}) + \lambda_{11s}\|\Phi_1\|^2 s_0^2 + \lambda_{22s}\|\Phi_2\|^2 s_0^2.
\end{aligned}
\tag{5.1}
$$

Here, I've excluded the standard 2HDM potential for brevity and clarity, and a_0 and s_0 are the new (pseudo)scalar singlet fields. It should be noted that I have pre-imposed the softly-broken $\mathbb{Z}_2$ symmetry on the Higgs doublets. The cubic terms μ_a, μ_s are also often taken to be zero [23, 62] for simplicity due to two main reasons. First, this term does not contribute anything new to the scalar mass spectrum, so it will be less directly relevant to present experiments [23]. In addition, the RGEs for the 2HDM+s/a always have solutions at $\mu_s, \mu_a = 0$, so one can impose symmetries on the model which would simultaneously ensure $\mu_s, \mu_a = 0$ while keeping all the other parameters free[1].

[1]One simple example is to let s or a to transform as $s, a \mapsto -s, -a$ under the 2HDM $\mathbb{Z}_2$ symmetry.

Such symmetries would presumably come from a more complete model, which would be out of the scope of this research project.

It should be noted however that in the scalar case, μ_s modifies the effective potential in a nontrivial way. Roughly, if two minima of the 2HDM+s potential occur at $s = \pm v_s$, then due to the $\frac{1}{3}\mu_s s_0^3$ term, the two minima will have their s_0 squared mass $\frac{\partial^2 V}{\partial s_0^2}$ differ by $\sim 4\mu_s v_s$. In addition, one minimum would be higher than the other, allowing for tunneling from the higher minimum. Interestingly, such a mechanism has recently been shown to allow for baryogenesis without beyond-SM CP violation [87]. However, even in this case their choice of μ_s is very small $\mu_s \ll v, m_h$ so it is unlikely that setting it to zero will have any major consequences on experimental observables. In addition, we do not expect that $\mu_s \neq 0$ provides interesting absolute stability constraints since we can always choose μ_s with the sign such that (v_1, v_2, v_s) is a minimum.

The 2HDM+s/a models are some of the most promising simplified dark matter models for collider searches [23, 88]. So, on top of the potential $V_{\text{2HDM}+s/a}$, we would also like to include the dark matter Yukawa couplings:

$$\mathcal{L}_{\text{Yukawa},a} = -iy_\chi a\bar{\chi}\gamma^5\chi, \quad \mathcal{L}_{\text{Yukawa},s} = -y_\chi s\bar{\chi}\chi. \tag{5.2}$$

Here, χ is the fermionic dark matter candidate and $\gamma^5 := i\gamma^0\gamma^1\gamma^2\gamma^3$ is the top element of the Dirac algebra. The parameter y_χ will be important to metastability as it will have negative contributions to the running of the quartic couplings λ_i. However, this term will be otherwise irrelevant to our effective potential.

Just as in the 2HDM, we would like to obtain a set of input variables for the 2HDM+a and the 2HDM+s. For the 2HDM+a, the situation is comparatively simpler. Since the new pseudoscalar a can only mix with the 2HDM pseudoscalar A, we introduce only one new mass m_a and one new mixing angle θ between a and A. It has previously been shown that by diagonalising the Hessian, [24]

$$\mu_{12a} = \frac{(m_a^2 - m_A^2)\sin(2\theta)}{2v}, \quad m_{A_0}^2 = m_a^2 \sin^2\theta + m_A^2 \cos^2\theta. \tag{5.3}$$

Here, m_{A_0} replaces the role of m_A in the 2HDM change of variables (3.2). Since the 2HDM+a does not come with any other new particles, we cannot substitute any more variables, and we are done. However, this simplicity comes at a cost: Since we are keeping $\lambda_a, \lambda_{11a}, \lambda_{22a}$ as input parameters, it is considerably more difficult to interpret our result in direct experimental terms. However, it has previously been noted that it is frequently reasonable to take $2\lambda_3 = \lambda_{11a} = \lambda_{22a}$ so that cubic $H \to aa$ and $A \to ha$ interactions are not too large [88]. Of course, we may also take $\theta, \lambda_{11a}, \lambda 22a \ll 1$ to recover the standard 2HDM. Due to the vastness of the 2HDM+a parameter space, I focus only on these two motivated scenarios in this thesis.

The case for the 2HDM+s is much more complicated, and to the best of our group's knowledge, no analytical change of variables to a satisfactory set of input variables has previously appeared in the literature. The first challenge is thus to obtain a reasonable change of variables so that our parameter scans can be kept efficient. First, it is straightforward to solve for the minimum of the potential $\frac{\partial V}{\partial \phi} = 0$ and solve for m_{11}, m_{22}, m_{s_0}. The main challenge is that the new scalar s can mix with both h and H. This means we would need to analytically diagonalise a 3×3 matrix while avoiding double-counting from permutations of the eigenvalues. To achieve this, I found that it is most efficient to solve[2]

$$M^2 := \left.\frac{\partial^2 V}{\partial\phi\partial\phi}\right|_{\phi=(v_1,v_2,v_s)} = Q \cdot \mathrm{diag}(m_H, m_h, m_s) \cdot Q^T, \quad Q := R^{12}_\gamma R^{13}_\delta R^{23}_\theta. \tag{5.4}$$

Here, R^{ij}_ξ is the matrix rotating coordinates i and j with angle ξ. It is also understood that $\phi = (\phi_1, \phi_2, s_0)$ with $\phi_{1,2}$ defined in (4.2). This way, by equating the off-diagonal components of this 3×3 matrix equation, we can solve for $\lambda_{11s}, \lambda_{22s}, m^2_{12}$ in terms of the new mixing angles γ, δ, θ, the new scalar mass m_s and the 2HDM input parameters.

The final three conditions can be obtained by instead solving $M^2 Q = Q \cdot \mathrm{diag}(m_H, m_h, m_s)$ with the equations appearing on the diagonal. I found that it is most efficient to solve for the parameters $\lambda_3, \lambda_2, \lambda_s$ this way.

With the above technique, I obtained an analytical, invertible change of variables of the following kind[3]:

$$\begin{pmatrix} m^2_{11} & m^2_{22} & m^2_{12} & \lambda_1 \\ \lambda_2 & \lambda_3 & \lambda_4 & \lambda_5 \\ m^2_{s_0} & \lambda_s & \mu_{12s} & \lambda_{11s} \\ \lambda_{22s} & \mu_s & & \end{pmatrix} \leftarrow \begin{pmatrix} v & \beta & \gamma & \lambda_1 \\ m_h & m_H & m_{H^\pm} & m_A \\ v_s & m_s & \mu_{12s} & \delta \\ \theta & \mu_s & & \end{pmatrix}. \tag{5.5}$$

[2]Note that our convention for the mixing angles differs from [62].

[3]The full expressions are provided in appendix A.1, as they are too long to include in the main text.

As we will take $\mu_s = 0$ in this thesis, the only new parameter not directly related to experimental masses is μ_{12s}. This parameter softly breaks the 2HDM $\mathbb{Z}_2$ symmetry[4] and directly mixes all three scalars Φ_1, Φ_2, s at tree-level. So I expect that μ_{12s} would directly modify the decay rate of processes like $H \to hs$.

Before we continue to discuss metastability constraints in the 2HDM+s/a model, I would like to first discuss a subtlety which arises in the 2HDM+s. Since the new scalar s attains a vev, and the μ_{12s} term breaks the $s \mapsto -s$ symmetry, the vev at (v_1, v_2, v_s) is not always the true vacuum. Indeed, for $\mu_{12s} \ll v_s$, we find that (v_1, v_2, v_s) and $(v_1, v_2, -v_s)$ are two nondegenerate vacua. The potential difference between the two vacua is approximately[5] $V(v_s) - V(-v_s) \approx 2\mu_{12s} v_s v_1 v_2$. For this reason, to ensure that the chosen vacuum at $+v_s$ is stable, I will take $\mu_{12s} < 0$ in this thesis.

5.2 Summary of Existing Constraints on the 2HDM+s/a

Just as in the 2HDM, the 2HDM+s/a models come with their own sets of PU and BFB constraints. Their explicit analytical expressions can be found in [23, 62, 89], and I will not reproduce them here as their full forms are rather long and uninsightful. However, as usual, I will make use of them to rule out uninteresting regions of parameter space. For example, due to the large mass difference $m_s \ll m_H$, the s, H mixing angle δ must be of order $\frac{v v_s}{m^2_{H^*,A}}$ to keep the coupling λ_{11s} perturbative. As such, I will frequently assume $\delta \sim 10^{-2}$ in this thesis. In addition, for small mixing angles, $\lambda_s \sim \frac{m_s^2}{2v_s^2}$. So I will frequently take $v_s \sim m_s$ to keep λ_s perturbative. Finally, for the 2HDM+a, the mixing angle θ also enters into $\lambda_4 \propto m_H^2 \theta^2 / v^2$. So for larger masses $m_H \sim 1000\,\text{GeV}$ we must keep $\theta \lesssim 0.2$

On top of the above theoretical constraints, I will take $m_{s,a} \gtrsim 100\,\text{GeV}$ to prevent $h \to a\bar{\chi}\chi$ decays, where χ is the DM candidate. If this process is energetically allowed, the decay rate would be on the order of $\Gamma(h \to a\bar{\chi}\chi) = O\left(\frac{m^4_{H^*,A} y_\chi^2}{32\pi^3 m_h v^2}\right)$ [90]. For a small $y_\chi \sim 0.1$ and a reasonable $m_{H^*,A} \sim 1000\,\text{GeV}$, this would yield an estimated decay rate of $\sim 1.3\,\text{GeV}$. However, the 125 GeV Higgs boson has a decay rate that has been measured to agree with the SM to within $\lesssim 0.4\,\text{MeV}$ [91], so the parameter space with

[4] If $s \mapsto s$ under this symmetry

[5] In reality, the value of the first two entries v_1, v_2 are not identical between the two vacua, but for small μ_{12s}, they will be approximately equal.

$m_{s,a} \lesssim 100\,\text{GeV}$ is severely constrained.

The mixing angle θ is also severely constrained by experiment. However their constraints vary wildly depending on the other parameter choices. For example, Bauer *et al.* found that $\sin\theta$ as large as $\frac{1}{\sqrt{2}}$ can be allowed in the 2HDM+a. The review paper [88] also finds that a large portion of parameter space with $m_a > 100\,\text{GeV}$ is still allowed by dark matter direct detection experiments even with $\sin\theta = 0.7$. As a result, I will not make any assumptions on the values of the mixing angles θ, δ based on experiment.

5.3 Radial Bounces in the 2HDM+s/a

The technique introduced in section 4.1 can be straightforwardly generalised to the 2HDM+s/a models. To do this, we denote $\psi_s = \psi\cos(\zeta)$ and multiply all the 2HDM fields in (4.1) by $\sin(\zeta)$. Unfortunately, some of the resulting angles θ, ξ, η, ζ solving equation (4.7) are very messy in the 2HDM+s/a, so I will omit them for brevity. In any case, their values are not important for our metastability constraints, and we are only interested in checking if the angles θ, ξ, η, ζ are all real[6]. Substituting these angles back into our quartic potential yields the effective quartic couplings λ_{eff} in table 5.1.

λ_{eff}
λ_a
$\frac{2\lambda_1\lambda_a-\lambda_{11a}^2}{2\lambda_1-4\lambda_{11a}+4\lambda_a}$
$\frac{2\lambda_2\lambda_a-\lambda_{22a}^2}{2\lambda_2-4\lambda_{22a}+4\lambda_a}$
$\frac{\lambda_1\left(\lambda_{22a}^2-2\lambda_2\lambda_a\right)+\lambda_{11a}^2\lambda_2-2\lambda_{11a}\lambda_{22a}\lambda_3+2\lambda_3^2\lambda_a}{2\left(-\lambda_1(\lambda_2-2\lambda_{22a}+2\lambda_a)+\lambda_{11a}^2+2\lambda_{11a}(\lambda_2-\lambda_{22a}-\lambda_3)-2\lambda_2\lambda_a+\lambda_{22a}^2-2\lambda_{22a}\lambda_3+\lambda_3^2+4\lambda_3\lambda_a\right)}$
$\frac{\lambda_1\left(\lambda_{22a}^2-2\lambda_2\lambda_a\right)+\lambda_{11a}^2\lambda_2-2\lambda_{11a}\lambda_{22a}(\lambda_3+\lambda_4+\lambda_5)+2\lambda_a(\lambda_3+\lambda_4+\lambda_5)^2}{2\left(-\lambda_1(\lambda_2-2\lambda_{22a}+2\lambda_a)+\lambda_{11a}^2+2\lambda_{11a}(\lambda_2-\lambda_{22a}-\lambda_3-\lambda_4-\lambda_5)-2\lambda_2\lambda_a+\lambda_{22a}^2-2\lambda_{22a}\lambda_3-2\lambda_{22a}\lambda_4-2\lambda_{22a}\lambda_5+\lambda_3^2+2\lambda_3\lambda_4+2\lambda_3\lambda_5+4\lambda_3\lambda_a+\lambda_4^2+2\lambda_4\lambda_5+4\lambda_4\lambda_a+\lambda_5^2+4\lambda_5\lambda_a\right)}$
$\frac{\lambda_1\left(\lambda_{22a}^2-2\lambda_2\lambda_a\right)+\lambda_{11a}^2\lambda_2-2\lambda_{11a}\lambda_{22a}(\lambda_3+\lambda_4-\lambda_5)+2\lambda_a(\lambda_3+\lambda_4-\lambda_5)^2}{2\left(-\lambda_1(\lambda_2-2\lambda_{22a}+2\lambda_a)+\lambda_{11a}^2+2\lambda_{11a}(\lambda_2-\lambda_{22a}-\lambda_3-\lambda_4+\lambda_5)-2\lambda_2\lambda_a+\lambda_{22a}^2-2\lambda_{22a}\lambda_3-2\lambda_{22a}\lambda_4+2\lambda_{22a}\lambda_5+\lambda_3^2+2\lambda_3\lambda_4-2\lambda_3\lambda_5+4\lambda_3\lambda_a+\lambda_4^2-2\lambda_4\lambda_5+4\lambda_4\lambda_a+\lambda_5^2-4\lambda_5\lambda_a\right)}$

Table 5.1: Summary of the different radial bounce solutions present in the 2HDM+a. The case for the 2HDM+s is identical by replacing all the a labels with s labels. The angles θ, ξ, η, ζ are omitted for brevity.

With these solutions, I performed a Monte Carlo sampling of the 2HDM+s/a parameter space and excluded all points which do not satisfy PU, BFB, and $\Lambda_{\text{L}} >$

[6]When an angle isn't real, then the corresponding solution to (4.7) doesn't exist. That is, the corresponding bounce solution isn't supported by the potential.

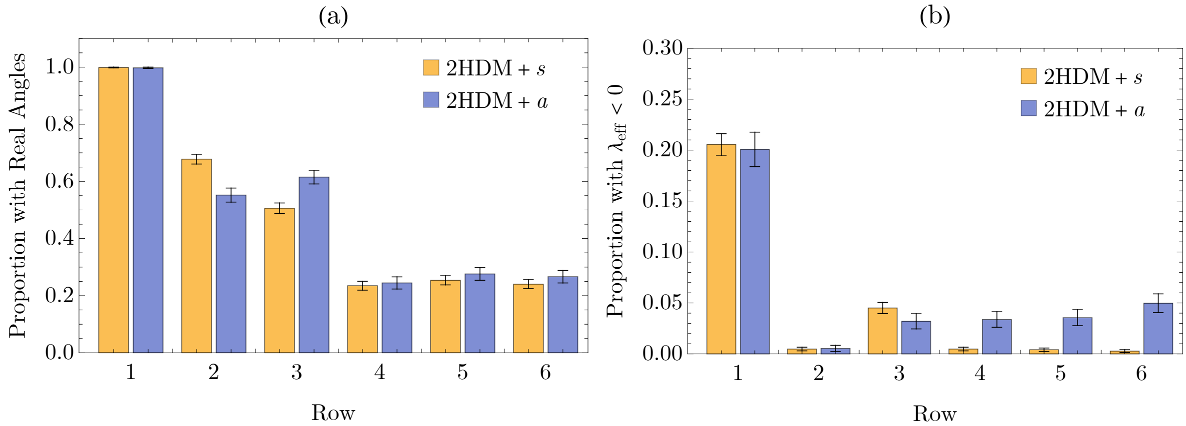

Figure 5.1: Proportions of 2HDM+s/a parameter space satisfying PU, BFB, and Landau pole $\Lambda_L > 10^{10}$ GeV constraints, which: (a) supports the radial bounce solution in the corresponding row (b) has $\lambda_{\text{eff}}(10^8\,\text{GeV}) < 0$. The aforementioned rows are the rows of table 5.1. The parameters are taken from the following intervals, distributed uniformly: $\tan\beta \in [0, 20]$, $\cos(\alpha - \beta) \in [-0.02, 0.02]$, $m_{H,H^*,A} \in [600, 1500]$, $m_{a/s} \in [100, 300]$, $v_{s/a} \in m_{s/a}[1, 2]$, $\lambda_1, \lambda_2, \lambda_a \in [0, 1]$, $\theta \in [-0.5, 0.5]$, $\delta \in [-0.01, 0.01]$, $\mu_{12s} \in [-200, 0]$, $\lambda_{11a} = \lambda_{22a} = 2\lambda_3$, and $y_\chi \in [0, 1]$.

10^{10} GeV Landau Pole constraints. Among the surviving points, the proportion of points which ensures the existence of each solution in table 5.1 is shown in figure 5.1a. We see that the angles corresponding to rows 2 to 6 of table 5.1 are real in a significant portion of parameter space ($\gtrsim 20\%$). This means we must take them all into account when determining the metastability of our vacuum. Similarly, the proportion of points which are not absolutely stable is shown in figure 5.1b. Overall, we see that all rows have nonzero contributions to stability bounds with the exception of row 2. So it seems important that we take all of these different ways the vacuum can become metastable into account. However, given that the proportion of points with $\lambda_{\text{eff}} < 0$ in rows 3 to 6 are small ($\lesssim 5\%$), I claim that it is reasonable to only check $\lambda_{\text{eff}} = \lambda_{s/a}$ for a first approximation to the full metastability bounds. This may be useful for future studies where metastability bounds are not the main focus.

However, for this thesis, I will take all rows of table 5.1 into account, as there is no harm in doing so.

5.4 Results for the 2HDM+s/a

With all our preliminary work done, we may now calculate the metastability constraints for the 2HDM+s/a. Given how many new parameters the 2HDM+s/a introduce, it is difficult to gain a comprehensive understanding of how metastability bounds constrain the 12-dimensional parameter space. Thus, we first need a qualitative understanding of how metastability bounds constrain the parameter space. To do this, I perform a Monte Carlo scan and analyse the resulting data as follows:

1. Generate a random set of input parameters randomly from a uniform distribution. This choice of distribution is arbitrary and chosen only for simplicity. In the end, our heuristic results will not be strongly dependent on the choice of distribution. The ranges of the 2HDM parameters are chosen as follows: $\tan\beta \in [0, 20], \cos(\alpha - \beta), \cos(\gamma - \beta) \in [-0.05, 0.05], m_{H^*,A} \in [600, 1500]\,\text{GeV}$, $\lambda_1 \in [0, 1]$. For the 2HDM+a, the new parameters are chosen as $\sin\theta \in [-0.5, 0.5]$, $\lambda_a \in [0, 1]$ and $\lambda_{11a}, \lambda_{22a} \in [0, 1]$. For the 2HDM+$s$, the new parameters are chosen as $v_s/m_s \in [0.5, 2]$, $\sin\theta \in [-1, 1]$, $\sin\delta \in [-0.05, 0.05]$, $\mu_{12s} \in [-200, 0]$. The new singlet mass and DM Yukawa coupling are chosen to be $m_{s,a} \in [100, 300]$ and $y_\chi \in [0, 1]$. Where parameters are dimensionful I have chosen them to be of the electroweak scale[7] $\sim m_h, v$ and where parameters are dimensionless I have chosen them to be < 1 to prevent low-energy Landau poles.

   With the above settings, I generated $\sim$ 160000 points for the 2HDM+a and $\sim$ 130000 points for the 2HDM+s satisfying PU and BFB constraints. Each run took 1 to 2 hours to complete on an Intel Core i7-14650HX processor.

2. For each set of input parameters which satisfy the PU, BFB, and perturbativity constraints, calculate the location of the Landau pole and calculate the lifetime of the desired vacuum using 5.1. If they are allowed by metastability or Landau pole constraints, label each point M and L respectively.

3. For each input parameter I, I organise the dataset into $N = 20$ uniform interval bins $\{b_i\}$ spanning the entire scanning range of I. Within each bin b_i, I calculate the proportion p_i of points satisfying M, given that it satisfies L. The uncertainty can be estimated using the standard deviation of the sample mean $\sqrt{\frac{p_i(1-p_i)}{N}}$.

4. How p_i varies with i will tell us how our input parameter I affects metastability constraints on average. However it is not very efficient to plot these p_i for all the

[7]This is because this is the approximate scale present colliders work in. In addition, this prevents large dimensionless parameters coming from ratios like μ_{12s}/v, which can cause the theory to be nonperturbative.

~ 20 input variables we have across both 2HDM+s/a models. As such, to obtain a qualitative metric for the nonuniformity of p_i, I obtain the reduced chi-squared deviation of the p_i with respect to the mean $\langle p \rangle$ as follows

$$\chi^2_{\text{red}} = \sum_i \frac{(p_i - \langle p \rangle)^2}{p_i(1-p_i)} \frac{N}{N-1}. \tag{5.6}$$

The χ^2_{red} for the 2HDM+a are shown in figure 5.2a. Here, we see that the parameters most significantly impacted by metastability constraints are $\tan\beta, \lambda_a$, and y_χ. The parameters $\cos(\alpha-\beta), \lambda_{22a}$ and θ are also significantly nonuniform, but they are impacted less by metastability. Figure 5.2b shows the proportions p_i for each of the 20 bins, and for each new significant parameter. We see that λ_{22a} and θ only affect the surviving proportion by $\sim 20\%$ while λ_a and y_χ show stronger trends. Most significantly, we see that the $\gtrsim 80\%$ of the region $y_\chi > 0.9$ is excluded by the metastability constraint. The small uncertainties also indicate that the number of points suriviving the PU, BFB, and Landau pole constraints in this region are large. So, metastability rules out a significant portion of parameter space this way.

Similarly, from figure 5.2b we see that $\gtrsim 60\%$ of the region $\lambda_a > 0.6$ is ruled out by metastability. However, the uncertainties in these regions are much larger, which means these regions correspond to a smaller portion of parameter space overall. As such, these constraints are not as significant as the constraint on y_χ.

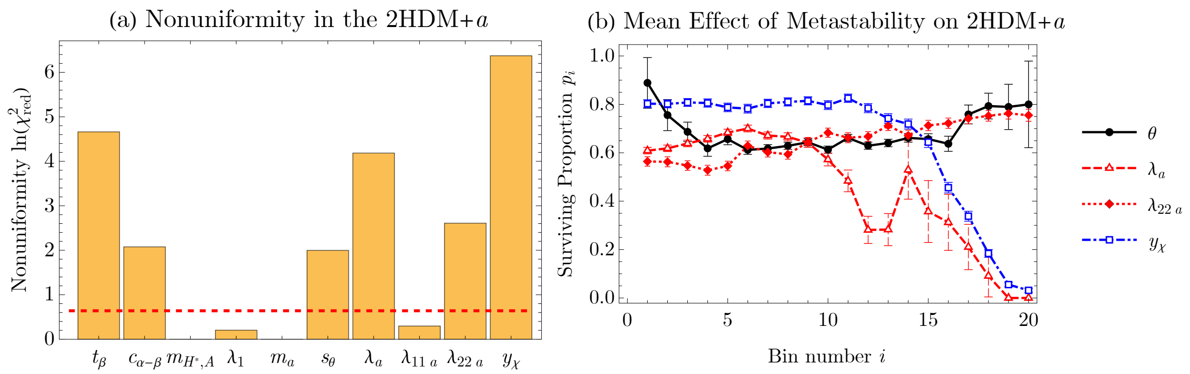

Figure 5.2: Effect of metastability constraints on the 2HDM+a parameter space. I have defined $t_\beta := \tan\beta$, and $s_\theta = \sin\theta$. (a) Nonuniformity χ^2_{red} for each 2HDM+a parameter. The red dashed line indicates a p-value of 1%. (b) Proportions p_i surviving metastability constraints given that the point survives the Landau pole constraint. I only plot here the 2HDM+a parameters which are absent in the 2HDM, and have nonuniformities χ^2_{red} above the red dashed line in (a).

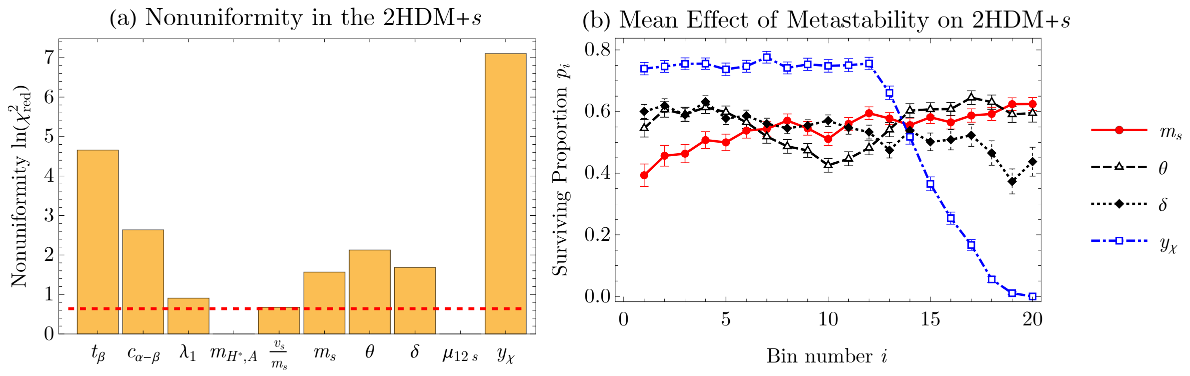

Figure 5.3: Effect of metastability constraints on the 2HDM+s parameter space. I have defined $t_\beta := \tan\beta$, and $s_\theta = \sin\theta$. (a) Nonuniformity χ^2_{red} for each 2HDM+s parameter. The red dashed line indicates a p-value of 1%. (b) Proportions p_i surviving metastability constraints given that the point survives the Landau pole constraint. I only plot here the 2HDM+s parameters which are absent in the 2HDM, and have nonuniformities χ^2_{red} above the red dashed line in (a).

Similar plots are shown for the 2HDM+s in figure 5.3. In contrast to the 2HDM+a, most of the new 2HDM+s parameters with the exception of y_χ have very low nonuniformities. This means that metastability bounds do not depend on most of the parameters in the 2HDM+s. This is highlighted in figure 5.3b where I plot the new 2HDM+s parameters with the highest χ^2_{red} values. With the exception of y_χ, we see that the surviving proportion p_i only vary by $\sim 20\%$ as m_s and θ are swept in their respective domains.

Now that we have identified the significant input parameters, we would like to perform a 2D parameter scan of the 2HDM+s/a models, just as we did for the 2HDM in Chapter 4. However, given that there are 6 to 7 input parameters with significant nonuniformities χ^2_{red}, we would have to scan 30 to 50 planes to identify the most informative pair of input parameters. To sidestep this issue, I take the data from the Monte Carlo scan and perform the following analysis:

1. For each pair of input parameters I and J, organise the data into $N = 20 \times 20$ uniform interval bins b_{ij}.

2. In each bin b_{ij}, estimate the probability p_{ij} of satisfying M given L. Due to the difficulty of getting enough data points in certain regions of parameter space, I

will use an estimate for p_{ij} given by

$$p_{ij} = \frac{n_{ij}(M \cap L) + \alpha}{n_{ij}(L) + 1} \pm \sqrt{\frac{p_{ij}(1-p_{ij})}{N}}, \quad \alpha = \frac{p_i + p_j}{2}.$$

Here, $n_{ij}(\square)$ is the number of parameter points in bin b_{ij} satisfying $\square$, and p_i and p_j are the probabilities in figures 5.2 and 5.3. This will reduce potential artifacts appearing due to insufficient data $n_{ij}(L) \ll 10$, without affecting our results for statistically significant sample sizes $n_{ij}(L) \gg 1$.

3. Calculate the correlation of the parameters I and J, treating p_{ij} as the (unnormalised) probability distribution. This can be done in several ways[8], but I found that the most robust method is one that takes into account the uncertainty of p_{ij}. This is done by computing the reduced χ^2 deviation of p_{ij} from a product distribution as follows:

$$\chi^2_{\text{red}} = \frac{(\bar{p}_{ij} - \sum_{i'j'} \bar{p}_{i'j}\bar{p}_{ij'})^2}{(\Delta\bar{p})^2}, \quad \bar{p}_{ij} = \frac{p_{ij}}{\sum_{i'j'} p_{i'j'}}. \tag{5.7}$$

Here, $\bar{p}$ is the normalised version of p and $\Delta\bar{p}$ is the uncertainty of p divided by the normalisation factor $\sum_{i'j'} p_{i'j'}$.

The results for both the 2HDM+s/a models are shown in figure 5.4. Here, we see that for the 2HDM+a, it is most informative[9] to scan over the planes $y_\chi \times \lambda_a$, $\theta \times y_\chi$, and $\cos(\alpha - \beta) \times y_\chi$. I will scan over the first two pairs of variables, but not $\cos(\alpha-\beta) \times y_\chi$, for brevity. In any case we will have at this point multiple 2D scans involving both $\cos(\alpha-\beta)$ and y_χ. For the 2HDM+s, figure 5.4b tells us that we should scan over $y_\chi \times \tan\beta$ and $\mu_{12s} \times \delta$. Just as in the 2HDM+a case, I will not scan over $y_\chi \times \frac{v_s}{m_s}$ and $y_\chi \times \cos(\alpha-\beta)$ for brevity. The reason that I ignore $y_\chi \times \frac{v_s}{m_s}$ is because in the limit $\theta = \delta = \mu_{12s} = 0$, we have $\frac{v_s}{m_s} = \frac{1}{\sqrt{2\lambda_s}}$. So since we perform a $\lambda_a \times y_\chi$ scan in the 2HDM+a, performing a $\lambda_s \times y_\chi$ scan in the 2HDM+s would be redundant[10].

[8] For example, I have tried calculating Pearson's correlation coefficient as well as Shannon's mutual information. Both result in false positives when any of the bins b_{ij} has an insufficient number of data points ($\lesssim 3$).

[9] Note that I ignore the $\tan\beta \times \cos(\alpha-\beta)$ plane since it produces a near-identical plot to figure 4.6a.

[10] This is because the one-loop RGEs of the 2HDM+s/a models are identical. Their differences only come from the relations between the particle masses and the parameters appearing in the potential. These are in turn different purely because the scalar attains a nonzero vev v_s.

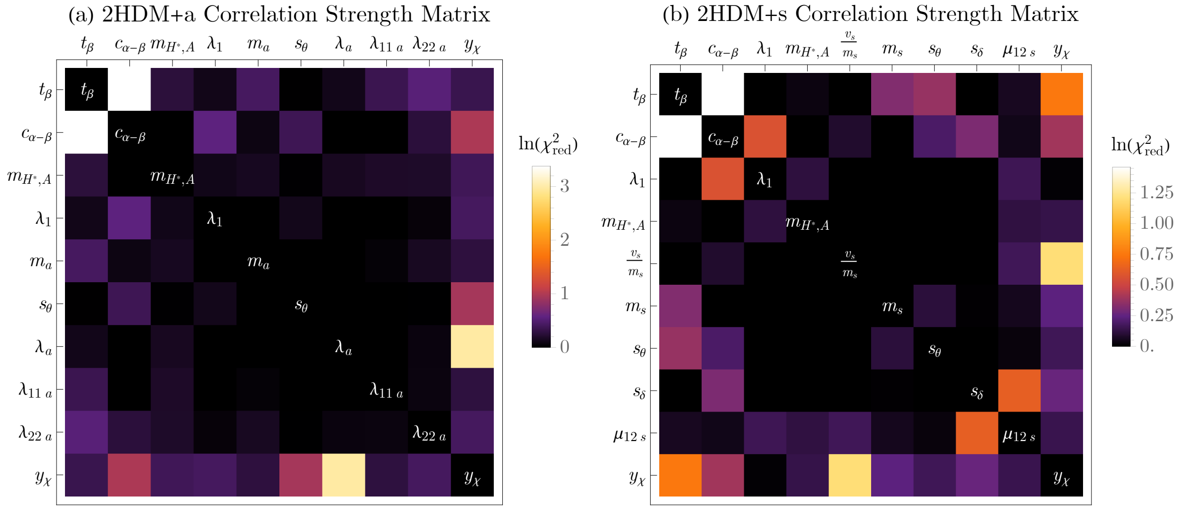

Figure 5.4: Correlation strengths of the effect of metastability constraints on each pair of input variables for the (a) 2HDM+a and (b) 2HDM+s models. The diagonal is set to zero for convenience. Here, a bright cell (I, J) indicates that the behaviour of metastability bounds is highly nontrivial in the pair of variables I and J, so it will be informative to scan over I and J.

The 2D parameter scans for the 2HDM+a is shown in figure 5.5. We see from both subfigures that large Yukawa couplings $y_\chi \gtrsim 0.8$ excludes all of the parameter space. However, the critical Yukawa coupling y^*_χ, above which the vacuum becomes unstable, varies with the other parameters. From figure 5.5a we see that increasing λ_a has the effect of stabilising the vacuum. However, we can only raise λ_a up to ~ 0.6 to 0.7 before we inevitably encounter a low energy Landau pole. From figure 5.5b we see that the dependence y^*_χ on $\sin\theta$ is very weak. Throughout the allowed interval for $\sin\theta$, the critical y^*_χ varies only by 1%. This, along with the observation that the other parameters in figures 5.2 and 5.4 impact metastability constraints less on average, suggest that most parameters do not impact metastability constraints. Indeed, we find that the only new metastable regions are induced by large Yukawa couplings $y_\chi \gtrsim 0.7$. This Yukawa coupling enters directly the one-loop beta function for λ_a:

$$\beta_{\lambda_a} := \frac{d\lambda_a}{d\ln\mu} = \frac{1}{8\pi^2}\left(9\lambda_a^2 + \lambda_{11a}^2 + \lambda_{22a}^2 + 4y_\chi^2\lambda_a - 4y_\chi^4\right). \tag{5.8}$$

Since the coefficient of y_χ^4 is negative, a large y_χ would cause λ_a to be negative at large energies $\mu \gg v$. So we expect that the new metastability constraints in the 2HDM+a is due to the λ_a bounce in table 5.1. Crucially, the 2HDM+a parameters do not significantly affect the tunneling rates as calculated from the 2HDM bounces.

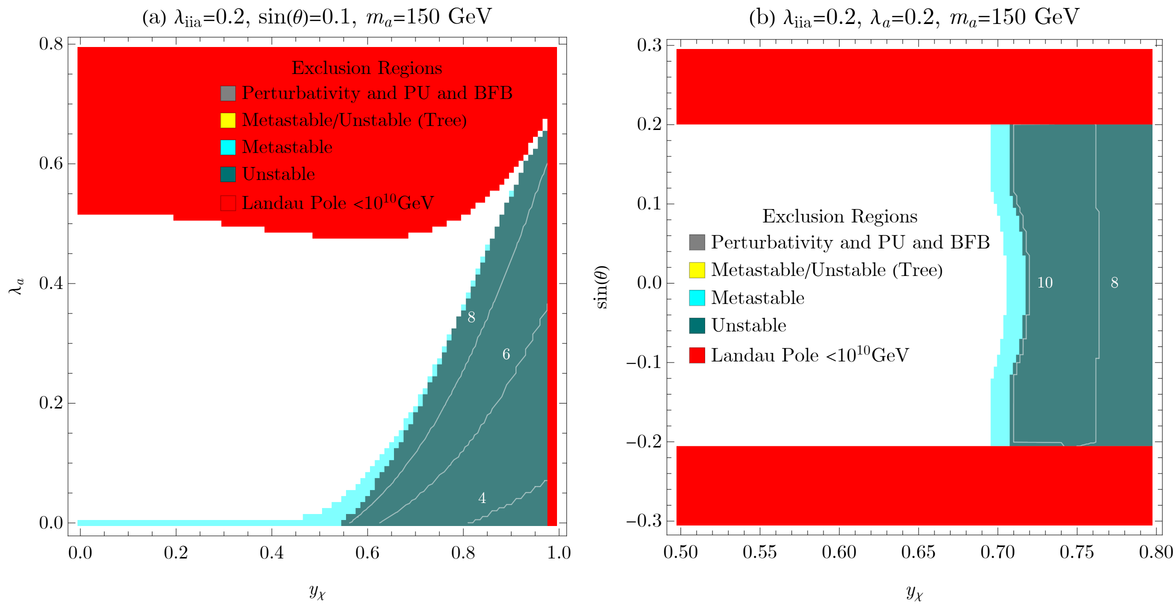

Figure 5.5: Parameter scans of stability bounds and Landau pole constraint in the 2HDM+a model. The white contours show the instability scale $\log_{10}(\Lambda_I/\mathrm{GeV})$. The 2HDM parameters are taken to be $\tan\beta = 5, \cos(\alpha-\beta) = -0.01, m_{H^*,A} = 1000\,\mathrm{GeV}, \lambda_1 = 0.6$. (a) Parameter scan in the $y_\chi \times \lambda_a$ plane. We see that metastability excludes large values of Yukawa couplings $y_\chi > 0.6$. However, larger values of Yukawa couplings $y_\chi \sim 0.8$ can still be allowed if λ_a is tuned between 0.4 and 0.6. (b) Parameter scan in the $y_\chi \times \sin(\theta)$ plane. Larger values of $\sin\theta$ marginally destabilises the vacuum. However, this effect is very small and is equivalent to shifting y_χ by about 1%.

This shows that the bounds on the 2HDM we derived in chapter 4 apply well to the 2HDM+s/a models.

The parameter scans for the 2HDM+s model are shown in 5.6. The left subfigure 5.6a shows that lowering μ_{12s} requires that δ also be lowered for the theory to evade perturbativity and Landau pole constraints. More negative values of μ_{12s} also seems to cause absolutely stable vacua to become metastable. But the proportion of metastable parameters seems to stay approximately fixed as μ_{12s} is varied. This is in agreement with the analysis in 5.3, where μ_{12s} makes no statistically significant impact on metastability constraints.

Note that for both models, the vacuum becomes unstable for larger Yukawa couplings y_χ. The role of the other 2HDM+s/a parameters are to minimally shift the critical y^*_χ above which the vacuum becomes unstable. Therefore, to leading order, my results tell us that the dark matter Yukawa coupling y_χ should not be too large $y_\chi \lesssim 0.8$. This is a novel constraint. A recent study by Arcadi *et al.* examined y_χ as large as 10,

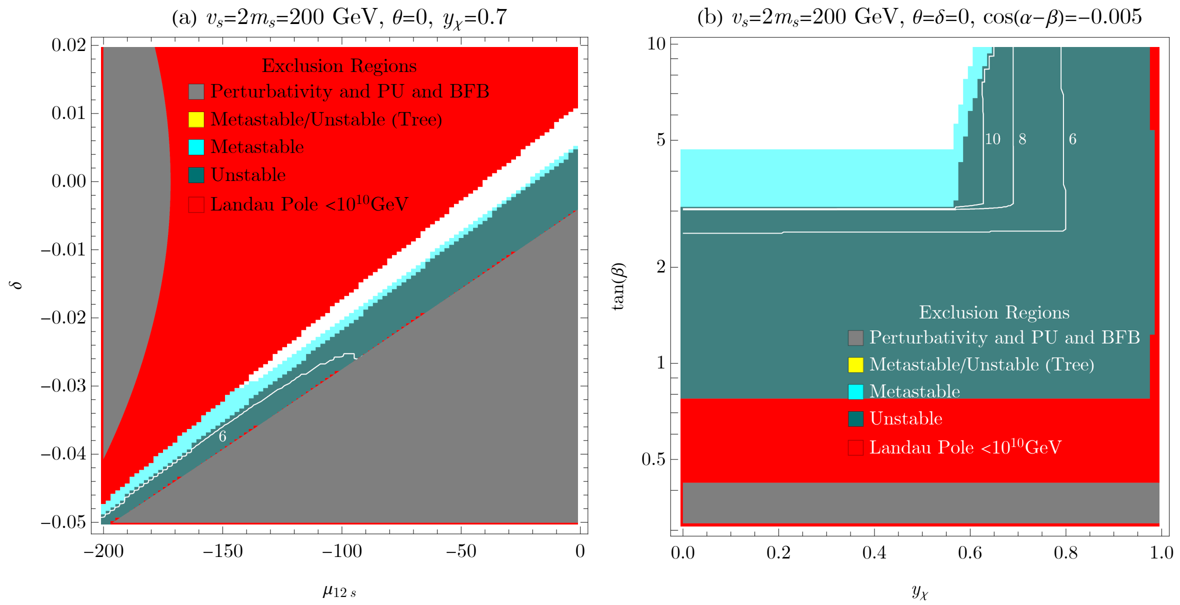

Figure 5.6: Parameter scans of stability bounds and Landau pole constraint in the 2HDM+s model. The white contours show the instability scale $\log_{10}(\Lambda_I/\text{GeV})$. (a) Parameter scan in the $\mu_{12s} \times \delta$ plane. The 2HDM parameters are set to $\tan\beta = 5, \cos(\alpha - \beta) = -0.01, m_{H^*,A} = 1000\,\text{GeV}$ and $\lambda_1 = 0.6$. We see that regions of more negative μ_{12s} prefers more negative values of δ. However, the proportion of parameter space excluded by metastability stays constant, as hinted by 5.3a. (b) Parameter scan in the $y_\chi \times \tan(\beta)$ plane. The 2HDM parameters other than $\cos(\alpha - \beta)$ are set the same as (a). We see that higher values of $\tan\beta$ can help stabilise the vacuum when $y_\chi \sim 0.6$.

and found points consistent with all considered constraints even at $y_\chi \sim 2$ [24]. Several other studies also perform parameter scans using a benchmark parameter of $y_\chi = 1$. [22, 88, 92]. The results of this chapter shows that, going forward, scanning beyond $y_\chi = 1$ is unnecessary as it is strongly disfavoured by metastability constraints. In addition, given that metastability disfavours $y_\chi \gtrsim 0.8$, future work on the 2HDM+s/a models should prefer smaller Yukawa couplings $y_\chi \lesssim 0.8$ as benchmark parameters.

Finally, most of the unstable regions in figures 5.5 and 5.6 have $\Lambda_I < 10^8$ GeV. This means that it would be difficult for new physics to stabilise the vacuum, and so we expect that the metastability bounds derived in this chapter should be relatively robust against new physics. In any case, just as in the 2HDM, if experiments somehow confirm a 2HDM+s/a model marked unstable in this chapter, then we immediately know that new physics must appear below $\Lambda_I \lesssim 10^6\,\text{GeV}$ to quickly stabilise the vacuum. In addition, the parameter space of these extended theories will be even more severely constrained by false vacuum decay, so I expect that the results in this thesis will be useful even then.

Chapter 6

Discussions and Conclusion

6.1 Summary and Discussion

In high-energy particle physics, simplified models have gained popularity due to their relative simplicity, and their rich phenomenology [19]. In particular, the 2HDM+s/a is one such promising simplified model, as it is a minimal SM extension which can simultaneously accommodate baryogenesis [30, 31], neutrino mass generation [25, 26], and a dark matter candidate [23, 90]. Unfortunately, just as with any quantum field theory, the 2HDM+s/a contains several free variables which must be fixed to keep the theory predictive. One goal of phenomenologists is thus to use whatever means necessary, from collider experiments to astrophysical signals, to constrain the model's parameter space.

In this thesis, I constrained the 2HDM(+s/a) parameter space using the observation that our universe has not decayed in the past 10^{10} years. I first analysed the behaviour of nearby vacua in the 2HDM in chapter 3, where I found that for large new 2HDM masses $m_{H^*,A} \gtrsim 800\,\text{GeV}$, the 2HDM only supports one vacuum. On one hand, this shows that our vacuum is unconditionally stable, when considering only vacua within $10^5\,\text{GeV}$ of our own. However, this also makes baryogenesis more difficult, as it generally requires a first-order phase transition from a higher vacuum state [30]. So it would be interesting to investigate more deeply the implications of high 2HDM masses, $m_{H^*,A} \gtrsim 800\,\text{GeV}$, on baryogenesis.

Contrastingly, renormalisation-induced vacua excludes a large region of parameter space with $\tan\beta < 3$ when the new 2HDM masses are set to be degenerate $m_H = m_{H^\pm} = m_A$. Note that this result complements constraints from electroweak and flavour physics, as they generally require the new 2HDM masses to be near-degenerate [77]. This way, I expect that the metastability constraints in this thesis will work together with future flavour and electroweak constraints to rule out most of the 2HDM parameter space with $\tan\beta < 3$. For the 2HDM+s/a, I found that in addition to the 2HDM constraints, our metastability constraint also requires the dark matter Yukawa coupling y_χ be small ($\lesssim 0.8$), regardless of the value of the other parameters. This is a considerable improvement upon the bound $y_\chi \lesssim 2$ in [24], and will help guide future phenomenological and experimental studies of the 2HDM+s/a, as researchers can now focus on the smaller region of parameter space $y_\chi \lesssim 0.8$.

However, there remains work to be done to fill in the gaps in this thesis. For example, throughout this thesis, I have only used the one-loop effective potential approximation to the observed Higgs mass m_h. While this is reasonably justified given that $m_h < v$ [40, 52], it is not strictly correct to one-loop order. Given we have seen how drastically m_h impacts tunneling rates (see figure 4.4), it is imperative that full one-loop corrections to m_h be included in future work. Along this line, I have also used in this thesis the choice $\bar{\mu}$ in (3.22). While simple, this hack comes at the cost of introducing numerical instabilities near the roots $\partial V^{(1)}/\partial \ln \mu = 0$. To further refine the results of this thesis, it would be beneficial to find a global way of ensuring that the one-loop corrections be small, while keeping the benefits of a mass-independent renormalisation scheme. One possible solution is to adapt the counterterm potential of Cline *et al.* [30, 78] into an iterative method. More precisely, at step k, we successively define the parameters $\lambda_i^{(k)}$ appearing in the potential as $\lambda_i^{(k)} := \lambda_i^{(k-1)} + \delta\lambda_i^{(k-1)}$. Here, $\delta\lambda_i$ are the counterterms defined by (3.17). I expect that this method will converge as the correction $\delta\lambda_i^{(k-1)}$ is formally at one-loop order. Finally, throughout this thesis I have only used the one-loop RGEs in studying the behaviour of renormalisation-induced vacua in the 2HDM. I do this mainly for consistency with chapter 3. However, more accurate results can be obtained by simply substituting in n-loop beta functions for λ_{eff}. Though, to be consistent, we would then also need to determine precisely measured observables like the Higgs mass m_h and the W/Z boson masses m_W, m_Z to n-loop order.

Regardless, in this thesis, I have taken the first step in comprehensively investigating the behaviour of metastability constraints in the 2HDM+s/a models. Chapters 4 and 5 in particular outline general methods which can be adapted to more refined studies of metastability in the 2HDM+s/a. Thus, I expect that the contributions of this thesis are also valuable for future studies of false vacuum decay in two-Higgs doublet models.

6.2 Future Work

Beyond the gaps mentioned in the previous section, there are also a number of new directions one can take from this point onward. As mentioned in the main text, I have not considered in this thesis the subject of early-universe phase transitions. It would be interesting to see to what extent the results of chapter 3 can be generalised to the early universe, where we must take into account thermal corrections. Further along the topic of baryogenesis, it would also be valuable to obtain metastability constraints for the more general CP-violating 2HDM[1]. This will require a re-derivation of the λ_{eff} with the CP-violating potential, but the general procedure outlined in this thesis will still be effective.

Another potential project to work on would be to fully automate the calculation of metastability constraints for general QFTs. Given that the Mathematica package SARAH is able to compute the two-loop RGEs, the only work left is to find a general procedure to solve for the straight line bounces (4.8), given a homogenous quartic potential. I expect that this would be difficult, if not impossible, to do for theories with a large number (> 5) of scalar fields, but in these cases, a numerical approach would be straightforward to implement. I expect that fully automating metastability constraints will allow for more high-energy physicists to adopt them as a quick way to disfavour large regions of parameter space on theoretical grounds. This will in turn make phenomenology more efficient, as phenomenologists can now refocus their efforts on a smaller region of parameter space. In addition, automation would simplify the study of how extensions to the QFT impact metastability constraints. Presently, this is often done in the SM using effective field theory techniques (see for example [93].) However, these fields tend to affect the decay rates only when $\phi \sim \Lambda$ the new physics scale. At this energy scale, effective field theory, as an expansion in ϕ/Λ becomes inaccurate, so it would be beneficial to study instead extensions of the QFT.

Recently, there has also been renewed interest in the possibility of false vacuum decay enhanced by primordial black holes [94, 95, 96, 97]. The basic idea is that the quantum field theory calculations in this thesis are done in a flat, Minkowski background. Since this approximation does not hold near black holes, we must

[1]These 2HDMs are frequently used in studies of baryogenesis, as CP-violation is an important ingredient for baryogenesis. See for example [30].

take the effects of curved spacetime into account. However, the possibility of this black-hole-assisted tunneling is still debated with some researchers [96] arguing that the enhancement is negligible, while some others [97] argue that these criticisms are flawed and that the tunneling rate must be enhanced. Overall, if there is indeed an enhancement on the tunneling rate, then much of the parameter space marked metastable (light cyan in figures 4.6, 4.7, 5.5, and 5.6) in this thesis may become unstable. We can then obtain new, more stringent metastability constraints with the assumption of black-hole-assisted tunneling.

Appendix

A.1 Analytical Change of Variables for the 2HDM+s

For completeness, I list here the analytical change of variables I obtained for the 2HDM+s. As usual, $c_\square := \cos(\square), s_\square := \sin(\square)$, and $t_\square := \tan(\square)$.

$$\begin{aligned}\lambda_s = \frac{1}{16v_s^3}\Big(&2v_s c_{2\delta}\left(m_h^2 - 2m_H^2 + m_s^2\right) + v_s\left(m_s^2 - m_h^2\right)c_{2(\delta-\theta)} - m_h^2 v_s c_{2(\delta+\theta)} \\ &-2m_h^2 v_s c_{2\theta} + m_s^2 v_s c_{2(\delta+\theta)} + 2m_s^2 v_s c_{2\theta} + 8\mu_{12s}v^2 c_\beta s_\beta + 12\mu_s v_s^2 + 2m_h^2 v_s + 4m_H^2 v_s + 2m_s^2 v_s\Big)\end{aligned} \tag{A.1}$$

$$\begin{aligned}m_{12}^2 = \frac{1}{4}\Bigg(&\frac{1}{t_\beta}\Big[4c_\theta^2\left(s_\gamma^2\left(m_h^2 - m_s^2 s_\delta^2\right) + m_s^2 s_\delta^2\right) - 2m_h^2 c_{2\gamma}s_\delta s_{2\theta}t_\gamma - 4m_H^2 c_\delta^2 s_\gamma^2 + 2m_s^2 c_{2\gamma}s_\delta s_{2\theta}t_\gamma \\ &-2\left(m_h^2 - m_s^2\right)s_\delta s_{2\theta}t_\gamma - 4m_h^2 s_\gamma^2 s_\delta^2 s_\theta^2 + 4m_h^2 s_\delta^2 s_\theta^2 - 4m_H^2 s_\delta^2 + 4m_H^2 + 4m_s^2 s_\gamma^2 s_\theta^2 - 3\lambda_1 v^2\Big] \\ &-\frac{\lambda_1 v^2 c_{3\beta}}{s_\beta} + 4\mu_{12s}v_s\Bigg)\end{aligned} \tag{A.2}$$

$$\lambda_{11s} = -\frac{c_\delta\left(c_\gamma s_\delta\left(-m_s^2 c_\theta^2 - m_h^2 s_\theta^2 + m_H^2\right) + c_\theta\left(m_h^2 - m_s^2\right)s_\gamma s_\theta\right) + \mu_{12s}v s_\beta}{v v_s c_\beta} \tag{A.3}$$

$$\lambda_{22s} = \frac{c_\delta\left(s_\gamma s_\delta\left(m_s^2 c_\theta^2 + m_h^2 s_\theta^2 - m_H^2\right) + c_\gamma c_\theta\left(m_h^2 - m_s^2\right)s_\theta\right) - \mu_{12s}v c_\beta}{v v_s s_\beta} \tag{A.4}$$

$$\begin{aligned}\lambda_2 = \frac{1}{32v^2 s_\beta^4}\Big[&-m_h^2 c_{2(\beta-\delta-\theta)} - m_h^2 c_{2(\beta+\delta-\theta)} - m_h^2 c_{2(\beta-\delta+\theta)} - m_h^2 c_{2(\beta+\delta+\theta)} + 2m_h^2 c_{2(\beta-\delta)} \\ &+2m_h^2 c_{2(\beta+\delta)} - 2m_h^2 c_{2(\beta-\theta)} - 2m_h^2 c_{2(\beta+\theta)} - m_h^2 c_{2(\gamma-\delta-\theta)} - m_h^2 c_{2(\gamma+\delta-\theta)} - m_h^2 c_{2(\gamma-\delta+\theta)} \\ &-m_h^2 c_{2(\gamma+\delta+\theta)} + 2m_h^2 c_{2(\gamma-\delta)} + 2m_h^2 c_{2(\gamma+\delta)} + 6m_h^2 c_{2(\gamma-\theta)} + 6m_h^2 c_{2(\gamma+\theta)} + 4m_h^2 c_{2\gamma} \\ &-4c_{2\beta}\left(3m_h^2 + 2m_H^2 + 3m_s^2 - 4\lambda_1 v^2\right) - 4m_H^2 c_{2(\beta-\delta)} - 4m_H^2 c_{2(\beta+\delta)} - 4m_H^2 c_{2(\gamma-\delta)} \\ &-4m_H^2 c_{2(\gamma+\delta)} - 8m_H^2 c_{2\gamma} + m_s^2 c_{2(\beta-\delta-\theta)} + m_s^2 c_{2(\beta+\delta-\theta)} + m_s^2 c_{2(\beta-\delta+\theta)} + m_s^2 c_{2(\beta+\delta+\theta)} \\ &+2m_s^2 c_{2(\beta-\delta)} + 2m_s^2 c_{2(\beta+\delta)} + 2m_s^2 c_{2(\beta-\theta)} + 2m_s^2 c_{2(\beta+\theta)} + m_s^2 c_{2(\gamma-\delta-\theta)} + m_s^2 c_{2(\gamma+\delta-\theta)}\end{aligned}$$

$$+m_s^2 c_{2(\gamma-\delta+\theta)} + m_s^2 c_{2(\gamma+\delta+\theta)} + 2m_s^2 c_{2(\gamma-\delta)} + 2m_s^2 c_{2(\gamma+\delta)} - 6m_s^2 c_{2(\gamma-\theta)} - 6m_s^2 c_{2(\gamma+\theta)}$$
$$+4m_s^2 c_{2\gamma} + 4\lambda_1 v^2 c_{4\beta} - 4m_h^2 s_{2\gamma-\delta-2\theta} + 4m_h^2 s_{2\gamma+\delta-2\theta} + 4m_h^2 s_{2\gamma-\delta+2\theta} - 4m_h^2 s_{2\gamma+\delta+2\theta}$$
$$+4m_s^2 s_{2\gamma-\delta-2\theta} - 4m_s^2 s_{2\gamma+\delta-2\theta} - 4m_s^2 s_{2\gamma-\delta+2\theta} + 4m_s^2 s_{2\gamma+\delta+2\theta} + 12\lambda_1 v^2\Big] \tag{A.5}$$

$$\lambda_5 = \frac{m_A^2\left(-c_\beta\right)s_\beta + m_{12}^2 - \mu_{12s}v_s}{v^2 c_\beta s_\beta} \tag{A.6}$$

$$\lambda_4 = \frac{-c_\beta s_\beta\left(2m_{H^\pm}^2 + \lambda_5 v^2\right) + 2m_{12}^2 - 2\mu_{12s}v_s}{v^2 c_\beta s_\beta} \tag{A.7}$$

$$\lambda_3 = -\frac{1}{4v^2 c_\beta s_\beta^2}\Big[-2s_\beta\Big(s_\delta\Big(c_{2\gamma}\left(m_h^2 - m_s^2\right)s_{2\theta} + m_s^2 c_\theta^2 s_{2\gamma}s_\delta + m_h^2 s_{2\gamma}s_\delta s_\theta^2\Big)$$
$$-2c_\gamma s_\gamma\left(m_h^2 c_\theta^2 + m_s^2 s_\theta^2\right) + m_H^2 c_\delta^2 s_{2\gamma}\Big) + c_\beta\Big(-4c_\theta^2\left(s_\gamma^2\left(m_h^2 - m_s^2 s_\delta^2\right) + m_s^2 s_\delta^2\right) +$$
$$4c_\theta\left(m_h^2 - m_s^2\right)s_\delta s_\theta t_\gamma + 2m_h^2 c_{2\gamma}s_\delta s_{2\theta}t_\gamma + 4m_H^2 c_\delta^2 s_\gamma^2 - 2m_s^2 c_{2\gamma}s_\delta s_{2\theta}t_\gamma + 4m_h^2 s_\gamma^2 s_\delta^2 s_\theta^2$$
$$-4m_h^2 s_\delta^2 s_\theta^2 + 4m_H^2 s_\delta^2 - 4m_H^2 - 4m_s^2 s_\gamma^2 s_\theta^2 + 4\lambda_4 v^2 s_\beta^2 + 4\lambda_5 v^2 s_\beta^2 + 3\lambda_1 v^2\Big) + \lambda_1 v^2 c_{3\beta}\Big] \tag{A.8}$$

$$m_{11}^2 = -\frac{s_\beta\left(c_\beta\left(v^2 s_\beta^2(\lambda_3+\lambda_4+\lambda_5) + \lambda_{11s}v_s^2\right) + \lambda_1 v^2 c_\beta^3 + 2s_\beta\left(\mu_{12s}v_s - m_{12}^2\right)\right)}{s_{2\beta}} \tag{A.9}$$

$$m_{22}^2 = \frac{1}{2}\left(\frac{2c_\beta\left(m_{12}^2 - \mu_{12s}v_s\right)}{s_\beta} - v^2 c_\beta^2(\lambda_3+\lambda_4+\lambda_5) - \lambda_2 v^2 s_\beta^2 - \lambda_{22s}v_s^2\right) \tag{A.10}$$

$$m_{s_0}^2 = -\frac{\lambda_{11s}v^2 v_s c_\beta^2 + 3\mu_s v_s^2 + \mu_{12s}v^2 s_{2\beta} + \lambda_{22s}v^2 v_s s_\beta^2 + 2\lambda_s v_s^3}{2v_s} \tag{A.11}$$

$$m_{12}^2 = \frac{1}{4}\Bigg(\frac{1}{t_\beta}\Big[4c_\theta^2\left(s_\gamma^2\left(m_h^2 - m_s^2 s_\delta^2\right) + m_s^2 s_\delta^2\right) - 2m_h^2 c_{2\gamma}s_\delta s_{2\theta}t_\gamma - 4m_H^2 c_\delta^2 s_\gamma^2$$
$$+2m_s^2 c_{2\gamma}s_\delta s_{2\theta}t_\gamma - 2\left(m_h^2 - m_s^2\right)s_\delta s_{2\theta}t_\gamma - 4m_h^2 s_\gamma^2 s_\delta^2 s_\theta^2 + 4m_h^2 s_\delta^2 s_\theta^2$$
$$-4m_H^2 s_\delta^2 + 4m_H^2 + 4m_s^2 s_\gamma^2 s_\theta^2 - 3\lambda_1 v^2\Big] - \frac{\lambda_1 v^2 c_{3\beta}}{s_\beta} + 4\mu_{12s}v_s\Bigg) \tag{A.12}$$

Note that some of the input variables are dependent on previous input variables. However, there are no dependency loops so the above equations provide an explicit change of variables.

Bibliography

1. **KLOE** Collaboration, "Precise measurement of $\Gamma(K\to e\ \nu(\gamma))/\Gamma(K\to\mu\ \nu(\gamma))$ and study of $K\to e\ \nu\ \gamma$," *Eur. Phys. J. C* **64** (Dec., 2009) 627–636. (cited on page 1)

2. **NA64** Collaboration, "Test of lepton flavour universality in $K+\to+\nu$ decays," *Phys. Lett. B* **698** (Apr., 2011) 105–114. (cited on page 1)

3. J. J. Aubert, U. Becker, P. J. Biggs, J. Burger, M. Chen, G. Everhart, P. Goldhagen, J. Leong, T. McCorriston, T. G. Rhoades, M. Rohde, S. C. C. Ting, S. L. Wu, and Y. Y. Lee, "Experimental Observation of a Heavy Particle J," *Phys. Rev. Lett.* **33** (Dec., 1974) 1404–1406. (cited on page 1)

4. **CDF** Collaboration, "Observation of Top Quark Production in $\bar{p}p$ Collisions with the Collider Detector at Fermilab," *Phys. Rev. Lett.* **74** (Apr., 1995) 2626–2631. (cited on page 1)

5. **D0** Collaboration, "Observation of the Top Quark," *Phys. Rev. Lett.* **74** (Apr., 1995) 2632–2637. (cited on page 1)

6. **UA1** Collaboration, "Experimental observation of isolated large transverse energy electrons with associated missing energy at s=540 GeV," *Phys. Lett. B* **122** (Feb., 1983) 103–116. (cited on page 1)

7. **UA2** Collaboration, "Observation of single isolated electrons of high transverse momentum in events with missing transverse energy at the CERN pp collider," *Phys. Lett. B* **122** (Mar., 1983) 476–485. (cited on page 1)

8. **UA1** Collaboration, "Experimental observation of lepton pairs of invariant mass around 95 GeV/c2 at the CERN SPS collider," *Phys. Lett. B* **126** (July, 1983) 398–410. (cited on page 1)

9. **UA2** Collaboration, "Evidence for $Z0\to e+e-$ at the CERN pp collider," *Phys. Lett. B* **129** (Sept., 1983) 130–140. (cited on page 1)

10. **ATLAS** Collaboration, "Observation of a new particle in the search for the Standard Model Higgs boson with the ATLAS detector at the LHC," *Phys. Lett. B* **716** (Sept., 2012) 1–29. (cited on pages 1 and 4)

11. **CMS** Collaboration, "Observation of a new boson at a mass of 125 GeV with the CMS experiment at the LHC," *Phys. Lett. B* **716** (Sept., 2012) 30–61. (cited on pages 1 and 4)

12. A. Arbey and F. Mahmoudi, "Dark matter and the early Universe: A review," *Prog. Part. Nucl. Phys.* **119** (July, 2021) 103865. (cited on page 1)

13. V. A. Kuzmin, V. A. Rubakov, and M. E. Shaposhnikov, "On anomalous electroweak baryon-number non-conservation in the early universe," *Phys. Lett. B* **155** (May, 1985) 36–42. (cited on page 1)

14. A. D. Sakharov, "Violation of CP invariance, C asymmetry, and baryon asymmetry of the universe," *Sov. Phys. Usp.* **34** (May, 1991) 392. (cited on pages 1 and 46)

15. K. Kajantie, M. Laine, K. Rummukainen, and M. Shaposhnikov, "Is There a Hot Electroweak Phase Transition at $m_H \gtrsim m_W$?," *Phys. Rev. Lett.* **77** (Sept., 1996) 2887–2890. (cited on page 1)

16. Y. Cai, J. Herrero García, M. A. Schmidt, A. Vicente, and R. R. Volkas, "From the Trees to the Forest: A Review of Radiative Neutrino Mass Models," *Front. Phys.* **5** (Dec., 2017) 296004. (cited on page 1)

17. S. Dimopoulos and H. Georgi, "Softly broken supersymmetry and SU(5)," *Nucl. Phys. B* **193** (Dec., 1981) 150–162. (cited on page 1)

18. N. Arkani-Hamed, A. G. Cohen, and H. Georgi, "Electroweak symmetry breaking from dimensional deconstruction," *Phys. Lett. B* **513** (July, 2001) 232–240. (cited on page 1)

19. J. Abdallah, H. Araujo, A. Arbey, *et al.*, "Simplified models for dark matter searches at the LHC," *Phys. Dark Universe* **9-10** (Sept., 2015) 8–23. (cited on pages 2 and 77)

20. V. Silveira and A. Zee, "Scalar Phantoms," *Phys. Lett. B* **161** (Oct., 1985) 136–140. (cited on page 2)

21. **ATLAS and CMS** Collaboration, "Measurements of the Higgs boson production and decay rates and constraints on its couplings from a combined ATLAS and CMS analysis of the LHC pp collision data at and 8 TeV," *J. High Energy Phys.* **2016** (Aug., 2016) 1–113. (cited on page 2)

22. G. Arcadi, A. Djouadi, and M. Raidal, "Dark Matter through the Higgs portal," *Phys. Rep.* **842** (Feb., 2020) 1–180. (cited on pages 2 and 76)

23. N. F. Bell, G. Busoni, and I. W. Sanderson, "Self-consistent Dark Matter simplified models with an s-channel scalar mediator," *J. Cosmol. Astropart. Phys.* **2017** (Mar., 2017) 015. (cited on pages 2, 53, 64, 65, 67, and 77)

24. G. Arcadi, N. Benincasa, A. Djouadi, and K. Kannike, "The 2HD+a model: collider, dark matter and gravitational wave signals," *arXiv* (Dec., 2022) , `2212.14788`. (cited on pages 2, 64, 65, 76, and 78)

25. E. Ma, "Verifiable radiative seesaw mechanism of neutrino mass and dark matter," *Phys. Rev. D* **73** (Apr., 2006) 077301. (cited on pages 3 and 77)

26. S. S. Correia, R. G. Felipe, and F. R. Joaquim, "Dirac neutrinos in the 2HDM with restrictive Abelian symmetries," *Phys. Rev. D* **100** (Dec., 2019) 115008. (cited on pages 3 and 77)

27. B. Holdom, "Two U(1)'s and xn–kza charge shifts," *Phys. Lett. B* **166** (Jan., 1986) 196–198. (cited on page 3)

28. P. Minkowski, "$\mu \to e\gamma$ at a rate of one out of 109 muon decays?," *Phys. Lett. B* **67** (Apr., 1977) 421–428. (cited on page 3)

29. J. A. Casas, J. R. Espinosa, and M. Quirós, "Improved Higgs mass stability bound in the standard model and implications for supersymmetry," *Phys. Lett. B* **342** (Jan., 1995) 171–179. (cited on page 4)

30. P. Basler, M. Krause, M. Mühlleitner, *et al.*, "Strong first order electroweak phase transition in the CP-conserving 2HDM revisited," *J. High Energy Phys.* **2017** (Feb., 2017) 121–38. (cited on pages 4, 38, 39, 46, 47, 77, 78, and 79)

31. S. J. Huber, K. Mimasu, and J. M. No, "Baryogenesis from transitional *CP* violation in the early Universe," *Phys. Rev. D* **107** (Apr., 2023) 075042. (cited on pages 4 and 77)

32. N. Chakrabarty and B. Mukhopadhyaya, "High-scale validity of a two-Higgs-doublet scenario: metastability included," *Eur. Phys. J. C* **77** (Mar., 2017) 1–14. (cited on page 4)

33. R. J. Baxter, *Exactly Solved Models in Statistical Mechanics*. Academic Press Inc, London, England, UK, Jan., 1982. (cited on page 7)

34. M. Kardar, *Statistical Physics of Particles*. Cambridge University Press, Cambridge, England, UK, June, 2007. (cited on pages 7, 10, 11, and 12)

35. H. Lehmann, K. Symanzik, and W. Zimmermann, "Zur Formulierung quantisierter Feldtheorien," *Nuovo Cim.* **1** (Jan., 1955) 205–225. (cited on page 9)

36. D. Schroeder and M. Peskin, *An Introduction To Quantum Field Theory*. Perseus, Boulder, CO, USA, Oct., 1995. (cited on pages 10, 11, 12, 13, 19, 20, and 55)

37. R. Shankar, "Renormalization-group approach to interacting fermions," *Rev. Mod. Phys.* **66** (Jan., 1994) 129–192. (cited on pages 10 and 11)

38. C. P. Burgess, "An Introduction to Effective Field Theory," *Annu. Rev. Nucl. Part. Sci.* (Nov., 2007) 329–362. (cited on page 11)

39. B. Delamotte, "An Introduction to the Nonperturbative Renormalization Group," in *Renormalization Group and Effective Field Theory Approaches to Many-Body Systems*, pp. 49–132. Springer, Berlin, Germany, June, 2012. (cited on page 11)

40. A. Andreassen, D. Farhi, W. Frost, and M. D. Schwartz, "Precision decay rate calculations in quantum field theory," *Phys. Rev. D* **95** (Apr., 2017) 085011. (cited on pages 12, 17, 18, 20, 59, and 78)

41. S. Coleman and E. Weinberg, "Radiative Corrections as the Origin of Spontaneous Symmetry Breaking," *Phys. Rev. D* **7** (Mar., 1973) 1888–1910. (cited on page 14)

42. L. Chataignier, T. Prokopec, M. G. Schmidt, *et al.*, "Single-scale renormalisation group improvement of multi-scale effective potentials," *J. High Energy Phys.* **2018** (Mar., 2018) 1–44. (cited on pages 14, 15, 16, 38, 40, 41, 43, 48, and 51)

43. M. B. Einhorn and D. R. Timothy Jones, "A new renormalization group approach to multiscale problems," *Nucl. Phys. B* **230** (Feb., 1984) 261–272. (cited on page 15)

44. M. Bando, T. Kugo, N. Maekawa, *et al.*, "Improving the Effective Potential: Multi-Mass-Scale Case," *Prog. Theor. Phys.* **90** (Aug., 1993) 405–417. (cited on page 15)

45. S. Coleman, "Fate of the false vacuum: Semiclassical theory," *Phys. Rev. D* **15** (May, 1977) 2929–2936. (cited on pages 16 and 17)

46. C. G. Callan and S. Coleman, "Fate of the false vacuum. II. First quantum corrections," *Phys. Rev. D* **16** (Sept., 1977) 1762–1768. (cited on pages 16, 17, and 18)

47. V. I. Arnold, *Mathematical Methods of Classical Mechanics*. Springer, New York, NY, USA. https://link.springer.com/book/10.1007/978-1-4757-2063-1. (cited on pages 16 and 17)

48. T. Banks, C. M. Bender, and T. T. Wu, "Coupled Anharmonic Oscillators. I. Equal-Mass Case," *Phys. Rev. D* **8** (Nov., 1973) 3346–3366. (cited on page 16)

49. G. V. Dunne and H. Min, "Beyond the thin-wall approximation: Precise numerical computation of prefactors in false vacuum decay," *Phys. Rev. D* **72** (Dec., 2005) 125004. (cited on page 17)

50. G. Isidori, G. Ridolfi, and A. Strumia, "On the metastability of the Standard Model vacuum," *Nucl. Phys. B* **609** (Aug., 2001) 387–409. (cited on pages 18, 21, 22, 23, 24, 25, and 59)

51. A. Andreassen, D. Farhi, W. Frost, *et al.*, "Direct Approach to Quantum Tunneling," *Phys. Rev. Lett.* **117** (Nov., 2016) 231601. (cited on page 18)

52. A. Brignole, "Radiative corrections to the supersymmetric neutral Higgs boson masses," *Phys. Lett. B* **281** (May, 1992) 284–294. (cited on pages 20 and 78)

53. S. Elitzur, "Impossibility of spontaneously breaking local symmetries," *Phys. Rev. D* **12** (Dec., 1975) 3978–3982. (cited on page 21)

54. J. Fröhlich, G. Morchio, and F. Strocchi, "Higgs phenomenon without a symmetry breaking order parameter," *Phys. Lett. B* **97** (Dec., 1980) 249–252. (cited on page 21)

55. J. Elias-Miró, J. R. Espinosa, G. F. Giudice, *et al.*, "Higgs mass implications on the stability of the electroweak vacuum," *Phys. Lett. B* **709** (Mar., 2012) 222–228. (cited on page 21)

56. M. Sher, "Precise vacuum stability bound in the standard model," *Phys. Lett. B* **317** (Nov., 1993) 159–163. (cited on page 21)

57. G. Ridolfi, "Search for the Higgs boson: theoretical perspectives," *arXiv* (June, 2001) , `hep-ph/0106300`. (cited on page 21)

58. D. Buttazzo, G. Degrassi, P. P. Giardino, *et al.*, "Investigating the near-criticality of the Higgs boson," *J. High Energy Phys.* **2013** (Dec., 2013) 1–49. (cited on pages 21, 24, and 25)

59. S. Fubini, "A new approach to conformal invariant field theories," *Nuov. Cim. A* **34** (Aug., 1976) 521–554. (cited on pages 22 and 49)

60. K. Lee and E. J. Weinberg, "Tunneling without barriers," *Nucl. Phys. B* **267** (Mar., 1986) 181–202. (cited on pages 22, 23, and 49)

61. V. Keus, S. F. King, S. Moretti, *et al.*, "CP Violating Two-Higgs-Doublet Model: Constraints and LHC Predictions," *arXiv* (Oct., 2015) , `1510.04028`. (cited on page 26)

62. G. Arcadi, G. Busoni, D. Cabo-Almeida, *et al.*, "Is there a (Pseudo)Scalar at 95 GeV?," *arXiv* (Nov., 2023) , `2311.14486`. (cited on pages 26, 31, 32, 62, 64, 66, and 67)

63. P. M. Ferreira, L. A. Morrison, and S. Profumo, "One-loop charge-breaking minima in the two-Higgs doublet model," *J. High Energy Phys.* **2020** (Apr., 2020) 1–33. (cited on pages 26, 27, 31, and 38)

64. Particle Data Group, M. Tanabashi, K. Hagiwara, *et al.*, "Review of Particle Physics," *Phys. Rev. D* **98** (Aug., 2018) 030001. (cited on page 26)

65. S. L. Glashow and S. Weinberg, "Natural conservation laws for neutral currents," *Phys. Rev. D* **15** (Apr., 1977) 1958–1965. (cited on page 26)

66. G. C. Branco, P. M. Ferreira, L. Lavoura, *et al.*, "Theory and phenomenology of two-Higgs-doublet models," *Phys. Rep.* **516** (July, 2012) 1–102. (cited on pages 26, 27, 29, 30, and 31)

67. **CMS** Collaboration, "Search for flavor-changing neutral current interactions of the top quark and the Higgs boson decaying to a bottom quark-antiquark pair at = 13 TeV," *J. High Energy Phys.* **2022** (Feb., 2022) 1–42. (cited on page 26)

68. G. C. Branco, "CP violation in the standard model and beyond," *AIP Conf. Proc.* **317** (1994) 82–94. (cited on pages 27 and 46)

69. I. P. Ivanov, "Minkowski space structure of the Higgs potential in the two-Higgs-doublet model," *Phys. Rev. D* **75** (Feb., 2007) 035001. (cited on page 27)

70. A. Barroso, P. M. Ferreira, I. P. Ivanov, *et al.*, "Metastability bounds on the two Higgs doublet model," *J. High Energy Phys.* **2013** (June, 2013) 45–33. (cited on pages 28, 30, and 33)

71. E. Tiesinga, P. J. Mohr, D. B. Newell, *et al.*, "CODATA recommended values of the fundamental physical constants: 2018," *Rev. Mod. Phys.* **93** (June, 2021) 025010. (cited on pages 29 and 55)

72. J. F. Gunion and H. E. Haber, "CP-conserving two-Higgs-doublet model: The approach to the decoupling limit," *Phys. Rev. D* **67** (Apr., 2003) 075019. (cited on page 29)

73. S. Argyropoulos, U. Haisch, and I. Kalaitzidou, "Novel collider signatures in the type-I 2HDM+a model," *arXiv* (Apr., 2024) , `2404.05704`. (cited on pages 31 and 32)

74. F. Arco, S. Heinemeyer, and M. J. Herrero, "Exploring sizable triple Higgs couplings in the 2HDM," *Eur. Phys. J. C* **80** (Sept., 2020) 884–33. (cited on pages 31 and 32)

75. P. Sikivie, L. Susskind, M. Voloshin, *et al.*, "Isospin breaking in technicolor models," *Nucl. Phys. B* **173** (Oct., 1980) 189–207. (cited on page 32)

76. M. E. Peskin and T. Takeuchi, "New constraint on a strongly interacting Higgs sector," *Phys. Rev. Lett.* **65** (Aug., 1990) 964–967. (cited on page 32)

77. A. S. Woodcock, "Investigation of Two-Higgs-Doublet Models," Master's thesis, 2023. https://digital.library.adelaide.edu.au/dspace/handle/2440/139281. (cited on pages 32, 61, 62, and 77)

78. J. M. Cline, K. Kainulainen, and M. Trott, "Electroweak baryogenesis in two Higgs doublet models and B meson anomalies," *J. High Energy Phys.* **2011** (Nov., 2011) 89–49. (cited on pages 39 and 78)

79. D. Curtin, P. Meade, and H. Ramani, "Thermal Resummation and Phase Transitions," *arXiv* (Dec., 2016) , `1612.00466`. (cited on page 47)

80. P. Basler, M. Mühlleitner, and J. Müller, "Electroweak phase transition in non-minimal Higgs sectors," *J. High Energy Phys.* **2020** (May, 2020) 16–45. (cited on page 47)

81. N. Blinov, J. Kozaczuk, D. E. Morrissey, and C. Tamarit, "Electroweak baryogenesis from exotic electroweak symmetry breaking," *Phys. Rev. D* **92** (Aug., 2015) 035012. (cited on page 47)

82. M. Aoki, T. Komatsu, and H. Shibuya, "Possibility of a multi-step electroweak phase transition in the two-Higgs doublet models," *Prog. Theor. Exp. Phys.* **2022** (June, 2022) 063B05. (cited on page 47)

83. Z.-g. Si, H.-x. Wang, L. Wang, and Y. Zhang, "Exploring multi-step electroweak phase transitions in the 2HDM+a," *arXiv* (Oct., 2024) , `2410.15975`. (cited on page 47)

84. K. Kannike, "Vacuum stability conditions from copositivity criteria," *Eur. Phys. J. C* **72** (July, 2012) 2093–7. (cited on page 53)

85. F. Staub, "Exploring new models in all detail with SARAH," *arXiv* (Mar., 2015) , `1503.04200`. (cited on page 55)

86. J. Greensite, *An Introduction to the Confinement Problem.* Springer, Berlin, Germany, 2011. https://link.springer.com/book/10.1007/978-3-642-14382-3. (cited on page 55)

87. G. Elor, R. Houtz, S. Ipek, and M. Ulloa, "The Standard Model CP Violation is Enough," *arXiv* (Aug., 2024) , `2408.12647`. (cited on page 65)

88. T. Abe, Y. Afik, A. Albert, C. R. Anelli, L. Barak, *et al.*, "LHC Dark Matter Working Group: Next-generation spin-0 dark matter models," *Phys. Dark Universe* **27** (Jan., 2020) 100351. (cited on pages 65, 66, 68, and 76)

89. T. Abe, M. Fujiwara, J. Hisano, and Y. Shoji, "Maximum value of the spin-independent cross section in the THDM+a," *arXiv* (Oct., 2019) , `1910.09771`. (cited on page 67)

90. M. Bauer, U. Haisch, and F. Kahlhoefer, "Simplified dark matter models with two Higgs doublets: I. Pseudoscalar mediators," *J. High Energy Phys.* **2017** (May, 2017) 138–38. (cited on pages 67 and 77)

91. **ATLAS** Collaboration, "Search for invisible Higgs-boson decays in events with vector-boson fusion signatures using 139 fb-1 of proton-proton data recorded by the ATLAS experiment," *J. High Energy Phys.* **2022** (Aug., 2022) 104–66. (cited on page 67)

92. U. Haisch and L. Schnell, "Long-lived particle phenomenology in the 2HDM+a model," *J. High Energy Phys.* **2023** (Apr., 2023) 134–20. (cited on page 76)

93. V. Branchina and E. Messina, "Stability, Higgs Boson Mass, and New Physics," *Phys. Rev. Lett.* **111** (Dec., 2013) 241801. (cited on page 79)

94. L. V. Iliesiu, "Black Holes Stimulate Higgs Vacuum Decay," July, 2015. https://inspirehep.net/literature/1384719. [Online; accessed 10. Oct. 2024]. (cited on page 79)

95. R. Gregory, I. G. Moss, and B. Withers, "Black holes as bubble nucleation sites," *J. High Energy Phys.* **2014** (Mar., 2014) 81–27. (cited on page 79)

96. A. Strumia, "Black holes don't source fast Higgs vacuum decay," *J. High Energy Phys.* **2023** (Mar., 2023) 39–14. (cited on pages 79 and 80)

97. L. Hamaide, L. Heurtier, S.-Q. Hu, and A. Cheek, "Primordial black holes are true vacuum nurseries," *Phys. Lett. B* **856** (Sept., 2024) 138895. (cited on pages 79 and 80)